

# Contributions towards a downscaling scheme for urban climate modeling integrating mobile measurements and improved roughness representation for Hamburg (Germany)

Dissertation

Zur Erlangung des Doktorgrades der Naturwissenschaften im Fachbereich  
Geowissenschaften der Universität Hamburg

vorgelegt von  
**Thomas Langkamp**  
aus  
Osnabrück

Hamburg  
2013

Als Dissertation angenommen vom Fachbereich Geowissenschaften der Universität Hamburg

Auf Grund der Gutachten von Prof. Dr. Böhner  
und Prof. Dr. Leidl

Hamburg, den 29. Januar 2013

Prof. Dr. Jürgen Oßenbrügge  
Leiter des Fachbereichs Geowissenschaften

# Abstract

Global climate change is affecting the local climate within the city, leading to potentially more heat waves and other health risks for the people. This research adds knowledge to improve numerical urban climate models. It implements a differentiated land use classification (LUC, available at 100 meter resolution) for Hamburg, Germany, within the open source regional climate model (RCM) Weather Research and Forecasting (WRF) at 1 kilometer resolution. While there are already different dynamical downscaling approaches available to model the urban canopy since WRF v3.1 (Noah LSM, SLUCM, BEP, BEP+BEM, and coupling to microscale models), they are all more demanding of scarce computing capacity. Thus, our approach uses the default WRF land surface model and demands almost no more computing time, while improving the model output. To save additional computing time, a benchmark of WRF using different compilers was accomplished.

The main enhancement of the new LUC (nLUC, Daneke, Bechtel, and Langkamp 2010, based on local climate zones (LCZ) by Stewart and Oke 2009, 2012) lies in providing more classes of urban roughness through a recently proposed roughness parameterization (cf. Bechtel and Langkamp et al. 2011). Further land use characteristics such as albedo, emissivity etc. could also be added to the classification and thus to WRF in the long run. At the same time the nLUC is backwards compatible to the LCZs and transferable to other cities in the world. The classes can automatically be derived from multisensor remote sensing data (Bechtel and Daneke 2012).

Another enhancement of the nLUC is, that future scenarios of the city's evolution are available because of its implementation in a dynamic urban land use model. Thus, changes of the city surface are also implementable in WRF or any other RCM using the nLUC. Current available RCMs and their urban canopy models implement static urban morphology only.

To evaluate its added value, a sensitivity study of WRF with the embedded nLUC was accomplished. For this evaluation – and to collect more data for statistical downscaling applications – this research also presents a mobile measurement campaign that utilized 15 buses of the local public transportation company Hochbahn AG. The huge amount of collected mobile air temperature data was implemented in a newly developed database together with numerous stationary data. The database is available to other scientists and is used here for evaluating different WRF runs for the metropolitan area of Hamburg, for May and June 2011.

# Zusammenfassung

Der globale Klimawandel verändert auch das städtische Klima. Dies führt potenziell zu häufigeren und stärkeren Hitzewellen und weiteren Gesundheitsrisiken für die Bevölkerung. Unter diesem Gesichtspunkt verbessert und ergänzt die vorliegende Forschungsarbeit das Know-How zur numerischen Modellierung des Stadtklimas durch die Nutzung einer differenzierten Landnutzungs-Klassifikation für Hamburg (verfügbar ab einer Auflösung von 100 m). Die Klassifikation wurde dazu bei einer Auflösung von einem Kilometer in das regionale, open source Klimamodell WRF integriert. Seit Version 3.1 verfügt WRF zwar bereits über mehrere auf das Stadtklima abgestimmte Oberfläche-Boden-Modelle, jedoch benötigen sie alle deutlich mehr Rechenkapazität. Deshalb ist der vorgestellte Ansatz rechenzeit-neutral, verbessert aber dennoch die Modellergebnisse. Um weitere wertvolle Rechenzeit einzusparen wurde eine Benchmark-Studie durchgeführt, die WRFs Leistung bei der Verwendung verschiedener Compiler vermisst.

Der Hauptvorteil der neuen Landnutzung (Daneke, Bechtel, und Langkamp 2010, basierend auf der Klassifikation der lokalen Klimazonen (LCZ) von Stewart und Oke 2009, 2012) liegt in der differenzierteren Darstellung städtischer Oberflächenrauigkeit, welche auf eine neue Rauigkeitsparameterisierung von Bechtel und Langkamp et al. 2011 zurückgreift. Auf lange Sicht, können weitere Landnutzungs-Parameter wie Albedo, Emissivität etc. in der Klassifikation und somit in WRF ergänzt werden.

Trotz einer weiter erhöhten Klassenzahl bleibt die Klassifikation nach Daneke, Bechtel, und Langkamp (2010) rückwärts-kompatibel zu den LCZs und kann auf andere Städte weltweit übertragen werden. Die Klassen können mit Hilfe von multi-sensorischen Fernerkundungsdaten automatisiert erhoben werden, wie in Bechtel und Danke 2012 beschrieben.

Ein weiterer Vorteil der neuen Klassifikation liegt darin, dass für sie Szenarien des Stadtwachstums verfügbar sind, da sie in ein dynamisches Landnutzungsmodell eingebettet ist. Somit können Veränderungen der städtischen Oberfläche auch in WRF oder anderen regionalen Modellen implementiert werden. Aktuelle verfügbare regionale Modelle und ihre Oberfläche-Boden-Modelle verfügen nur über statische städtische Oberflächen.

Um WRF in Kombination mit der neuen Landnutzung zu validieren und mehr Daten für ein statistisches Downscaling zu erhalten, welches die Auflösung der WRF-Ergebnisse auf 100 Meter erhöhen soll, wurde zudem eine mobile Messkampagne mit 15 Bussen des öffentlichen Personennahverkehrs der Hochbahn AG durchgeführt. Die große Menge gesammelter Luft-Temperaturdaten wurde zusammen mit zahlreichen stationären Messungen in eine neu entwickelte Datenbank integriert. Die Datenbank steht anderen Wissenschaftlern für ihre Forschungsfragen oder zur Erweiterung der Datenbasis offen. In dieser Arbeit diente ihr Datenbestand der Auswertung verschiedener WRF-Simulationen im Gebiet der Metropolregion Hamburg über den Zeitraum von Mai bis Juni 2011.

# Structure

<b>1 Introduction</b>	<b>8</b>
<b>2 State of the art</b>	<b>10</b>
2.1 Key characteristics of the UHI .....	10
2.2 Theoretical background of dynamical and statistical downscaling approaches .....	12
2.3 Urban land surface models and WRF .....	14
2.4 Impact of wind and roughness on the UHI .....	16
2.5 The importance of a land use classification optimized for urban climate studies .....	17
2.6 Urban roughness length parameterization .....	19
<b>3 Empirical data and methods</b>	<b>22</b>
3.1 Mobile measurements complementing met station data .....	22
3.2 Mobile measurement equipment .....	23
3.3 Logger offset .....	24
3.4 Lower speed boundary and logger position .....	25
3.5 Measurement resolution, bias, and representativeness .....	29
3.6 Measurement yield and data aggregation .....	31
3.7 Verification of mobile measurements with met station data .....	34
<b>4 Parameterization of urban roughness</b>	<b>39</b>
4.1 The IFSAR based digital elevation model .....	39
4.2 Morphological land use and roughness classification .....	40
4.3 Improved roughness mapping by sector height statistics .....	42
4.4 Improved roughness mapping by class specific height statistics .....	45
4.5 Implementation of the new roughness data into WRF .....	49
<b>5 Dynamical downscaling</b>	<b>52</b>
5.1 Optimizing WRF performance for a HPC .....	52
5.2 ERA Interim preprocessing and domain setup .....	53
5.3 WRF roughness sensitivity tests .....	55
<b>6 Sensitivity study results of the improved LSM</b>	<b>59</b>
6.1 Temperature .....	59
6.2 Surface wind field .....	64
6.3 Circulation types .....	66
6.4 Discussion .....	69
<b>7 Conclusions and Outlook</b>	<b>70</b>
Appendix .....	72
A Met station data sources and details .....	72
B Bus data processing R-script with hints and comments .....	74
C Python script to find non-unique GPS values .....	76
D SAGA GIS manuals to aggregate the bus measurements .....	77
E Data formats and constraints handled by the DBMS .....	78
F SQL queries to calculate the UHI .....	78
G Sources and contents of the default WRF surface data .....	79
H How to edit WRFs land surface with SAGA GIS .....	80

I	The new LANDUSE.TBL .....	81
J	Configure.wrf for PGI compiler .....	83
K	ERA-Interim grid transformation scripts utilizing CDO .....	84
L	WPS' runtime configuration file namelist.wps .....	85
M	WRFs runtime configuration file namelist.input .....	85
N	How-To execute ecmwf_calc_p.exe for ERA-I with model levels .....	86
O	The jobscript used on Tornado .....	87
P	WRF Post Processing and evaluation through combined DB data .....	87
	Abbreviations and acronyms .....	91
	Units .....	92
	Acknowledgments .....	93
	Bibliography .....	94
	Erklärung .....	100

## List of Figures

Fig. 2.1.1	Climate processes in the urban boundary layer (UBL). .....	10
Fig. 2.1.2	Relative diurnal temperatures of the climate stations from 10 July 2010. ....	11
Fig. 2.2.1	A general downscaling structure with exemplary resolution values and lower boundary layers. ....	12
Fig. 2.2.2	Changing global and urban climate in comparison to the city-growth. ....	13
Fig. 2.3.1	A scheme of the WRF modeling system. ....	15
Fig. 2.5.1	Local climate zones (LCZs) in the city series. ....	18
Fig. 2.6.1	Conceptual relation between morphometric and roughness parameters. ....	19
Fig. 3.1.1	Locations and sources of the collected met station data. ....	22
Fig. 3.2.1	Qstarz BT-Q1000XT GPS logger (left) and Mobile Power Pack VT-PP-320b (right). ....	23
Fig. 3.2.2	The instrumentation on the bus roof. ....	23
Fig. 3.4.1	Offset-corrected means of T and ST measurements regardless of driving speed. ....	26
Fig. 3.4.2	Roof pictures of bus 2 from front to back. ....	27
Fig. 3.4.3	Roof pictures of bus 3 from front to back. ....	27
Fig. 3.4.4	The temperature and speed measurements from bus 1. ....	27
Fig. 3.4.5	The measurements from bus 2. ....	28
Fig. 3.4.6	The measurements from bus 2, day 4, at 5 s frequency. ....	28
Fig. 3.4.7	The measurements from bus 3. ....	29
Fig. 3.5.1	The classified bus driving speeds of the 15 buses' raw data. ....	30
Fig. 3.5.2	The minimal resolution of the T sensor based on driving speed. ....	30
Fig. 3.6.1	Daytimes when the buses were traveling of the whole campaign. ....	32
Fig. 3.6.2	The database design for the climatological stations. ....	32
Fig. 3.6.3	Bus routes map with the usually operated lines of depot Mesterkamp (red). ....	33
Fig. 3.6.4	Spatial extent of bus-measurements aggregated in an irregular 100 m spaced network. ....	34
Fig. 3.7.1	T of mobile and stationary measurements relative to the MI-station. ....	35
Fig. 3.7.2	T of mobile and stationary measurements relative to the MI-station. ....	36
Fig. 3.7.3	Absolute T of mobile and stationary measurements. ....	37
Fig. 3.7.4	Absolute T of mobile and stationary measurements. ....	38
Fig. 4.1.1	IFSAR derived DEM maps of different parts of Hamburg. ....	39
Fig. 4.2.1	The different counties (Landkreise) of the metropolitan area (green and blue) of Hamburg. ....	41

Fig. 4.2.2	The nLUC over a part of the metropolitan area of Hamburg (Fig. 4.2.1).	42
Fig. 4.3.1	$z_0$ derived from wind profile measurements at the MI-station.	43
Fig. 4.3.2	VSH for Hamburgs inner city, the Elbe estuary and the Elbe island.	44
Fig. 4.3.3	Pearson's $r$ of VSH0.5 to $z_0$ in dependence of radius and tolerance for 250 m SLH (Fig. 4.3.1).	44
Fig. 4.4.1	$\sigma$ (colored) of the DEM (gray scale) for a raster of 250 m.	46
Fig. 4.4.2	Mean class HV for the 100 m resolved LUC polygons.	46
Fig. 4.4.3	The logarithmized mean HVs of the nLUCs plotted towards their literature $z_0$ -values.	47
Fig. 4.4.4	The IFSAR DEM for a central part of Hamburg, used in the evaluation of Table 4.4.2.	49
Fig. 4.5.1	WRFs original LUC (oLUC) for the inner 1 km domain.	50
Fig. 4.5.2	The nLUC after its integration in the inner 1 km domain of WRF.	51
Fig. 5.1.1	The 2048 core HPC Tornado of the DKRZ.	52
Fig. 5.2.1	The WRF domains with three nests and the ERA-I land-sea mask.	53
Fig. 5.2.2	WRF vegetation fraction, dominant soil category, and terrain height.	54
Fig. 5.3.1	Maps of WRF ARW T2 and wind for the three alternative roughness settings (A, B, C).	56
Fig. 5.3.2	0.2 K contours of B and C, the nLUC, and the C-B difference.	57
Fig. 5.3.3	Vertical temperature and RH for a 90° cross-section of the plots in Fig. 5.3.1.	58
Fig. 6.1.1	Daily means of T2 from measurements and WRF runs.	60
Fig. 6.1.2	6 hourly data of temperatures from measurements and WRF runs.	61
Fig. 6.1.3	6 hourly data of temperatures from measurements and ERA-I.	61
Fig. 6.1.4	Diurnal hourly temperature for measurements, WRF, and ERA-I.	62
Fig. 6.1.5	Diurnal hourly bias of temperature.	62
Fig. 6.1.6	WRF oLUC and nLUC T2 and wind for 8 May 2011, 12:00 to 13:00 UTC.	63
Fig. 6.2.1	Daily 10 m wind speed of WRF and measurements.	64
Fig. 6.2.2	The diurnal hourly 10 m wind speed for measurements and WRF.	65
Fig. 6.2.3	Daily surface pressure of WRF and measurements.	65
Fig. 6.3.1	Average T2 deviation of daily data for objective DWD circulation types (DWD HP 2012a).	67
Fig. 6.3.2	Average T2 deviation of the oLUC hourly data	67
Fig. 6.3.3	Average T2 deviation of the nLUC hourly data	68
Fig. 6.3.4	ANOVA with given $R^2$ of different circulation type combinations (colored).	68

## List of Tables

Table 3.2.1	Details on the evaluated loggers and sensors.	24
Table 3.3.1	Evaluation of the sensor offsets as their deviation of the measured mean of all sensors.	25
Table 4.2.1	Original LCZs and reclassified nLUCs with their assigned roughness class.	41
Table 4.4.1	HV and new $z_0$ for the nLUC, plus Spearman ( $\rho$ ) between HV and original $z_0$ .	48
Table 4.4.2	$\rho$ of mean HV for different LUCs correlated with the original $z_0$ (Table 4.4.1).	48
Table 6.1.1	Some statistics on the 6 hourly data.	60
Table 6.1.2	Pearson's $r$ on the data that was available for ERA-I's temporal resolution (6 h).	60
Table 6.2.1	Statistics of the hourly 10 m mean wind velocities.	64
Table 6.3.1	The objective circulation type classification by the DWD.	66
Table 7.1	Detailed station meta data for evaluated stations only.	73
Table 7.2	Table of $z_0$ values in centimeter from different LUC versions.	83

# 1 Introduction

Climate change is affecting the planet and with it the local climate in cities. The urban climate is an important determinant of people's lives, because of well known effects like the urban heat island (UHI). The UHI is defined as the highest nocturnal air temperature difference at screen height (Stewart and Oke 2009) between a measuring site in the city and another situated outside of the city. In short: The city is often warmer than the surrounding rural area. The extension and amplitude of the (many) UHIs are of imminent concern for human health during heat waves, besides coupled problems like air pollutants (ozone), soil sealing, hazardous flooding, or other extreme weather conditions including their ecological and economic implications.

The shape of the city is constantly changing, for example in form of a densification process, when the guidelines of urban development are following the compact city (Wentz 2000). This is supposed to lead to an even stronger UHI. There are already development guidelines to counter a stronger UHI (Ruth 2006), but especially in developing countries there are wild growing cities, without any guideline even implementable. Thus, a "smart growth" is needed, taking climate change into account (Ruth 2006).

Until then problematic climate conditions may rise more frequently, affecting the health of an increasing number of people. This research aims to support the bio-climatological risk management of heat waves within the UHI area, knowing that this is probably not the most severe threat for the research area Hamburg (1.8 million inhabitants; 53° 33' N, 10° 0' O). Hamburg was used nonetheless as a test case to develop new modeling approaches, which aim to improve the knowledge about **where** and **when heat waves may arise**. In the long run the basic research accomplished in this work should serve politicians and city planners to better adapt the city environment and to mitigate climate impacts.

To achieve these advancements, urban climate models have to be merged with high resolution land surface models (LSMs) and land use models, to assure a sufficient representation of the heterogeneous and dynamic urban morphology, determining the enormous small scale variation of urban climate. This small scale variation, however, is very difficult to handle due to two major problems:

The first problem can be found within the current regional climate models (RCMs) frequently used for numerical dynamical downscaling (DD) of global climate model (GCM) output. Most RCMs are not optimized for resolutions higher than 1 km, while an urban planning relevant resolution should yield around 100 m resolution at the building block level. And even if a RCM optimized for 100 m would be used – or a building resolving modeling approach (Schlünzen et al. 2003) – there is currently no capacity to compute big cities and time spans such as years at such a resolution.

The second problem covers the representation of the heterogeneous urban surface within the modeling system. Certainly, increasing computing capacities will bring along improvements within the RCMs for the meteorological processes and their resolution during the next decades. Unfortunately those advancements will not automatically improve the representation of the urban surface. The varying structure and material of the urban surface is quintessential to see effects like the UHI in a model. However, structure- and material-characteristics are strongly generalized in models and are often represented by only a single urban land use class (LUC, also used for land use classification). This results in an unrealistically homogenous and monolithic city model. There are already research projects in progress that aim to improve the urban land use and atmosphere data basis on a large scale, but they are not yet available for large regions or in an RCM-implemented operational state (Chen 2010, Ching 2009, ICDC 2012, JU03 2003, NUDAPT 2012, Sailor 2006).

In conclusion, while the resolution problem might be overcome by waiting for adequate computing capacity, an increased resolution does not introduce the missing LUCs.

This though can be solved by including new remotely sensed data sources on urban morphology and meteorology to generate new LUCs (nLUCs). This would also benefit an alternate approach to DD known as empirical statistical downscaling (SD). SD is not as demanding in computing capacity, but needs more measurement data to build upon. At best, the new measurement data improves SD and LUCs. Then ideally, they all work hand in hand as a hierarchical modeling chain: First a DD step embedding the nLUC is done to reach for example a resolution of 1 km (as a main topic of this research), followed up by a SD step to 100 m, building upon the DD output and also utilizing the nLUC data.

To derive morphology data such as building density or building height variance remote sensing data can be used by translating it into LUC characteristics such as albedo, heat capacity, or surface roughness. The data source should be ubiquitously available, because it is important to enable transfer, of models developed on data of a limited region, to greater regions. Hence, the developed urban model components based on data of Hamburg are transferable to other European cities. With some adjustment they should even serve very different cities with severe climate problems. This research, however, was embedded in the CliSAP cluster, area D4 urban systems, and focused on Hamburg, because of data availability, expert knowledge, and strategical reasons.

To give a summary, this research, utilizes new mobile measurement data on Hamburg, ubiquitously available remote sensing data to parameterize the urban heterogeneity, and a new LUC to implement dynamic urban surface data into a RCM. Although the parameterization of topographically determined processes is an emerging field in SD and DD (Böhner & Antonic 2008) refining climate model outputs for environmental modeling applications (Herzschuh et al. 2010), the parameter-definition from remotely sensed raster topographies in urban climate modeling is apparently new and not yet implemented often by the RCM modeling community. In this context, this research focuses on a number of questions:

- Are remotely sensed raster topographies suitable to parameterize the heterogeneous urban surface roughness and its influence on the surface wind field?
- How can the parameterization be linked to a new LUC – optimized on use in urban climate studies – to implement it into RCMs, enabling RCM scenario runs also including scenarios of urban development?
- Leads such a surface roughness parameterization to an added value in a RCM?
- Which systematic biases of RCM results compared to measurements can be identified in dependence to meteorology (especially circulation types) to develop SD methods?
- Can high resolution mobile measurements be suitable to enlarge the data basis needed for SD and are they suitable to evaluate RCMs? Which conceptual requirements are needed to make them suitable?

## 2 State of the art

### 2.1 Key characteristics of the UHI

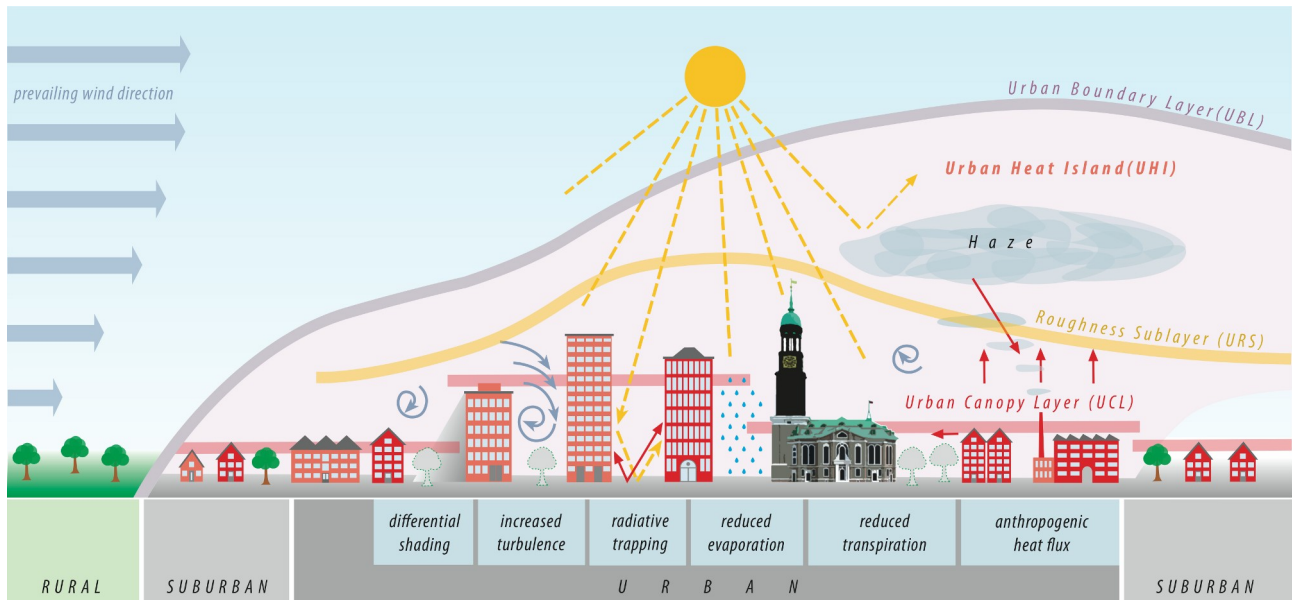


**Fig. 2.1.1** Climate processes in the urban boundary layer (UBL).

Morphology and climate interact due to different processes named in the figure and form an urban heat island (UHI) within the UBL. (Bechtel and Schmidt 2011, modified Oßenbrügge and Bechtel 2010)

The magnitude of the UHI is the most widely recognized indicator of urban climate modification in environmental sciences. It has been measured and reported at numerous sites around the world since the early 20<sup>th</sup> century (Stewart and Oke 2009:1). Where the UHI is the strongest, the most severe heat waves are potentially taking place. The UHI varies from city to city ranging from 0.6 to 12 K (Memon et al. 2010).

In general, the UHI is stronger at night than during day time and it is more pronounced in winter than in summer – at least for cities that do not heavily use air conditioning. Furthermore, the UHI signal decreases with increasing wind speed and cloud cover (Souch and Grimmond 2006). In this context, a warmer city would also increase energy and water consumption. Thus, its mitigation could achieve financial and environmental benefits (Memon et al. 2010). Memon et al. (2008) also point out that the wind is the perhaps most important natural factor influencing the UHI, while the perhaps most important man-made factor is the design of urban morphology. However, there is no agreement on the quantification of both factors yet (Memon et al. 2008).

Referring to urban morphology, the UHI's shape – as the urban climate in general – is formed by the distribution of LUCs. Urban LUCs are mostly characterized by increased turbulence, heat capacity, radiative trapping, sealing, surface runoff, reduced vegetation and latent heat flux (Fig. 2.1.1).

For instance, a densely built up inner-city with high buildings, a high degree of soil sealing, no evaporating vegetation, and huge anthropogenic heat emissions produce a large UHI, whereas a less dense center with buildings of same height, some parks, and wide streets as ventilation pathways creates a cooler micro climate. According to Souch and Grimmond (2006:271f) this result can be explained by the following effects: **First**, the geometry and materials of buildings and streets influence radiative fluxes. Shortwave radiation comes in and is reflected, depending on the albedo, and is scattered, depending on geometry and surface composition.

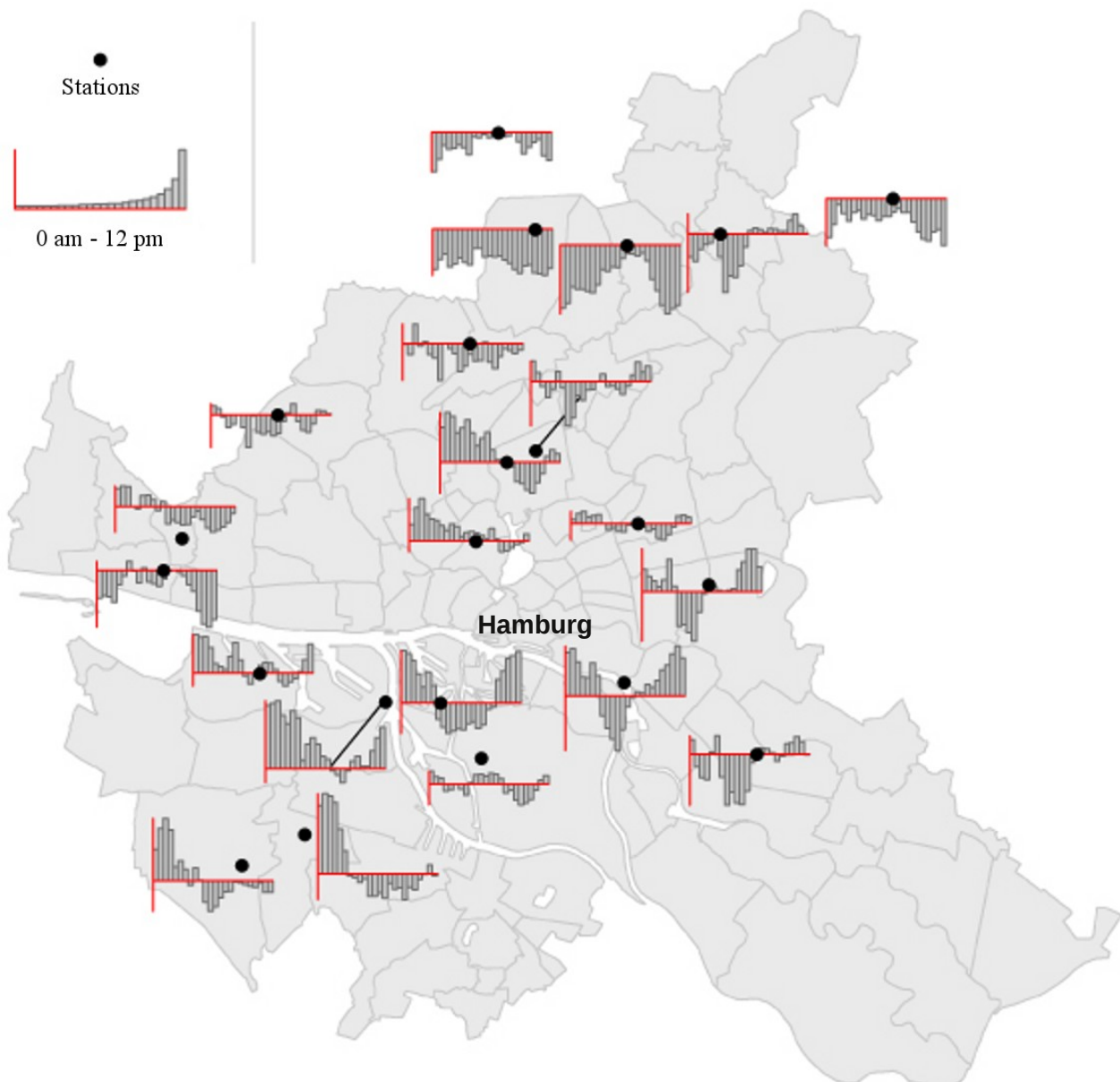


**Fig. 2.1.2** Relative diurnal temperatures of the climate stations from 10 July 2010.

The gray shapes show the districts of Hamburg. The MI-station (Appendix A) was used as the reference station to calculate the hourly mean differences shown here. The difference is high during the night and often negative during the day. Even if some planned stations were not yet installed in July 2010, the day was chosen for this visualization because it was the hottest in Hamburg during the last years (with a max. of 33.8 °C, mean of 3 to 4 p.m., airport DWD station Fuhlsbüttel). (Figure by C Daneke)

If absorbed and transformed to sensible heat, the incoming short waves are radiated back as long waves after some time, depending on the heat capacity of the material. Because the urban materials have a high heat capacity compared to the rural area materials, the heat stored during the day is released largely at night. This creates the even stronger nocturnal UHI (Fig. 2.1.2). **Second**, the latent heat flux has a cooling effect through evapotranspiration. At the same time increased humidity raises the human felt temperature.

Although important, radiative and latent heat fluxes are not addressed further in this research, due to the focus on the impact of wind and aerodynamic surface roughness on the UHI (Section 2.4).

## 2.2 Theoretical background of dynamical and statistical downscaling approaches

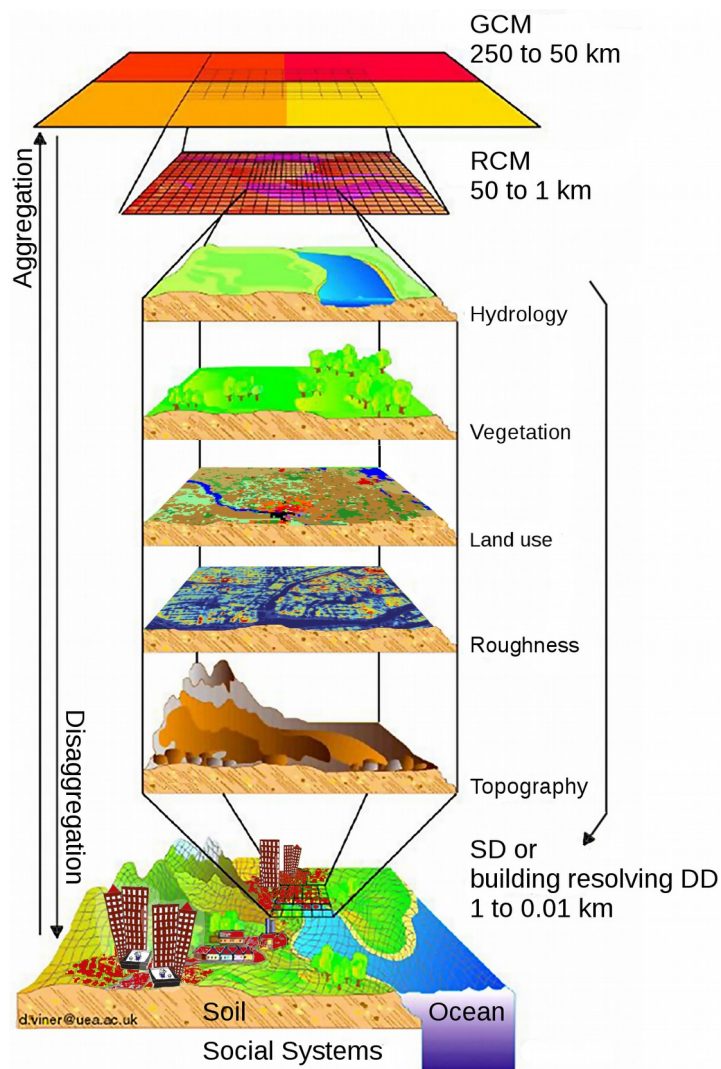


**Fig. 2.2.1** A general downscaling structure with exemplary resolution values and lower boundary layers. (modified CCCSN HP 2012)

For various reasons established approaches to model and project the urban climate using DD or SD are still restricted and far away from urban planning purposes. The RCMs urban canopy modules take the heterogeneous surface of cities into account by using an increased vertical resolution to resolve vertical urban energy and mass fluxes (Fig. 2.2.1). They are able to roughly show urban characteristics like the UHI. However, shortcomings remain. First, the parameterizations used in RCMs neglect some of the mentioned processes altering the urban climate. Second, they represent surface characteristics in a limited number of classes instead of "more fundamental descriptors" (Voogt and Oke 2003:370). Due to this reduction of complexity, the spatial variability of urban climates is systematically underestimated. Thirdly, RCM resolution is primarily limited by the scarcely available computing capacity.

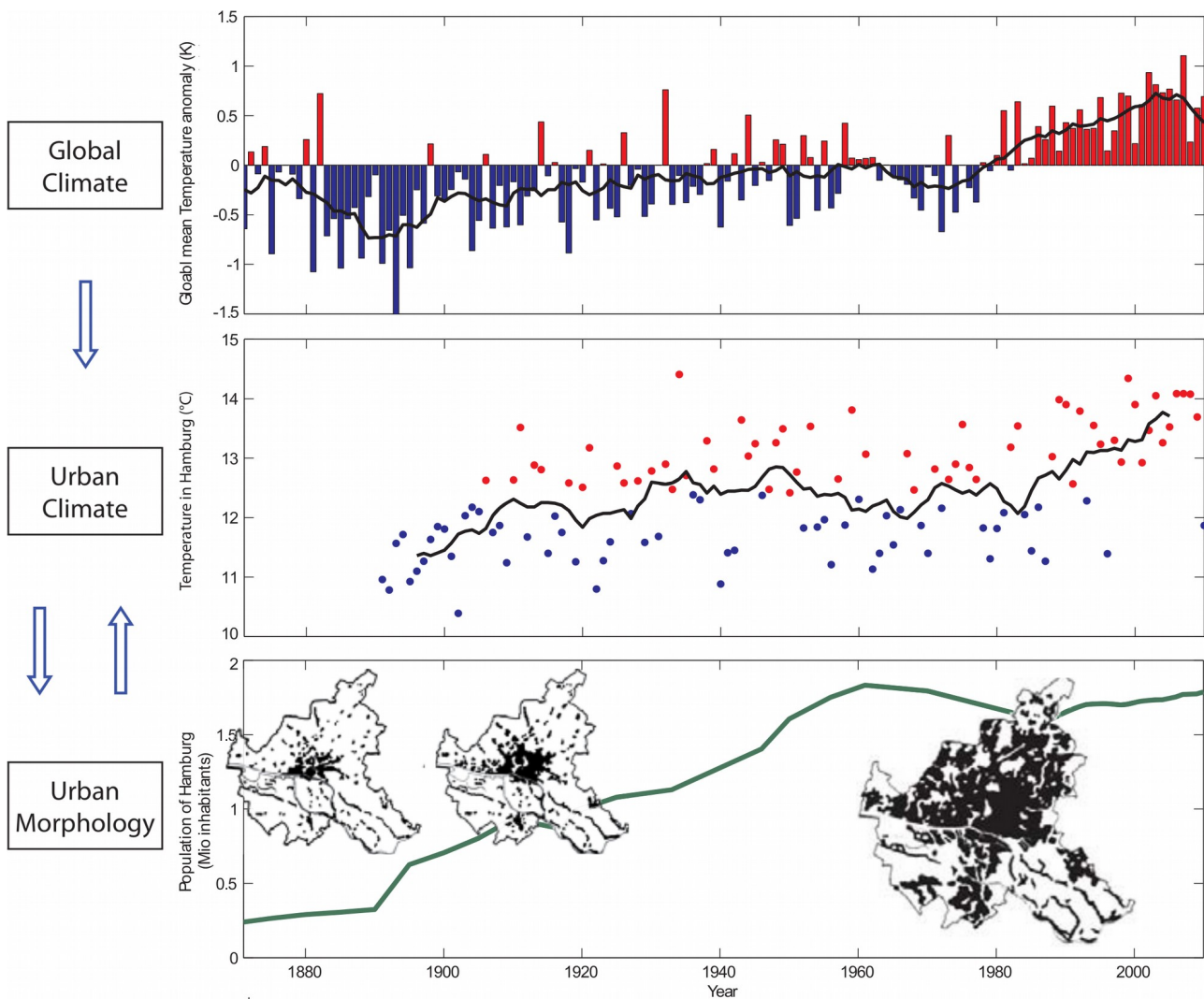


**Fig. 2.2.2** Changing global and urban climate in comparison to the city-growth.  
(modified Oßenbrügge et al. 2012)

Nowadays this resolution gap can be filled by SD. It is based on the analysis of empirical relationships between large-scale atmospheric driving parameters like pressure fields and local weather parameters such as the near-ground temperature (Wilby 2008).

For example, there are SD methods that involve linking observational station data to circulation type classifications. A circulation type is defined as a discrete atmospheric condition over a large area, for example Europe, which remains stable for some days and shares a synoptic similarity (Wilby 2008). Baur (1944) published the first calendar of the type classification of Grosswetterlagen (GWL) in Central Europe.

This classification was first extended by Hess and Brezowsky (1973) and more recently by Werner and Gerstengarbe (2010) who defined 29 objective GWL for Central Europe to describe the current weather. Those classifications can be derived subjectively via circulation classifications or objectively via a cluster analysis on the atmospheric fields like the one by Werner and Gerstengarbe (2010). An advantage of SD methods using circulation types is its applicability to different areas simultaneously, since the circulation type remains for decades for large regions. A limitation is that local weather parameter changes, produced by changes in the frequency of circulation types, could be inconsistent with the changes produced by the host GCM (Wilby et al. 2004).

A general advantage of SD methods is that they are computationally less demanding, enabling the evaluation of different UHI scenarios, emerging from different driving RCMs and multiple emission scenarios. A general shortcoming of SD is that the net effects of complex processes are aggregated in a single transfer function. Furthermore, the transfer function assumes the relationship between the driving forces and the climate to be static even for different climate and land use scenarios. This implies a static structure of the urban land use. However, urban land use is dynamic and changes occur on time scales which can be short compared to climate change (Fig. 2.2.2). Thus, it is partly misleading to analyze the interaction of a present city with a potential future climate of 2100, although this is still common procedure (Oßenbrügge et al. 2012) and has to be solved by including nLUC data of dynamic land use models (Chapter 4).

To give a summary of the section (2.2): The most promising possibility of improvement in filling the gap of spatial resolution, is seen in the combination of SD and DD. For the improvement of the surface layer new parameterization methods are needed such as the urban roughness parameterization approach described in Chapter 4. Further aspects such as advanced radiation schemes, improved layers of soil sealing, albedo, vegetation fraction, or heat storage have to be incorporated too. They are, however, not part of this research.

## 2.3 Urban land surface models and WRF

As so many factors influence the urban climate (Section 2.1), modeling a process like the UHI is complex. It demands a good spatiotemporal representation of morphological settings and surface-atmosphere interactions. Looking at available urban climate data, its resolution is too coarse. It is either represented by few measuring spots or by coarsely gridded data from numerical models, mostly RCMs with special urban LSMs. There are simple LSMs that represent the city as a concrete slab, or more detailed ones, also representing momentum and energy fluxes within the UBL (Grimmond et al. 2009). They model them based on this fundamental function:

$$Q_* + Q_F = Q_H + Q_E + Q_S$$

Those are the net wave radiation  $Q_*$ , anthropogenic heat flux  $Q_F$ , turbulent sensible heat flux  $Q_H$ , turbulent latent heat flux  $Q_E$ , and net heat storage flux  $Q_S$  (Grimmond et al. 2009).

Thirty-three urban LSMs implementing those fluxes (partly running independent from RCMs) were compared in "The International Urban Energy Balance Models Comparison Project" (Grimmond et al. 2009, 2010, 2011). The results of phase 1 (2010) and phase 2 (2011) show that every LSM has its own strengths and weaknesses and that the simpler models

"[...] often showed a net improvement with additional [surface] information [while] the more complex models did not. [...] But] it is expected that more complex models may have more potential for future improvements as they are able to resolve more details without deteriorating their performance." (Grimmond et al. 2011)

The observation, that simple models can perform just as well as the complex ones when utilizing additional surface information, confirms our choice of testing a simple (computationally cheap) LSM that is not particularly designed for the urban area. By integrating new urban surface descriptors, we aim to perform as well as urbanized LSMs. Due to former experience of our working group with the Weather Research and Forecasting model (WRF), this RCM was chosen in combination with its simple default 5-layer thermal diffusion LSM. For comparison, the urbanized LSMs available since WRF v3.1 (Chen et al. 2010) shall be introduced:

- the Noah LSM, including a bulk urban parameterization (Mitchell et al. 2005);
- the single layer urban canopy model (SLUCM), predicting surface skin temperatures and temperature profiles, both for roofs, walls, and roads (Chen et al. 2010);

- the multilayer urban canopy model (or BEP for building effect parameterization), additionally reproducing the effects of urban surfaces on momentum, turbulent kinetic energy, potential temperature, and radiation (Martilli et al. 2002, Martilli 2007);
- the outdoor exchange model (or BEM for building energy model), which is coupled with BEP to model effects on indoor temperature and moisture at different floors through diffusion of heat through walls, roofs, and floors, window and indoor radiation exchange, heat generation, and air conditioning (Martilli 2007);
- WRF coupling to microscale (~10 m) building-resolving models, e.g. Eulerian / semi-Lagrangian fluid solver (EULAG) or computational fluid dynamic (CFD) models; those can be coupled in real time through WRFs model coupling environment library (Chen et al. 2010).

As mentioned above, those urbanized LSMs, however, are computationally expensive. Thus, urban DD was performed with WRFs default LSM incorporating nLUC data.

An overview about WRF in general shall complete the picture: WRF is a mesoscale numerical weather prediction system and also a regional to global (experimental stage) climate model allowing simulations reflecting either real data or idealized configurations. WRF features a 4-dimensional variational (4DVAR) data assimilation system, and an open source software architecture, allowing for computational parallelism and system extensibility due to the modularity of its components (Fig. 2.3.1).

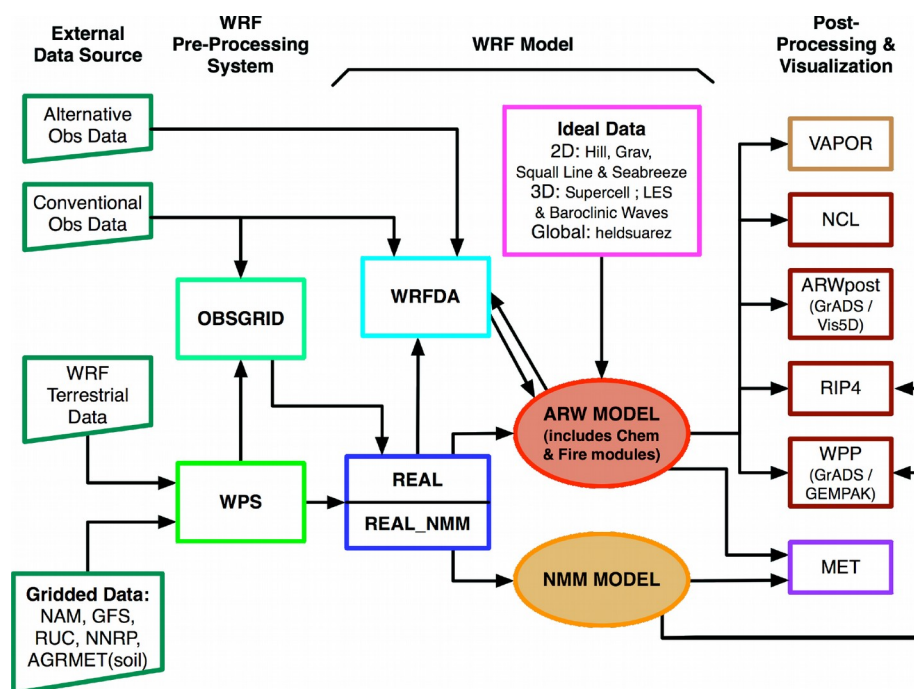


**Fig. 2.3.1** A scheme of the WRF modeling system.

It mainly consists of the WRF preprocessing system (WPS) and the physical core Advanced Research WRF (ARW). The NMM core is an alternative, used in operational weather forecast. (Wang et al. 2012)

WRF can be run with two dynamical cores, the Nonhydrostatic Mesoscale Model (NMM) and ARW<sup>1</sup>. ARW-only features are regional climate and seasonal time-scale research, coupled-chemistry applications, and global and idealized simulations - while both cores are suitable to do research on atmospheric physics/parameterizations, case-studies, real-time forecast systems, and data assimilation (Dudhia 2011).

<sup>1</sup> Both are freely available via the same source code package at <http://www.mmm.ucar.edu/wrf/src> for v2.0 up to v3.x for Linux and Unix only. Precompiled binaries are available for v3.x and x86 CPUs via Robert Rozumalski of the U.S. NWS at <http://strc.comet.ucar.edu/software/newrems>.

WRFs development is organized and promoted by NOAA consisting of NCEP and the Forecast Systems Laboratory, and also by the Air Force Weather Agency, the Naval Research Laboratory, the University of Oklahoma, the Federal Aviation Administration, and NCAR. WRFs advances in physics, numerics, and data assimilation are contributions by a broad and growing research community (WRF HP 2011). Details can be found in the user's guide by Wang et al. (2012) and in the technical physical documentation by Skamarock et al. (2008).

For longer climate simulations the better suited climate WRFs (CWRF and CLWRF) are available:

CWRF is available since 21 May 2012 (CWRF HP 2012), however, its improved surface descriptors are only available at 30 km resolution for the U.S. According to a personal communication by Xin-Zhong Liang, the main developer of CWRF, this is soon to be extended to China and Singapore, but "the automatic construction of surface boundary conditions for different resolutions and regions is still in development" (24 June 2012).

In contrast, CLWRF does not improve the crucial surface descriptors but adds some small advancements to the code base of WRF ARW v3.1.1. It is published and maintained by the Santander Meteorology Group (SMG) to "perform more flexible regional climate simulations by adding flexible GHG scenario usage and output of mean and extreme statistics of surface variables" (CLWRF HP 2012). The statistics feature is already backported to WRF ARW v3.3.1. The GHG feature was not of interest for this research, because only very long climate runs would benefit, while we did runs over two months.

## 2.4 Impact of wind and roughness on the UHI

The urban LSMs of WRF are able to capture urban climate characteristics to different degrees, but are demanding in terms of computing time and also need additional input data that is not delivered with WRF. Thus, we searched for a computing time neutral and not too input data intensive approach to fill the current gap of spatial resolution. As there are so many processes that shape the UHI, we aim to improve its modeling one by one. This research focuses on the impact of wind on the urban air temperature distribution.

The urban wind is highly variable in speed and direction because of the city's heterogeneous surface (Oke 1978, Bechtel and Langkamp et al. 2011). One speaks of the aerodynamic roughness of the city's surface. Buildings, cars, trees and other structures act as obstacles for the wind flow and in consequence "cities [are] the roughest of all aerodynamic boundaries" (Oke 1978:298). This results in an increased drag effect and enhanced turbulent momentum flux which alters the energy balance (Oke 1978). The drag slows down the mean wind, which decreases the transportation of heat out of the city and therefore intensifies the UHI (Oke 1978). The enhanced turbulent momentum flux, in contrast, results in increased maximum wind speed near outstanding buildings. Above a certain height, the flow is determined by the pattern and arrangement of obstacles rather than by single buildings, thereby creating a roughness of the surface. Over a homogenous surface the roughness binds the wind speed to a logarithmic profile (Oke 1978:115). Close to the ground within a heterogeneous morphology like the city, there is no regular flow. Nevertheless, for modeling purposes, it is necessary to idealize the turbulent behavior of the momentum flux. The most common idealization of the wind speed profile in the city is based on the power law equation (Davenport 1960). It provides reasonable fit to observed wind velocity profiles from the street canyons up to the lower planetary boundary layer (Counihan 1975), often accompanied by a vertical displacement height if the buildings stand very close.

The dependence of wind and morphology was structured into classes of effective aerodynamic roughness for real terrain types (Davenport et al. 2000, Wieringa et al. 2001). Davenport and Wieringa name eight roughness classes which are related to the aerodynamic roughness length of the surface (known as  $z_0$ , measured in m). They range from Sea (0.0002 m) over Rough (0.25 m) to Chaotic (2 m).

The aerodynamic roughness  $z_0$  is accompanied by the zero-plane displacement height  $z_d$ , the mean height of the momentum sink. When extra roughness elements such buildings are added to a flat surface the element density and  $z_0$  increase. But as  $z_0$  peaks further, elements begin to reduce the effective drag due to mutual sheltering. Thus, drag and  $z_0$  decrease, while the offset  $z_d$  increases. When  $z_0$  returns to its background value, elements are as close as a new surface. (Grimmond and Oke 1999)

The following further characteristics of the roughness should be noted in regard to this research:

First, Souch and Grimmond (2006:272) state that even small-scale features of the street architecture play an important role for the wind field. One example is the roof configuration that effects the vortex within street canyons. The scalar flux of the vortex varies by a factor of two or more with different geometries. This leads to the conclusion that a roughness data set suitable for urban climate modeling should either resolve such small elements or aggregate their effects through a parameterization at a lower resolution.<sup>2</sup>

Second, Gál and Unger (2009) and Wong et al. (2010) defined urban roughness mapping methods to detect ventilation paths of a city. These pathways play a significant role in the development of the UHI and result in reduction of air pollution. To detect them, the frontal area index of the buildings defined as  $\lambda_F$  was calculated. The index  $\lambda_F$  is the measure of buildings' walls facing the wind flow in a particular direction (frontal area per unit horizontal area). It has a strong relationship with the surface roughness and is related to the flow regime within urban street canyons (Burian et al. 2002). Based on the results of Gál and Unger (2009) and Wong et al. (2010), areas can be identified, where the city government should conserve the paths for a more comfortable urban climate. But their calculations are based on a 3D building data base. Such data is not easily available for many cities, especially less developed ones, which are often affected stronger by climate change impacts than more developed ones. Furthermore, these 3D data sets often consist of buildings only. This neglects the effect of trees and other obstacles on the wind<sup>3</sup>. (cf. Bechtel and Langkamp et al. 2011)

## 2.5 The importance of a land use classification optimized for urban climate studies

Instead of a spatially discrete isotropic island, the UHI appears as a scattered field of temperature variations. Yokobori and Ohta (2009:72) for instance recorded mobile vehicle temperature traverses and found that the intensity of the parent UHI is not mainly influenced by a monolithic parameter like the cities size, as argued by Oke (1987). In contrast they found a strong Intra-UHI (IUHI) with clear boundaries between different LUCs. Hart and Sailor (2007) developed a GIS based method for quantifying causes of the IUHI by combining mobile vehicle temperature traverses with a LUC. It turned out that for Portland the most important IUHI factor was canopy cover because of Portland's big forest park, while the warmest area of the city was found to be one of industrial land use. Due to the combination of the lack of vegetation and steady anthropogenic heat emissions it was even warmer than downtown. This illustrates the use of defining specific LUCs, that combine the characteristics from roughness over heat capacity and albedo to humidity, all in all optimally resulting in an unique urban climate per LUC (Section 4.2).

Different LUCs have been proposed and utilized in planning (cf. Bechtel and Langkamp et al. 2011). The most relevant in Germany is the *Klimatop* classification (VDI 1997). According to Baumüller et al. (2008) a *Klimatop* describes an area with similar microclimatic response. They differ within thermal diurnal variation and vertical roughness. Other discriminant factors are the topographic situation (exposition) and the land use like Industrial, Trade, City Core, Periphery or Garden Town (Baumüller et al. 2008). This is a simplifying and pragmatic approach, since it explains a large share of the urban climate response. The challenge for such classifications, however, is to neither have a too deterministic view nor a too detailed

<sup>2</sup> This research will make use of a 3 to 5 m resolving data set (Section 4.1) to approximate the urban roughness for use in lower resolving models.

<sup>3</sup> This research will use only ubiquitously available data also including all obstacles (Section 4.1).

differentiation to be both universal and manageable. A main shortcoming of the *Klimatop* classification is the qualitative description of the classes and the classification procedure, which requires substantial expert knowledge.

Further classifications include land use and vegetative cover (Auer 1978), urban terrain zones (Ellefsen 1991), the aerodynamic roughness classification (Davenport et al. 2000, Wieringa et al. 2001), and urban climate zones (Oke 2004). Those are more or less based on urban geometric features and building material properties. (cf. Bechtel and Langkamp et al. 2011)

Besides the detection and analysis of morphological characteristics that affect the IUHI, there remains an important problem in defining the paramount UHI in the first place. In UHI literature it is often roughly defined as the highest urban to rural temperature difference, with no definition of urban or rural. Regarding this inconsistent methodology in UHI measurement combined with a need for an easy assessment of exposures to heat wave risks, it would be beneficial to have LUCs of comparable climate response.

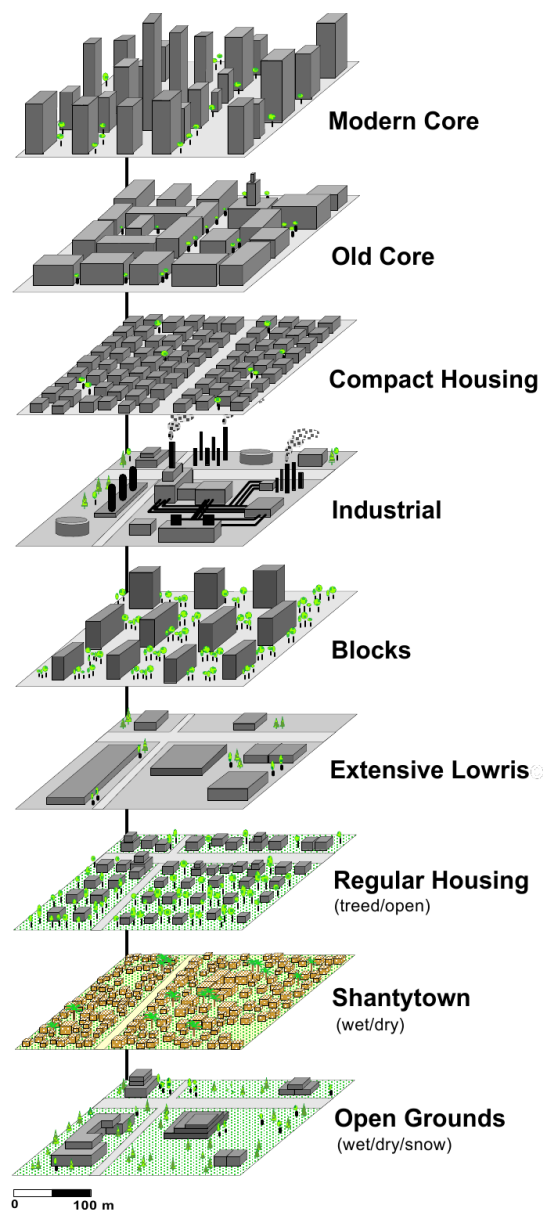


**Fig. 2.5.1** Local climate zones (LCZs) in the city series.

As this LUC is optimized for morphologies in the United States it had to be adapted for Hamburg, resulting in a new LUC (nLUC), see Section 4.2. (Stewart and Oke 2009)

In this regard, a more recent LUC, named local climate zones<sup>4</sup> (LCZs, Stewart and Oke 2009 and 2012), offers improvement. The LCZs integrate former classifications in a more consistent, objective and generic one. First, they divide in four classes: city, agricultural, natural and mixed. Second, they define subclasses on the microscale as shown for the city series in Fig. 2.5.1. The major benefit of the LCZs are that they are defined through qualitative descriptions and quantitative morphological and meteorological features like the aerodynamic roughness. This opens the opportunity for a semi-automated LUC; not fully automated, because the classification cannot represent every type of land use worldwide. Because the LCZs of Stewart and Oke (2009) refer to cities in the USA, Daneke, Bechtel, and Langkamp (2010) examined how the system can be evolved and transferred to European cities, what resulted in the new LUC (nLUC, Section 4.2).

Utilizing the fact that the original LCZs as the nLUC comprise  $z_0$ , we developed tools to derive roughness maps by combining the nLUC with remote sensing data. These roughness maps improve the accurate computation of urban winds and temperatures and thus benefit the detection of the IUHIs. This is of value for planning purposes similar to the identification of potential ventilation paths by Gál and Unger (2009). It also overcomes the disadvantage of needing 3D building data. 3D data is not that readily available and is expensive compared to most remotely sensed data. Its sparse availability may change in the future as large enterprises such as Google, Apple, Nokia, and Microsoft have started investing into their map services (Golem.de 2012). However, quality, price, and time of availability cannot be foreseen yet.

## 2.6 Urban roughness length parameterization

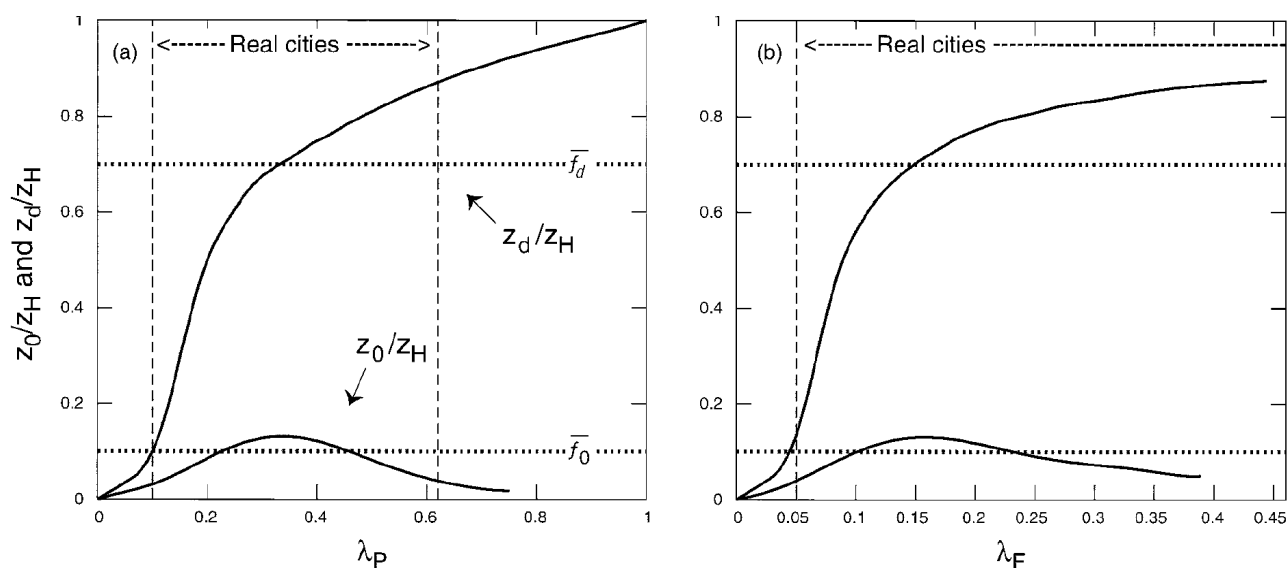


**Fig. 2.6.1** Conceptual relation between morphometric and roughness parameters.

$\lambda_P$  and  $\lambda_F$  are morphometric and  $z_0$  and  $z_d$  are roughness parameters. The dashed lines indicate the reasonable values for real cities; the dotted line represents the "rule of thumb", explained below. (Grimmond and Oke 1999:1263)

Before being able to link remote sensing data to the given roughness classes of the nLUC, a functional relation between both has to be found. Such a relation is known as a roughness length parameterization. To find it, detailed knowledge about the physical characteristics of the roughness and the already existing parameterization approaches is needed. Therefore Fig. 2.6.1 shows the idealized physical relation between morphology and  $z_0$  and  $z_d$  (Grimmond and Oke 1999). They depend on:

<sup>4</sup> In Stewart and Oke (2009) the name for LCZ was TCZ (thermal climate zones).

- packaging density of roughness elements ( $z_0$  peaks at intermediate density,  $z_d$  at max. density);
- variance of roughness elements height ( $z_0$  peaks at max. variance);
- element shape and street geometry in combination with the attack angle of the wind ( $z_0$  peaks with max. irregularity of geometry and shape);
- size and height of roughness elements ( $z_d$  peaks with max. height and size).

Building on the results of their GIS-based survey of urban forms, Grimmond and Oke (1999) deduced that roughness can directly be linked to surface morphometry (**morphometric measures**), or can be derived empirically from field observations and wind tunnel experiments (**empirical measures**).<sup>5</sup>

**Morphometric measures:** Grimmond and Oke (1999) compared 16 morphometric methods in a sensitivity analysis. The compared algorithms represent the relationship between aerodynamic parameters (like  $z_d$  and  $z_0$ ) and measurements of the city morphology. The methods differ in their respective combination of roughness attributes and weighting functions. They are divided into four sets based on (cf. Bechtel and Langkamp et al. 2011):

- the height of the roughness elements also known as "rule of thumb" (Raupach et al. 1991, Garratt 1992, Hanna and Chang 1992);
- height and plan areal fraction ( $\lambda_p$ ), also known as roof share (Kutzbach 1961, Kondo and Yamazawa 1986, Bottema 1995a);
- height and frontal area index ( $\lambda_f$ ), also known as wall share (Raupach 1992, 1994, 1995, Bottema 1997);
- further obstacle geometry parameters (Bottema 1995b, 1997).

**Empirical measures:** The micro-meteorological methods use anemometric wind tunnel data, or occasionally field observation data of wind or turbulence to derive aerodynamic parameters. Grimmond and Oke (1999) compared their morphometric roughness estimates with 74 anemometric observations, but only few have been considered to be acceptable, which vary widely in magnitude. This lack of suitable roughness measurements (Grimmond and Oke 1999, Chang and Huynh 2007, Bechtel and Langkamp et al. 2011) is partly related to the fluid-mechanical problem that the logarithmic wind profile can only be assumed after a longer fetch over a homogeneous surface. Furthermore, the instrumentation with tall towers or wind tunnel models is expensive and appropriate conditions may not occur for all wind directions during a field campaign.

**Morphometric measures** also have numerous shortcomings. The methods neglect the varying porosity of obstacles and the variance of obstacle heights, although "it is known, that inhomogeneity or patchiness of obstacle distribution generally increases formdrag" (Davenport et al. 2000). Additionally, methods based on  $\lambda_p$  completely neglect the orientation of obstacles, although, flow normal to the street axis causes greater roughness than parallel flow (cf. Bechtel and Langkamp et al. 2011). Furthermore, the geometry parameters are constructed on regular arrays of obstacles and therefore they are not well defined for irregular cities. Another problem is the available resolution: Due to the discretisation of  $\lambda_f$  (Ratti et al. 2006), the possible maximum slope in a grid depends on the quotient of obstacle height and grid cell spacing. Therefore, it has to be small compared to the obstacle height to properly represent walls. Also for  $\lambda_p$  pixels have to be classified as building or ground, which requires a high resolution. In addition, the processing of the geometry parameters is hardly standardized and depends on expensive 3D building data. According to "the need to account for trees in any morphometric assessment" (Grimmond and Oke 1999:1287) data on tree position, size, and geometry is also necessary. Eventually, the available methods rarely discuss the considered source area and therefore the parameters are extracted for areas of different size. Since the application of the logarithmic wind profile assumes homogeneous fetch conditions over certain distances and is only feasible above the blending height, it is physically unjustified to calculate roughness parameters for solitary building structures. Nevertheless, Gál and Unger (2009) tried to calculate roughness parameters for single building blocks and

<sup>5</sup> A further method suggested by Gál and Unger (2009) utilizes roughness classes and visual estimations of  $z_d$  and  $z_0$ . However, this method is not suitable for automation.

consequently derived  $z_0$  values of more than 10 m even for a small town. (cf. Bechtel and Langkamp et al. 2011)

To give a summary of the section (2.6): Grimmond and Oke (1999) stated that "none of the descriptors we used were able to capture fully the geometry appropriate for aerodynamic purposes" and that there can be no final statement of the "real-world significance of any differences between [the investigated] methods". Thus, the descriptors do not provide a standard against which to test the morphometric algorithms. Al-Jiboori and Fei (2005) confirmed this in a comparison of the morphometric method that was recommended by Grimmond and Oke (1999)<sup>6</sup>. Burian et al. (2004) also stated that analyzing wind measurements to determine  $z_0$  for a large number of an atmospheric model's grid cells, covering representative urban LUCs, is not practical, because **there are no adequate methods which "efficiently and accurately produce gridded coverage of roughness parameters"** (Burian et al. 2004:6).

Against this background, we propose a new method based on high resolution airborne Interferometric Synthetic Aperture Radar (IFSAR) data. The entire approach discussed in Chapter 4 is based on the assumption that instead of the individual geometry of a building, the determining factors for the aerodynamic roughness are the overall morphology, isotropy, and texture of all obstacles. Burian et al. (2004) already made an attempt to use Synthetic Aperture Radar (SAR) data and stressed the preliminary results to be promising and easy to handle. In view of future improved availability of high resolution SAR data, they assessed their results to be promising. Jeyachandran et al. (2008) also found SAR data in comparison to multispectral Landsat and InSAR (SRTM) data as the most promising data to capture the roughness characteristics best. (cf. Bechtel and Langkamp et al. 2011)

To give a summary of the whole chapter (2): The urban morphology has several important effects on urban climate and should be included in climate change assessments in more detail. The thermal conditions are mainly determined by a specific urban energy balance, altered wind fields, and turbulent exchange. For universal applicability we argued that features, that can be derived from highly available geodata should be preferred. IFSAR gives the chance to derive highly resolved, spatially extensive, and consistent information about the urban morphology and form at building block level, including all roughness elements.

Chapter 4 addresses our methods to estimate roughness parameters from IFSAR data. Before, the empirical data base used in this research is introduced in Chapter 3.

---

6 This method, namely Bottema (1995a) utilizing  $\lambda_p$ , was compared with slow and fast response anemometric wind measurements of a tower in Beijing.

# 3 Empirical data and methods

For the evaluation of the DD data – modeled with WRF and its nLUC layer – a vast amount of **air temperature measurements (T)** is needed. To collect a spatially denser coverage of climate observations than possible through collecting met station data (Section 3.1), we additionally carried out extensive mobile measurements (Section 3.1 and following), using city buses as "riding thermometers" (Buttstädt et al. 2011).

## 3.1 Mobile measurements complementing met station data

The met station data includes numerous parameters (T, RH, pressure, wind, air quality etc.) of which T was evaluated in this research. The data was collected for the metropolitan area of Hamburg (Fig. 4.2.1) from different sources. The temporal cover of the final selection, which was stored in a newly developed data base (Section 3.6), mainly comprises the period from 2009 til 2011 at different temporal resolutions (Appendix A, Table 7.1). About 20 of the 39 stations are situated within an urban environment (Fig. 3.1.1), and only half a dozen within the city center where the UHI is potentially the strongest (Fig. 3.2.2). Hence, a mobile measurement campaign covering the urban core was needed.

The campaign was carried out in cooperation with the local public transportation provider Hochbahn AG from 22 May till 29 October 2011. We measured T for the full period at a frequency of 5 s and relative humidity (RH) from 29 August 2011 till the end at a frequency of 10 s (it needed double the storage capacity). The GPS measured coordinates, speed, heading, and altitude every 20 m. Further details on the campaign are given in the following sections.

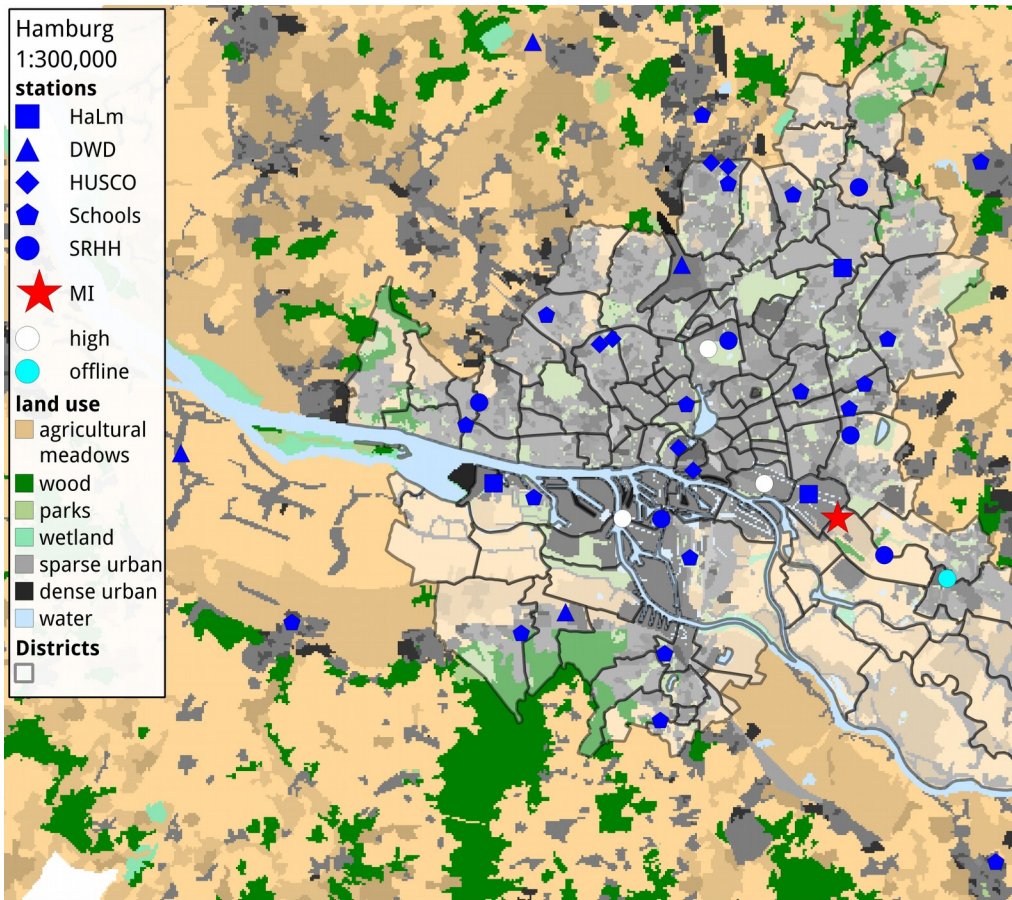


**Fig. 3.1.1** Locations and sources of the collected met station data. Boundaries are for Hamburg city districts laid over the nLUC (Daneke, Bechtel, and Langkamp 2010) at 100 m resolution. The coloration shall give a quick impression on how urban and natural land use is distributed in Hamburg. The darker the gray the denser the urban land use. For the detailed classification see Fig. 4.2.2. The legend names the station sources (Appendix A). Blue and red marked stations were used, white and light blue ones not. The white ones were placed on too high buildings, the light blue one was not operative in 2011.

### 3.2 Mobile measurement equipment



**Fig. 3.2.1** Qstarz BT-Q1000XT GPS logger (left) and Mobile Power Pack VT-PP-320b (right). Both were packed in a waterproof OtterBox 3000.



**Fig. 3.2.2** The instrumentation on the bus roof. The logger is glued on the OtterBox and could easily be turned up in order to read the data via USB cable.

First we considered the same logger than Buttstädt et al. (2011) of the company Onset (Table 3.2.1). In the end we equipped 15 buses with T and RH sensors of Driesen+Kern (DK), chosen because of their higher storing capacity and responsiveness to changes of the measurement variable<sup>7</sup> (Table 3.2.1, Section 3.5). The selection criteria for the equipment in detail were:

- storage capacity of at least 100.000 measurements ( $\approx 6$  d at 5 s logging frequency);
- high responsiveness to reach a spatial resolution around 100 m;
- waterproof and robust<sup>8</sup> against hot bus-roofs and possible branch or hail beats;
- accuracy of  $\pm 0.2$  K for T and  $\pm 2\%$  for RH.

The DK311 logger was combined with the CO325 temperature sensor, or the RFT325 humidity sensor<sup>9</sup>, and a radiation protection housing combined with a custom magnet holder (Westfalia Ltd. HP 2011). Flanked by the Qstarz BT-Q1000XT GPS logger (Variotek HP 2012a) and an external battery<sup>10</sup> (Variotek HP 2012b) they were packed in a waterproof OtterBox 3000 (OtterBox HP 2012). The instrumentation was mounted on the front roof (Fig. 3.2.2), where the thermal impact of the bus itself was minimal (Section 3.4).

<sup>7</sup> We tested the Onset against the DK logger beforehand, to not rely on the responsiveness information of the manufacturer alone. Both sensors measured at a frequency of 10 s over 6 sunny days. They were mounted at the same center position of the bus roof while it was driving different routes. The analysis showed up to 0.5 K lower and 1 K higher T peaks for the DK logger due to its higher responsiveness.

<sup>8</sup> The DK logger can be destroyed by trying to unscrew the sensor cable. If it is unscrewed with lateral force the inflexible contact to the board breaks, instantly recognizable by the loosened screw thread.

<sup>9</sup> We had to provide extra DK311 to log RH. They were custom builds, because we only needed a single channel logger (the normal RH logger DK325 has 2 channels). The RH measurements are not further discussed here.

<sup>10</sup> One needs at least twice as many batteries as loggers to charge one set during the week, while the other set is in use.

Manufacturer	Onset	Driesen+Kern
<b>Logger</b>	<b>HOBO Pro v2</b> ; models U23-001 with internal sensors, -002 with external sensors, -003 and -004 only with external T sensor	<b>DK311</b> Temp/HumiLog "rugged"
<b>Dimensions</b>	long cylindrical, D = 38 mm, H = 102 mm	flat cylindrical, D = 50 mm, H = 30 mm
<b>Battery lifetime</b>	3 years @ 1 min measurement frequency	120 days @ 5 s measurement frequency
<b>Storage capacity</b>	42,000 measurements	100,000 measurements
<b>operating range</b>	-40...+70 °C	-30...+70 °C
<b>Temperature sensor</b>	<b>U23-003 and -004</b> fixed cable with external sensor for T only	exchangeable cable <b>CO325</b> sensor and magnetic surface sensor <b>EUM325</b>
<b>Responsiveness</b>	50 s / 180 s at 63% / 90% registration of a temperature jump with ventilation of 5 m/s / 1 m/s	11 s / 50 s at 63% / 90% registration of a temperature jump without ventilation
<b>Accuracy</b>	max. $\pm 0.2$ K from 0 to 50 °C min. $\pm 0.18$ K from 0 to 30 °C	max. $\pm 0.2$ K from -40 to 50 °C min. $\pm 0.1$ K @ 0 °C
<b>operating range</b>	-40...+70 °C	-20...+80 °C -70...+250 °C with Teflon cable
<b>Humidity sensor</b>	<b>U23-002</b> fixed cable with external sensor for T and RH	<b>RFT325</b> exchangeable cable
<b>Responsiveness</b>	300 s at 90% registration of a temperature jump with ventilation of 1 m/s	16 s / 36 s at 63% / 90% registration of a temperature jump without ventilation
<b>Accuracy</b>	$\pm 2.5\%$ from 10% to 90% RH, max. $\pm 3.5\%$	$\pm 2\%$ from 10% to 90% RH, max. $\pm 4\%$
<b>operating range</b>	-40...+70 °C and 0...100% RH	-20...+80 °C and 0...100% RH -40...+120 °C with Teflon cable
<b>Price</b>	~ €200 (model U23-002)	~ €630 (2x DK311+ RFT325 + CO325)

**Table 3.2.1** Details on the evaluated loggers and sensors.  
(HOBO 2010, DK 2010, Buttstädt et al. 2011)

### 3.3 Logger offset

Even if the sensors are already calibrated, it is likely that they have a small offset from each other. To quantify the offset, preceding the measurement campaign, all 15 T and RH sensors were placed bound together in a cabinet for three days, in order to receive measurements from an almost identical point. The measured means were calculated over the same time period for each sensor. Therefore, the mean of all 15 means is the reference. The deviations from the reference temperature were high compared to the claimed accuracy of  $\pm 0.1$  to  $\pm 0.2$  K. For two T sensors it reached -0.29 and 0.27 K. It was low for all RH sensors with -0.90% and 0.47% compared to the accuracy of  $\pm 2\%$  (Table 3.2.1).

Sensor Number	T reference deviation [K]	RH reference deviation [%]
1	-0.07	-0.37
2	0.10	-0.04
3	0.27	0.33
4	0.01	0.29
5	-0.03	-0.05
6	0.03	0.31
7	0.00	-0.33
8	0.10	-0.07
9	-0.13	0.47
10	0.13	0.34
11	-0.12	-0.15
12	-0.29	0.00
13	-0.02	0.09
14	0.03	-0.90
15	-0.02	0.09
<b>Reference</b>	22.02	57.43
<b>Min</b>	<b>-0.29</b>	<b>-0.90</b>
<b>Max</b>	<b>0.27</b>	<b>0.47</b>
<b><math>\sigma</math></b>	0.13	0.35

**Table 3.3.1** Evaluation of the sensor offsets as their deviation of the measured mean of all sensors.

### 3.4 Lower speed boundary and logger position

The introduction of a lower speed boundary was needed because the roof temperature of the bus can significantly affect T at low travel velocities especially during sunny weather conditions (Fig. 3.4.6), especially because the T sensor was mounted only 15 cm above the roof. If the speed boundary is chosen too high, too much valid data is lost, whereas if the boundary is chosen too low, T can be distorted. The position was finally chosen based on a sensitivity analysis:

We detected significant T drops after bus stops upon reaching the speed of 12 km/h. This became especially apparent at the bus stop Altona (inner city setting, Fig. 3.6.3) where many buses park unshaded. When driving again T rapidly fell by more than 2 K within less than 1 minute, and reached a constant level within 0.5 to 1 minute. To automatically find all those cases, the speed at which T usually stopped falling was identified. Therefore, it was assumed that all temperature differences of more than 5 K between the bus measurements and the rural MI-station (Appendix A) were suspicious. All suspicious data was analyzed chronologically for the rapidly falling Ts. The speed boundary of 12 km/h proved suitable given that only one case was left above this speed boundary. Compared to the HOBO logger employed by Buttstädt et al. (2011) who identified 18 km/h, the lower threshold stresses the higher responsiveness of the DK logger.

To further minimize potential thermal influence of the bus roof – regardless of driving speed – we additionally identified the least thermally influenced of three different roof positions with the help of the DK EUM325 (Table 3.2.1) surface temperature (ST) sensor in a pre-evaluation campaign. See Fig. 3.4.4 and following for the raw data<sup>11</sup> and Fig. 3.4.1 for the aggregated data.

<sup>11</sup> The buses measured at a frequency of 5 s, the raw data, however, is displayed at a frequency of 150 s. For bus 2 and 3 speed measurements are available for the first two days only due to problems with the external GPS batteries.

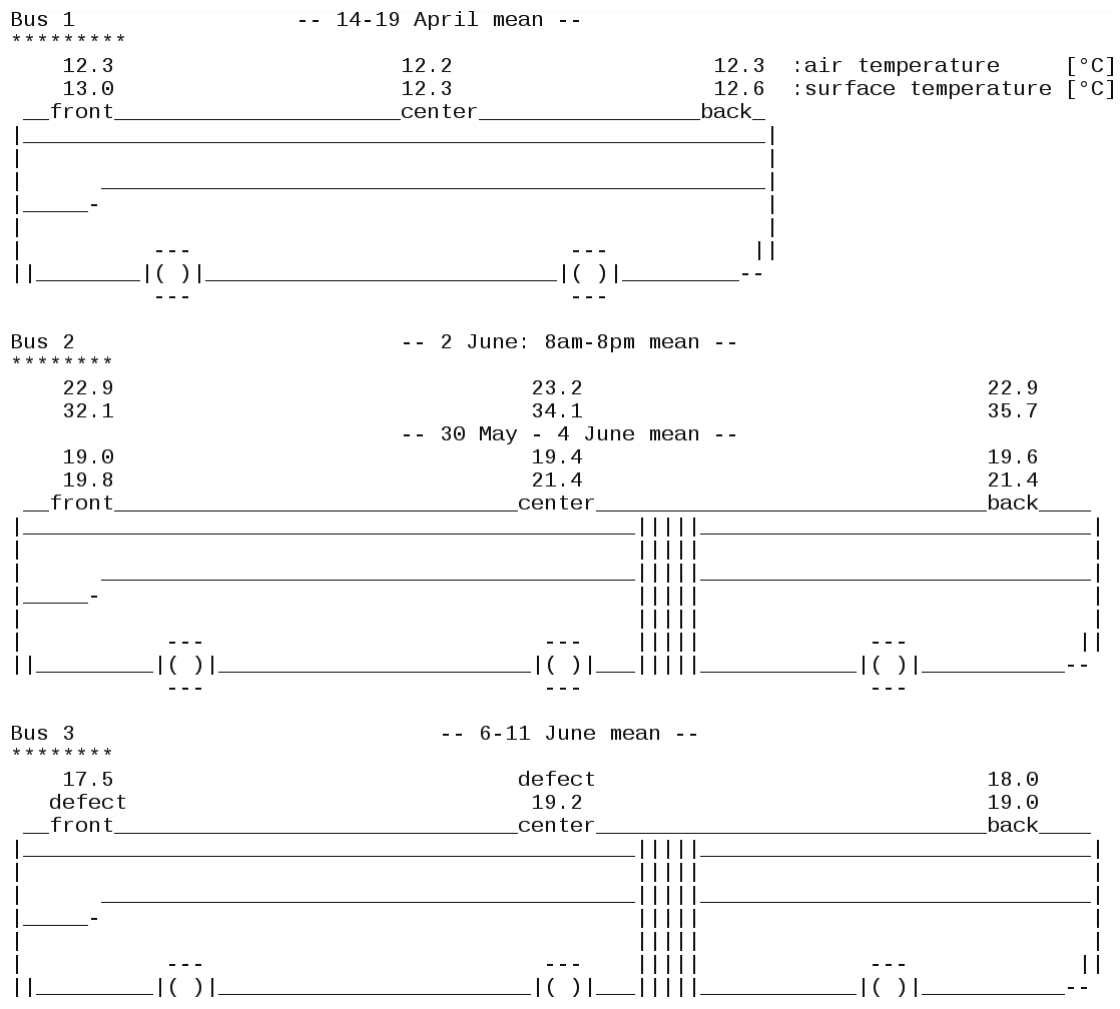


**Fig. 3.4.1** Offset-corrected means of T and ST measurements regardless of driving speed.

This pre-evaluation campaign started with a shorter bus type (bus 1). Despite a higher front and back ST for **bus 1**, T was not significantly affected. **Bus 2** had lower front T, raising towards the back in correspondence with the ST. **Bus 3** had two defective loggers, but generally showed the same characteristics as bus 2. For bus 2 an additional mean was calculated over 12 h while the bus was traveling during a particularly sunny day. Despite high ST differences (2 K) between the three position, T showed no corresponding heat up from front to back (see also Fig. 3.4.6). All those results do not change significantly if only data at a boundary speed of 12 km/h is used to calculate the means.

In general, the measurements reveal low T variations quite independent from the roof position. To better explain the ST distribution on the roofs, we took pictures of the logger positions (Fig. 3.4.2 and 3.4.3) that show that the albedo affects the ST. For almost all buses the center and back positions were more polluted than the front and included the black joint lamella (center) and a black hatch (back). This shows that the ST pattern is in correspondence with the albedo<sup>12</sup>. Given that only the longer bus type was available for the final campaign, which typically had a clean front, we decided to place the instrumentation there.

<sup>12</sup> Another factor influencing ST is the heat capacity for different roof parts. This could be observed during some nights (no albedo effect possible), when ST offsets between different positions got bigger (see following raw data).



**Fig. 3.4.2** Roof pictures of **bus 2** from front to back. The center position shows black dirt and dark elastic lamella, both lowering the albedo. The back position has a black emergency exit hatch.



**Fig. 3.4.3** Roof pictures of **bus 3** from front to back. The same as in Fig. 3.4.2, but with a partly gray hatch at the front. This was painted white on most other buses.

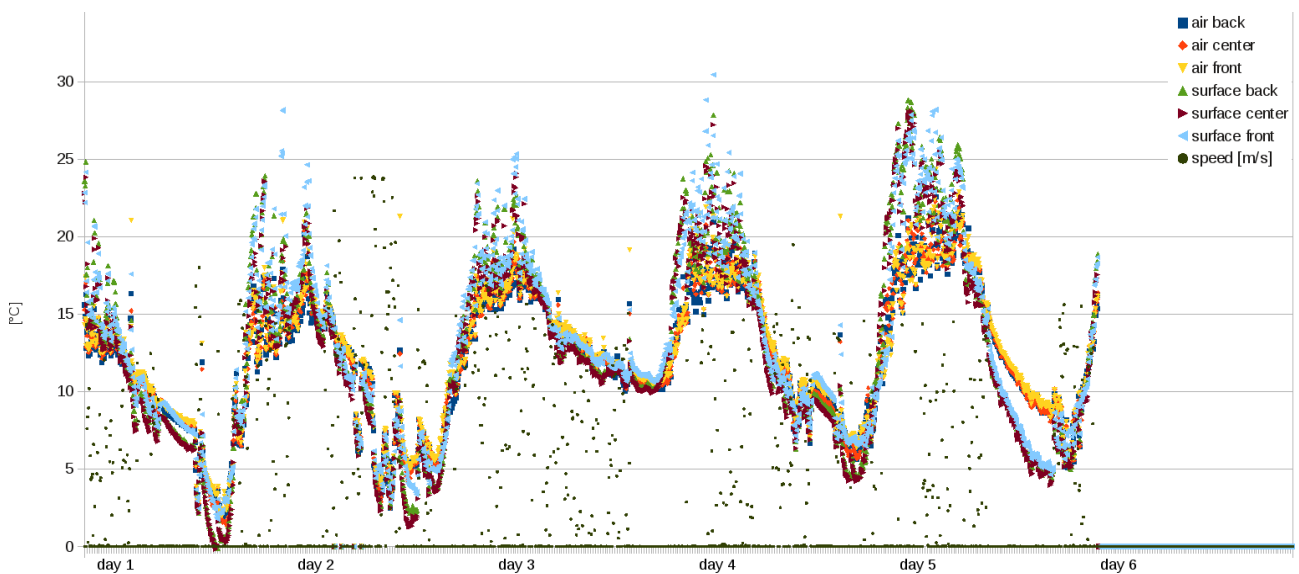


**Fig. 3.4.4** The temperature and speed measurements from **bus 1**. T follows ST with a delay and a offset that gets bigger when the bus stops. Missing ventilation leads to a slower cooling of the T sensors during night (between day 5 and 6). Generally T is lower than ST during day vice versa during night. The front ST often has a bigger offset to the center and back ST during night, indicating a different heat capacity of different roof parts (same for bus 2, Fig. 3.4.5).

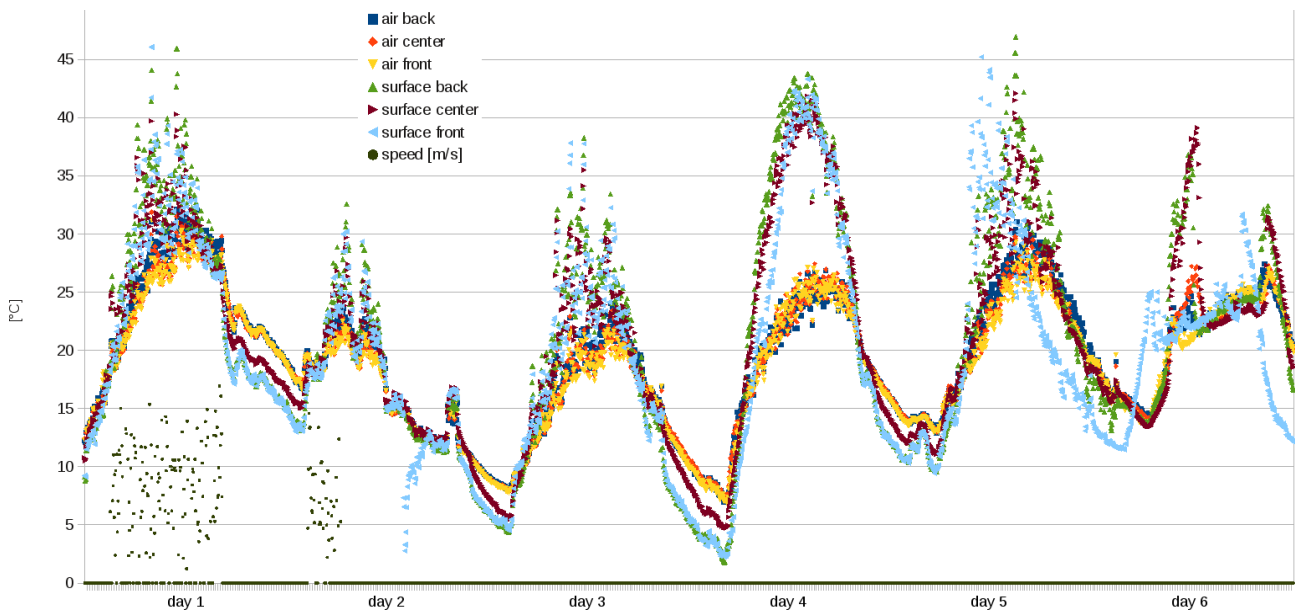


**Fig. 3.4.5** The measurements from **bus 2**.

During day, especially day 4 (2 June 2011), there is a huge offset between T and ST, which is explained in Fig. 3.4.6. Day 2 shows a front ST drop, induced by a storm, when a hailstone landed onto the sensor. Those measurements were discarded before calculating the means in Fig. 3.4.1.

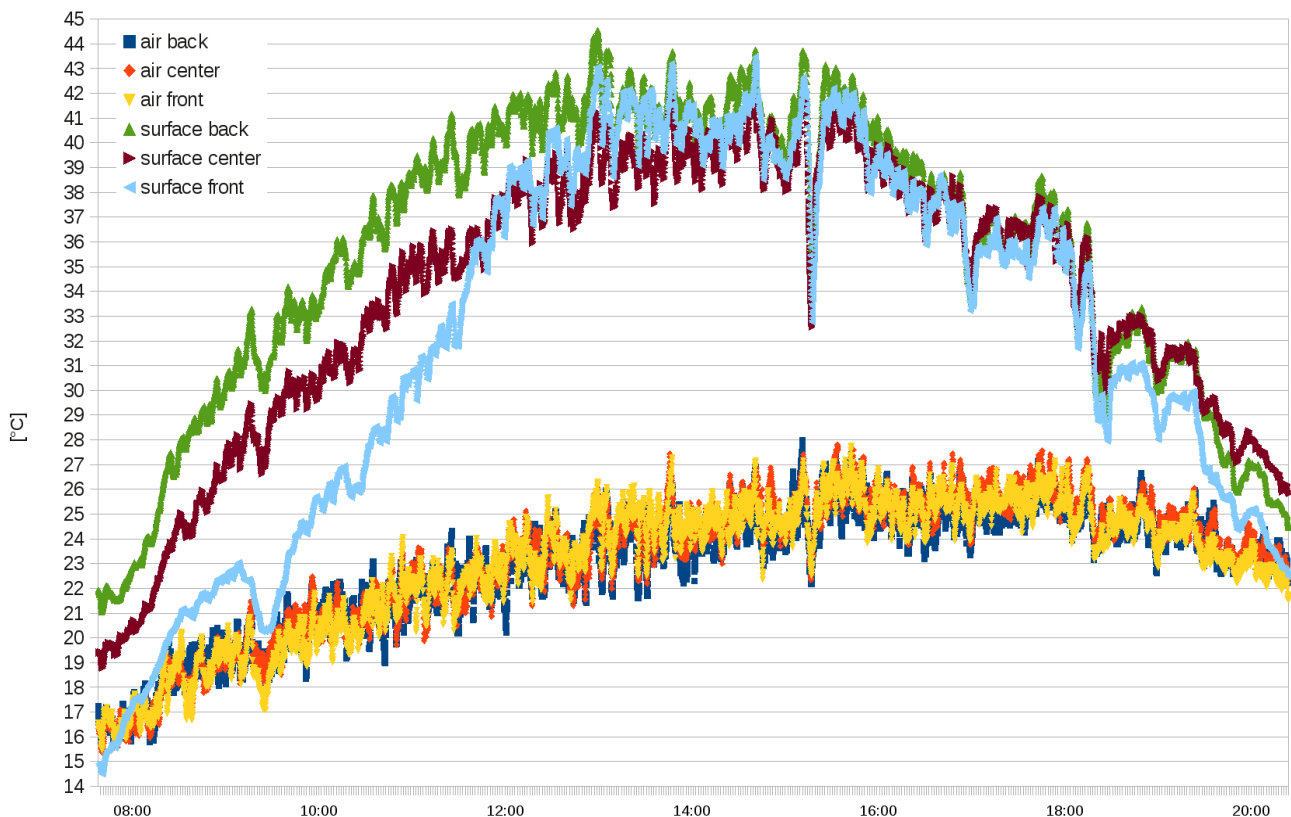


**Fig. 3.4.6** The measurements from **bus 2**, **day 4**, at 5 s frequency.

This 2 June 2011 shows a huge offset between T and ST. It was a particularly sunny day with up to 22.8 °C in the city center (4:00 p.m., 1 h mean of school station Altstadt), while the bus T goes up to 25.7 °C (4:00 p.m., 1 h mean of center roof position). The difference of 2.9 K has to be attributed to higher T in the street than at the station. This is because the front ST is much lower than the other STs from 8 to 11 a.m., whereas the front T is not lower than the other Ts, showing that ST has almost no effect on T. This implies that the bus measurements of warmer conditions in the street are real.

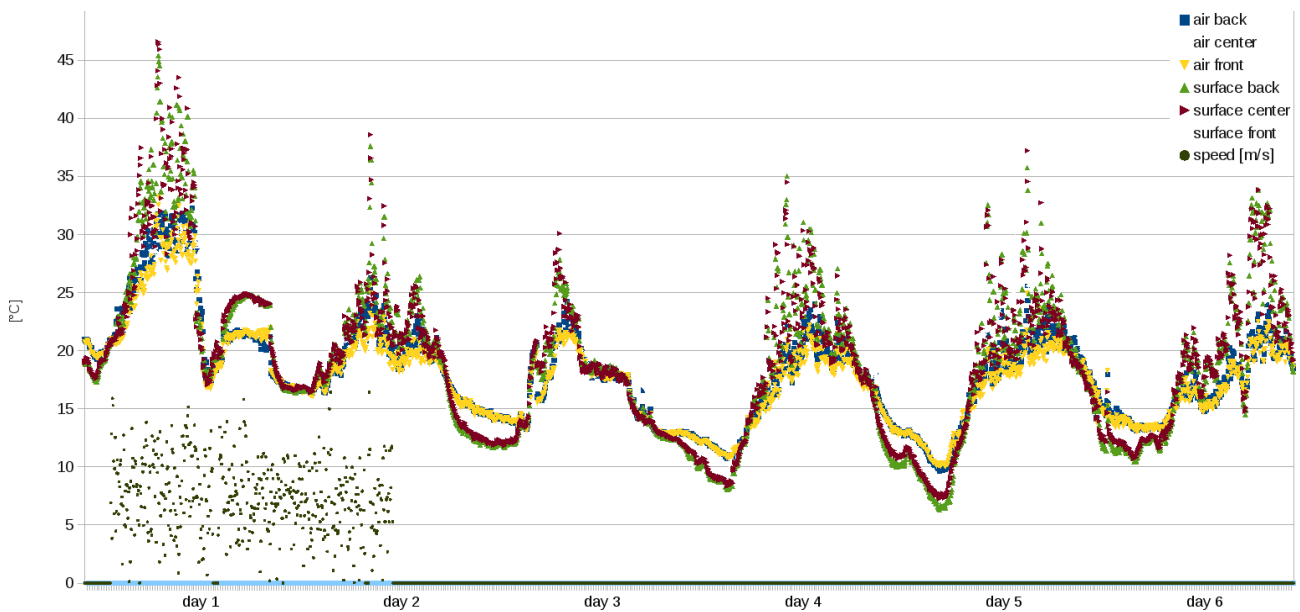


**Fig. 3.4.7** The measurements from **bus 3**.

Two loggers were defective, but in the overall picture it is the same as for bus 2. One difference is the offset between center and back ST, that is smaller. Another one is a T and ST drop during day 1 (5 p.m., 6 June 2011) due to a thunderstorm.

To give a summary of this section (3.4): Already the T means on these three different positions (Fig. 3.4.1) indicated that T is not relevantly influenced by ST. The raw data of bus 2 showed additional insights. Despite a huge offset between T and ST while the bus was driving<sup>13</sup>, T did not differ much at the three positions while ST clearly did. Thus, the impact of ST on T is negligible at a sufficient speed that we could specify to 12 km/h. Additionally, we evaluated the front as the best logger position regardless of driving speed (considering albedo, heat capacity, and T and ST measurements).

### 3.5 Measurement resolution, bias, and representativeness

To specify the maximum spatial resolution of the T sensor, as the minimum distance between the evaluation points along the bus routes, the logger's responsiveness to changing T needs to be ascertained (Buttstädt et al. 2011). This is especially important on the fast moving buses (usually up to 80 km/h; Fig. 3.5.1).

According to Liljequist and Cehak (1984), the adaption time of T sensors is described by a coefficient of thermal inertia. This is the time necessary to cover 63% of a T difference. Driesen+Kern give a time of 11 s for the 63% range for the non-ventilated logger. Thus, the ventilated loggers on the bus roofs will cover 63% even faster. However, the sensor's resolution is calculated based on the 11 s as the coefficient of thermal inertia. At the minimal driving speed to be evaluated (12 km/h) a distance of 36.7 m can be driven in 11 s. This represents the minimal resolution of the sensor at this speed. The real resolution will be higher due to ventilation. At increased travel speeds, say 50 km/h, which is the maximum speed allowed within the city, the bus travels 152.8 m, which exceeds the intended 100 m resolution. However, looking at Fig. 3.5.2, 48% of the driven speeds result in a minimal – non-ventilated – resolution of 100 m and 90% result in 140 m. All evaluated data was measured under ventilated conditions, thus, the resolution reached 100 m most times. (cf. Buttstädt et al. 2011)

<sup>13</sup> Despite the missing GPS data the bus is definitely moving, seen at the regular fluctuations. The figures before show linear measurements during night, when the bus was not moving.

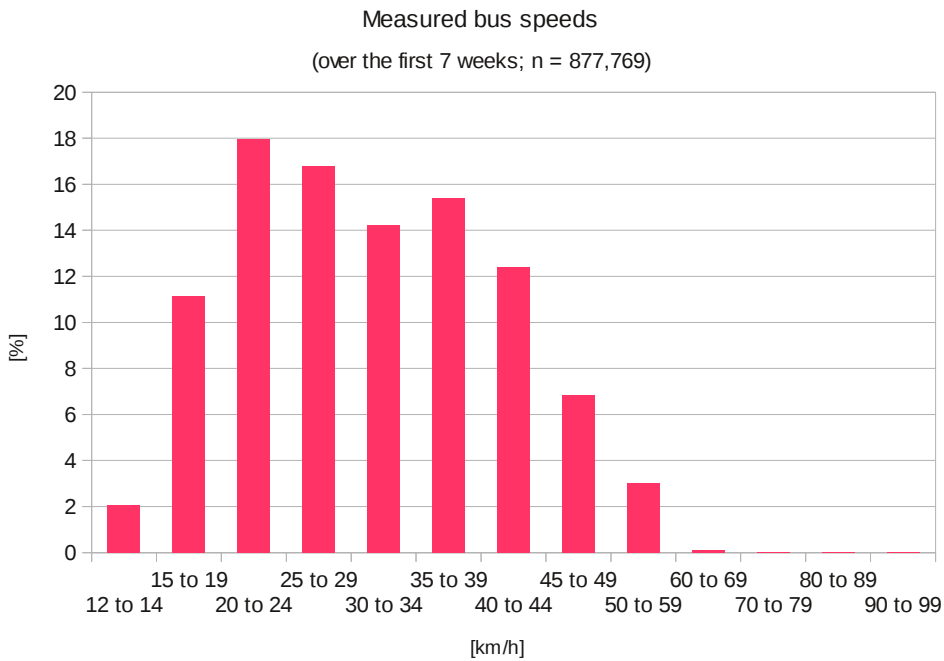


**Fig. 3.5.1** The classified bus driving speeds of the 15 buses' raw data. The first seven weeks of the campaign were classified. The GPS measured every 20 m and speeds below 12 km/h were discarded, see Section 3.4.

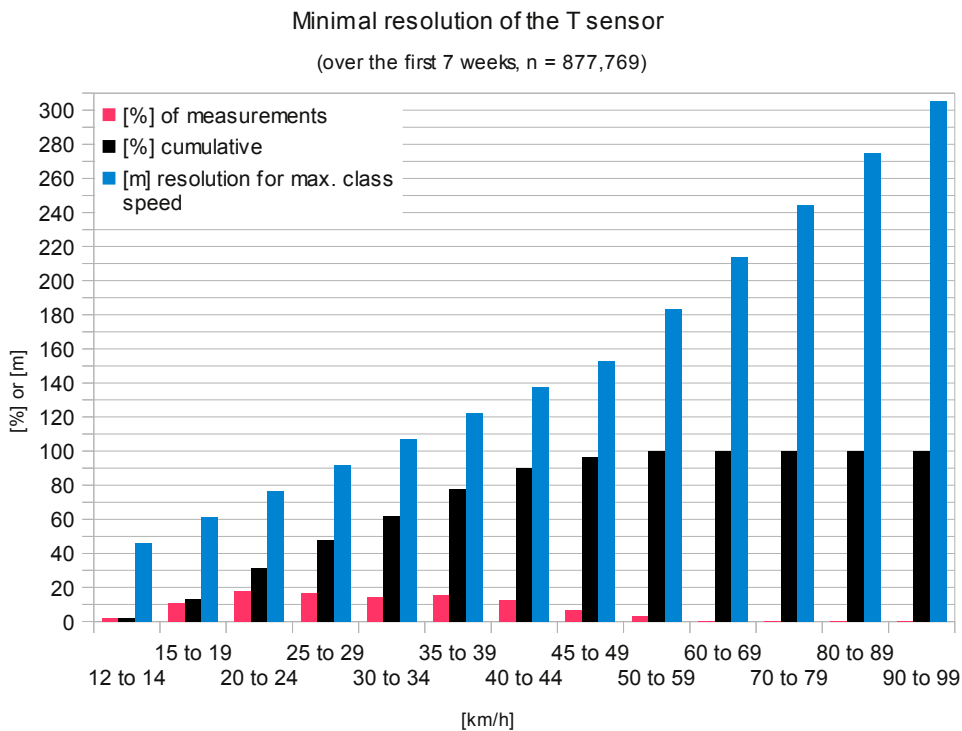


**Fig. 3.5.2** The minimal resolution of the T sensor based on driving speed. Classified bus speeds from the raw data as in Fig. 3.5.1 with additional cumulative values. The resolution is the potential minimum (non-ventilated) for each class. The real blue curve would be flatter with increased speeds.

Taking the T measurements from the bus traveling above 12 km/h, 90% of all T changes were smaller than 0.02 K/s. Thus, 90% of all T measurements are expected to register a T change of less than  $0.02 \text{ K/s} \cdot 11 \text{ s} = 0.22 \text{ K}$ . Due to thermal inertia, 0.22 K represent 63% of the real T change. Thus, 100% result in a real change of 0.35 K. The difference between measured (0.22 K) and real change (0.35 K) results in an acceptable bias of 0.13 K. This is acceptable as it is in range within the sensors' accuracy of  $\pm 0.1$  to  $\pm 0.2 \text{ K}$  (Table 7.1). For comparison the HOBO logger (model U23-003, Table 3.2.1) has a bias of 0.29 K and a resolution of 250 m at a bus speed of 5 m/s. (cf. Buttstädt et al. 2011)

Beside the logger resolution, we also discussed the spatial representativeness of the measurements. Due to the traffic producing constant turbulence the mobile measurement can not be regarded as a point measurement. To confirm that 100 m is a reasonable resolution for the measurements in this regard, a wind tunnel experiment quantifying the aerodynamics of a bus model would have been beneficial, but is not part of this research.

### 3.6 Measurement yield and data aggregation

The bus type used in the final campaign is the so called Metro Bus with one joint. Metro Buses – in contrast to Regio Buses – usually drive long routes through the city centers and are served at least every 10 min. Only special night buses operate in Hamburg during night. Hence, measurements at night and on weekends were rare, while most measurements were taken on Mondays and between 6 and 8 a.m. (Fig. 3.6.1).

We chose the bus depot Mesterkamp (one of five depots) because its lines (6, 7, 8, 20, and 25<sup>14</sup>) were judged to have the best spatial cover of different urban LUCs (Fig. 3.6.3). The logistics<sup>15</sup> at the depot were negotiated with dedicated middleman, Mr. Thomas Blümel, of the vehicle workshop FFG<sup>16</sup>. Altogether the produced maximum amount of data could have been 45 million T and RH measurements. The yield, however, was 56% (25.3 million) due to missing buses<sup>17</sup>, further reduced to 20 million measurements because of GPS and battery failures<sup>18</sup>. Still, this amount of T and RH measurements at different locations and times, flanked by even more GPS data for coordinates, speed, height, and heading had to be further aggregated to be handled:

First, the GPS data was merged with the climatological data. Therefore, the T (RH) measurements were linearly interpolated from a frequency of 5 s (10 s) to 1 s to pair them with the irregular GPS timestamp. This, and other data operations (12 km/h cut off, offset correction) were done with R-script and Python (Appendix B and C). Then the data was averaged temporally to 1 min and spatially to about 100 m (matching the nLUC resolution) with SAGA GIS (Appendix D), resulting in 1.6 million rows, still gathering the informational content needed for our purpose.

The spatial extent of the virtual 100 m station network was larger than expected beforehand (Fig. 3.6.3). However, when narrowing the set of virtual stations temporarily to those with at least 10, 100, and 1000 measurements, the covered area shrinks, not covering as many nLUCs as anticipated anymore. For at least 1000 measurements (Fig. 3.6.4 bottom right) only the routes of the bus lines 6, 20, and 25 are left. With their high temporal cover, their data complements the stationary network (Fig. 3.2.2) well for the inner city.

14 Lines 4 and 5 – at another depot – are very long and extend from the outer to the inner city, crossing many different land use types. However, it was not feasible to operate at two depots.

15 With the support of two student assistants, the maintenance work at the buses (emptying loggers, replacing batteries) was done every Sunday, when the buses were usually in the depot.

16 The Fahrzeugwerkstätten Falkenried GmbH is a subsidiary of the bus provider Hochbahn AG.

17 Special "shopping weekends" or other events resulted in a data loss, because the loggers could not be emptied.

18 The battery life time depends on how much a bus was driving, because the GPS goes to standby if the bus is not operating (integrated vibration sensor). The white model of the Variotek battery, however, goes to standby if the GPS goes to standby. Be sure to get batteries without a standby function like the black model.

To combine the processed bus measurements with the met station observations and to further discard unreasonable measurements<sup>19</sup> a DB management system (DBMS) was implemented, supporting the management of various data formats and constraints (Appendix E), easing data consistency. Fig. 3.6.2 displays the DB design<sup>20</sup> for the station data. The bus measurements were transferred to a similar but separate DB due to their different structure.

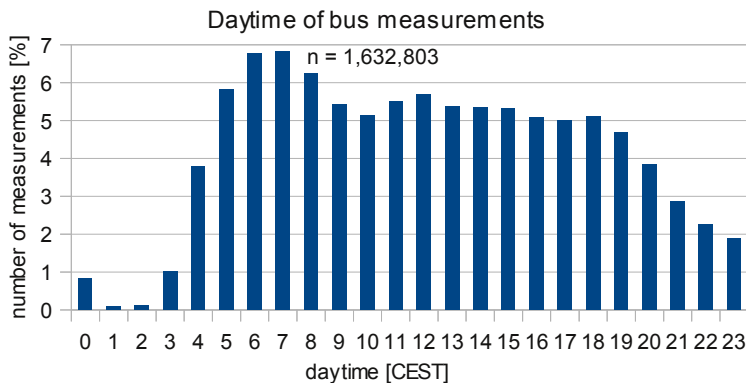


**Fig. 3.6.1** Daytimes when the buses were traveling of the whole campaign. The graph is based on the final edited data set.

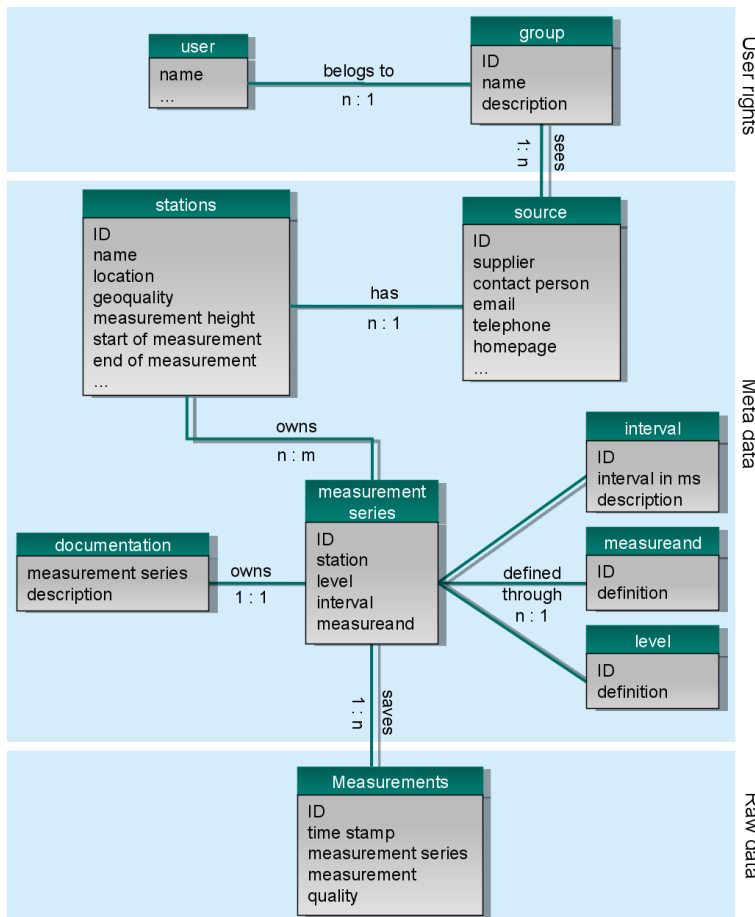


**Fig. 3.6.2** The database design for the climatological stations. (Fig. by C Daneke)

19 Measurements discarded: > 50 °C, > 95 km/h, < -2 m, > 105 m (found with 1 m vertically resolved DEM), location depot Mesterkamp (heaters in the maintenance hall)

20 The DB was developed by our urban climates working group, but mainly by C Daneke. The documentation (also of unused data and SQL scripts etc.) can be found on the server Pulaski. It was purchased exclusively for this purpose and can be accessed from within the ZMAW network and the network of the Institute of Geography: klimadb@pulaski.zmaw.de://scratch/local1/klimadb/FILESERVER\_klimadaten/README.txt

If others wish access, we would be delighted to arrange it. Contact [langkamp@tomblog.de](mailto:langkamp@tomblog.de)

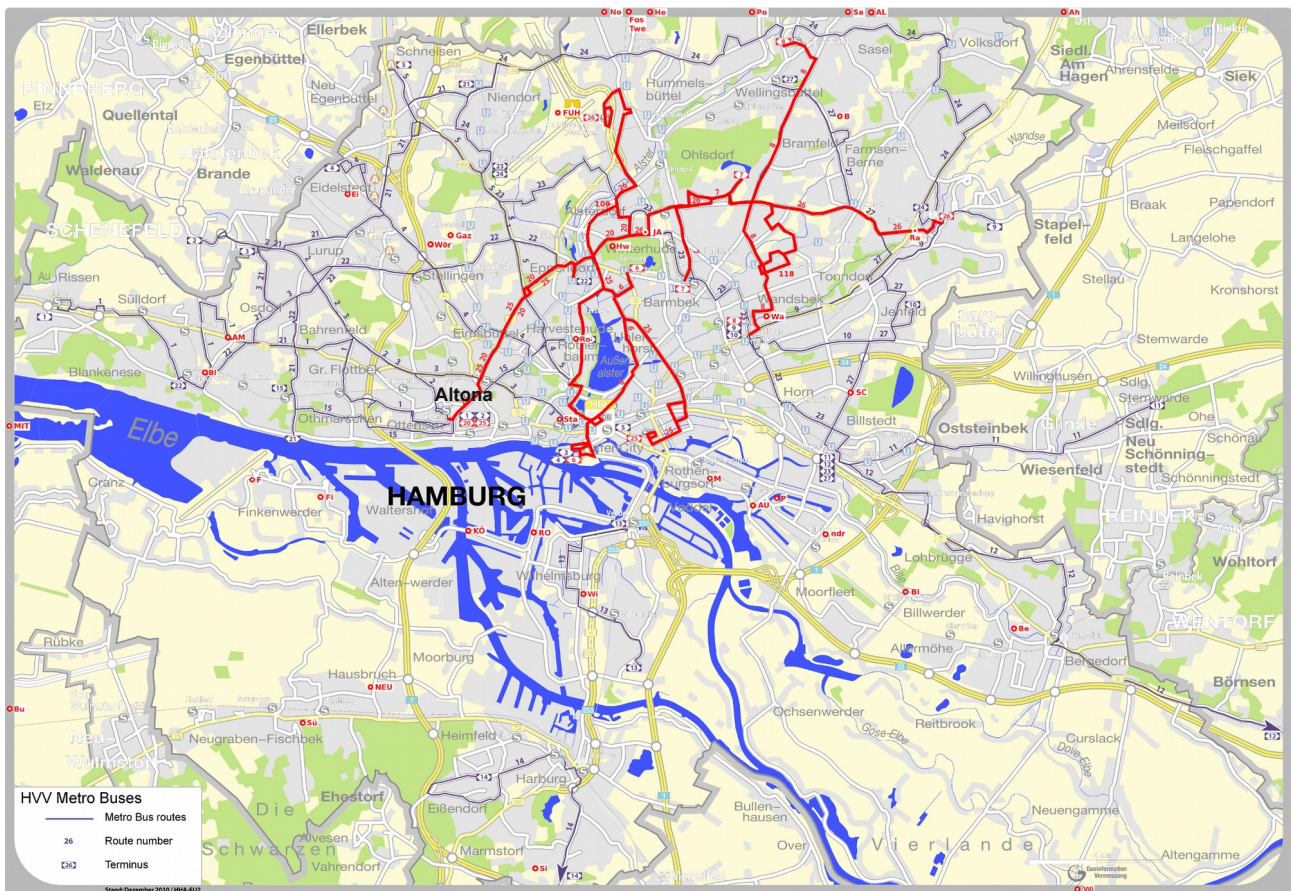


**Fig. 3.6.3** Bus routes map with the usually operated lines of depot Mesterkamp (red).

All other lines of the bus traffic service (Hamburger Verkehrs-Verein, HVV) are shown in purple. The map was created to evaluate the line coverage before the campaign. The lines cross many land use classes like the old city core of Altona in the southwest center (lines 20, 25), the airport in the north (line 26), the modern core with the new HafenCity in the south center (line 6), two routes along the lake Alster (lines 6, 109), big parks like the Winterhuder Stadtpark (lines 20, 26), or the Ohlsdorfer Cemetery (lines 7, 8), and outer residential areas in the east (lines 8, 26, 118). However, since the buses drive other lines as needed, there was no way to exactly predict the spatial cover. Additionally shown (red-white dots) are the positions of the stationary measurements that were collected at that time. For the final collection of stationary measurements see Fig. 3.1.1 and Table 7.1. Some of them are located beyond the map area and are drawn on the edge. (Base map from HVV 2010)

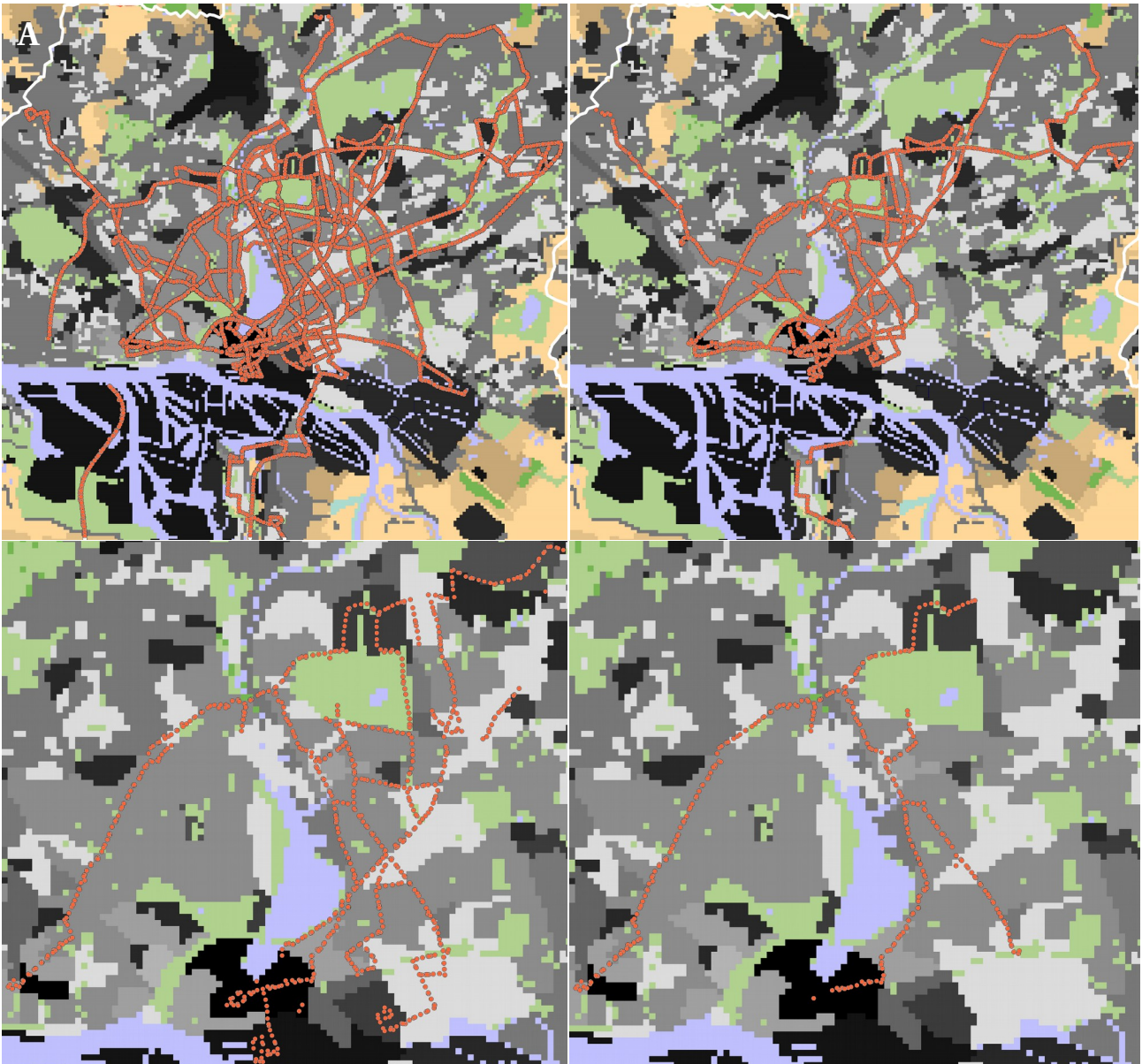


**Fig. 3.6.4** Spatial extent of bus-measurements aggregated in an irregular 100 m spaced network. All maps show the nLUC for central Hamburg with the lake Alster in the map's center. Overlaid maps show the bus measurements aggregated to the virtual station network (orange dots). They show the extent for A all stations, B stations with  $> 10$  Ts, C  $> 100$  Ts, D  $> 1000$  Ts (all counted for the aggregated 1 min means).

### 3.7 Verification of mobile measurements with met station data

To verify the quality of the aggregated mobile measurements, they were compared to met station data with a maximal distance of 130 m and a maximal temporal deviation of  $\pm 2.5$  min. Under these settings  $n = 108$  pairs of measurements were available for comparison. They showed a mean difference between stationary and mobile measurements of  $-0.15$  K (standard deviation,  $\sigma$  0.66 K) and a mean absolute difference of 0.51 K ( $\sigma$  0.44 K).

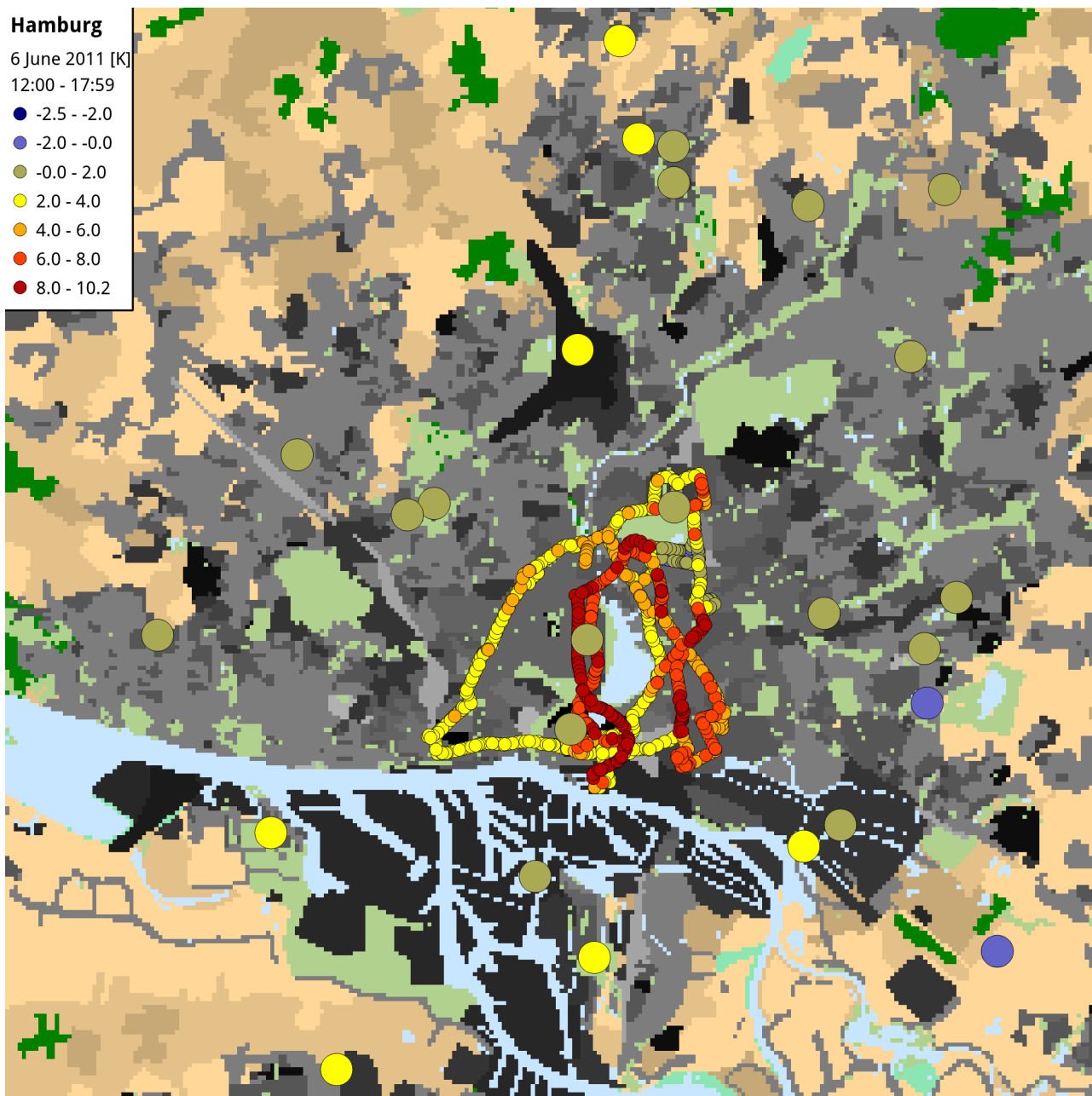


**Fig. 3.7.1**  $T$  of mobile and stationary measurements relative to the MI-station.

Although the MI-station contains some urban effects, the offset to the real UHI can be neglected for these figures.

This is a satisfactory result since the data was not measured at exactly the same time or location. If the difference between station and mobile measurements is weighted by distance in time and space, the mean absolute difference shrinks even further.

The urban temperature distribution relative to a station that measured at 1 min frequency (same as the aggregated bus  $T_s$ ) is displayed in Fig. 3.7.1 and 3.7.2, the absolute  $T_s$  in Fig. 3.7.3 and 3.7.4, for two 6 hourly periods of the warmth day during the campaign (6 June 2011). Such visualization of the current UHI is important to identify potential regions of high vulnerability for risk mapping applications. However, for risk and urban planning applications also a long time mean of UHI-extremes is needed<sup>21</sup>.

<sup>21</sup> Therefore, the bus measurement campaign would have to continue. Interested? Contact [langkamp@tomblog.de](mailto:langkamp@tomblog.de)

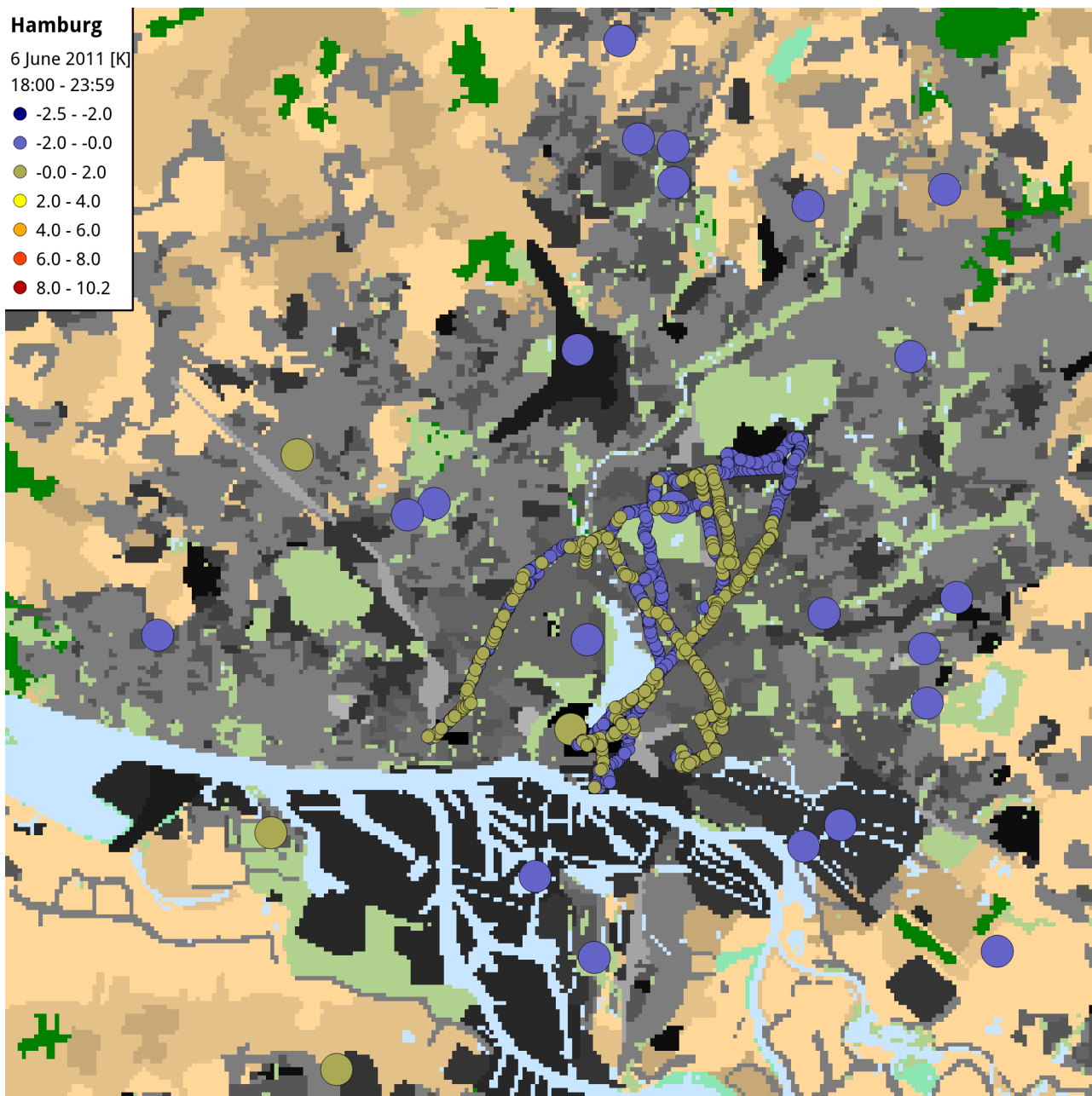


**Fig. 3.7.2** T of mobile and stationary measurements relative to the MI-station.

The depicted UHI is weak, however, most bus measurements were made at the evening (Fig. 3.7.4), thus the real UHI of this period at the bus measurement locations might have been stronger (Chapter 2.1)

Furthermore, to project the UHI into the future DD and SD (for a planning relevant resolution) are needed. Hence, the presented map is intended to give a first impression and cannot be representative, neither spatial, nor temporal. Not to forgotten, that the bus measurements reflect the UHI of an unspecified time span during the depicted six hours, while the stationary measurements reflect the whole period mean, since they measure constantly. To enable a better comparability between bus and met station UHIs, Fig. 3.7.3 and Fig. 3.7.4 depict the absolute Ts. Especially Fig. 3.7.4 shows that most of the bus measurements were made early in the period between 6 p.m. and midnight on that day.

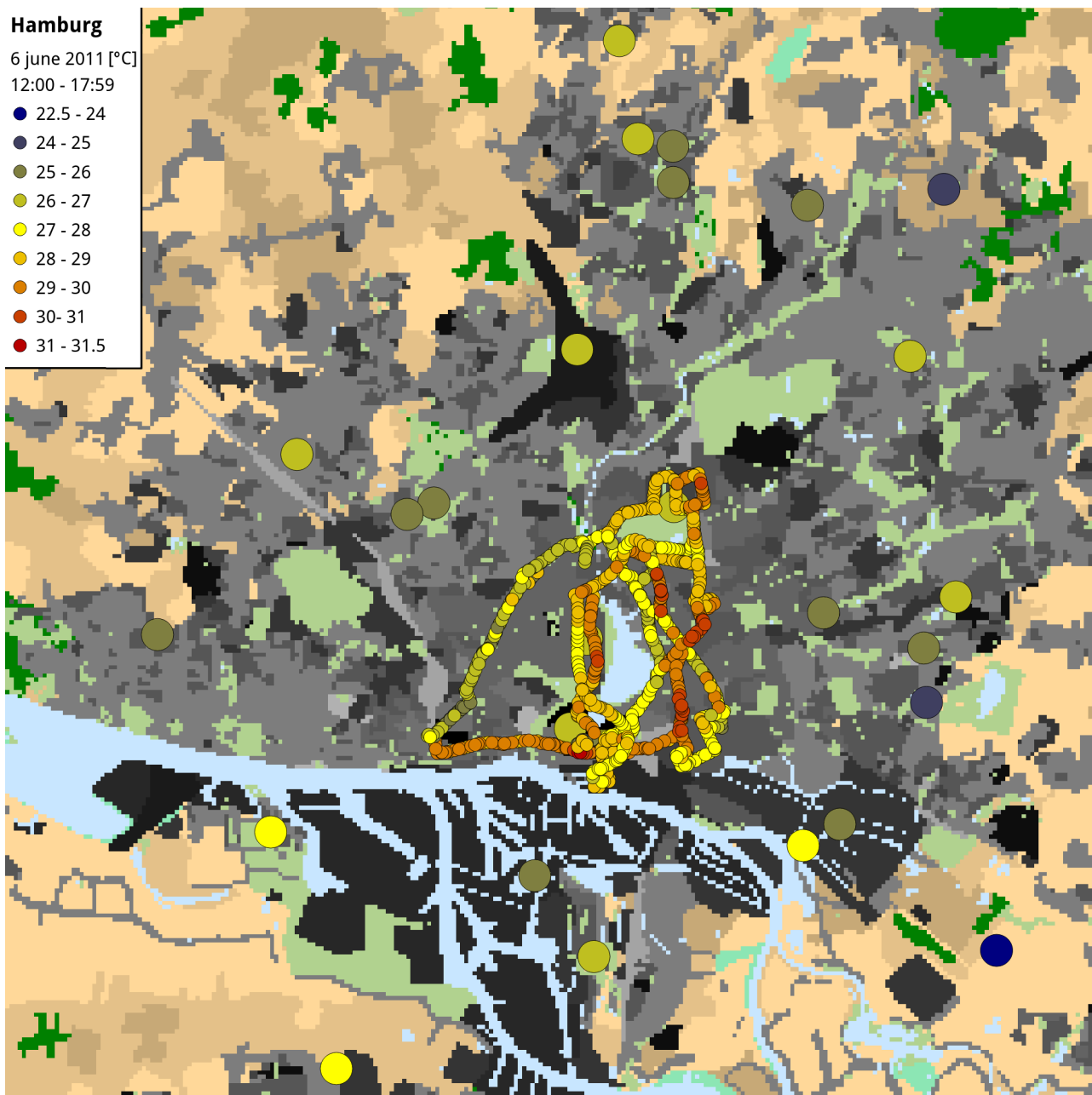


**Fig. 3.7.3** Absolute T of mobile and stationary measurements.

The bus measurements here are comparable to the stationary means, since the measurement frequency of the buses is quite high on afternoons (Fig. 3.6.1).

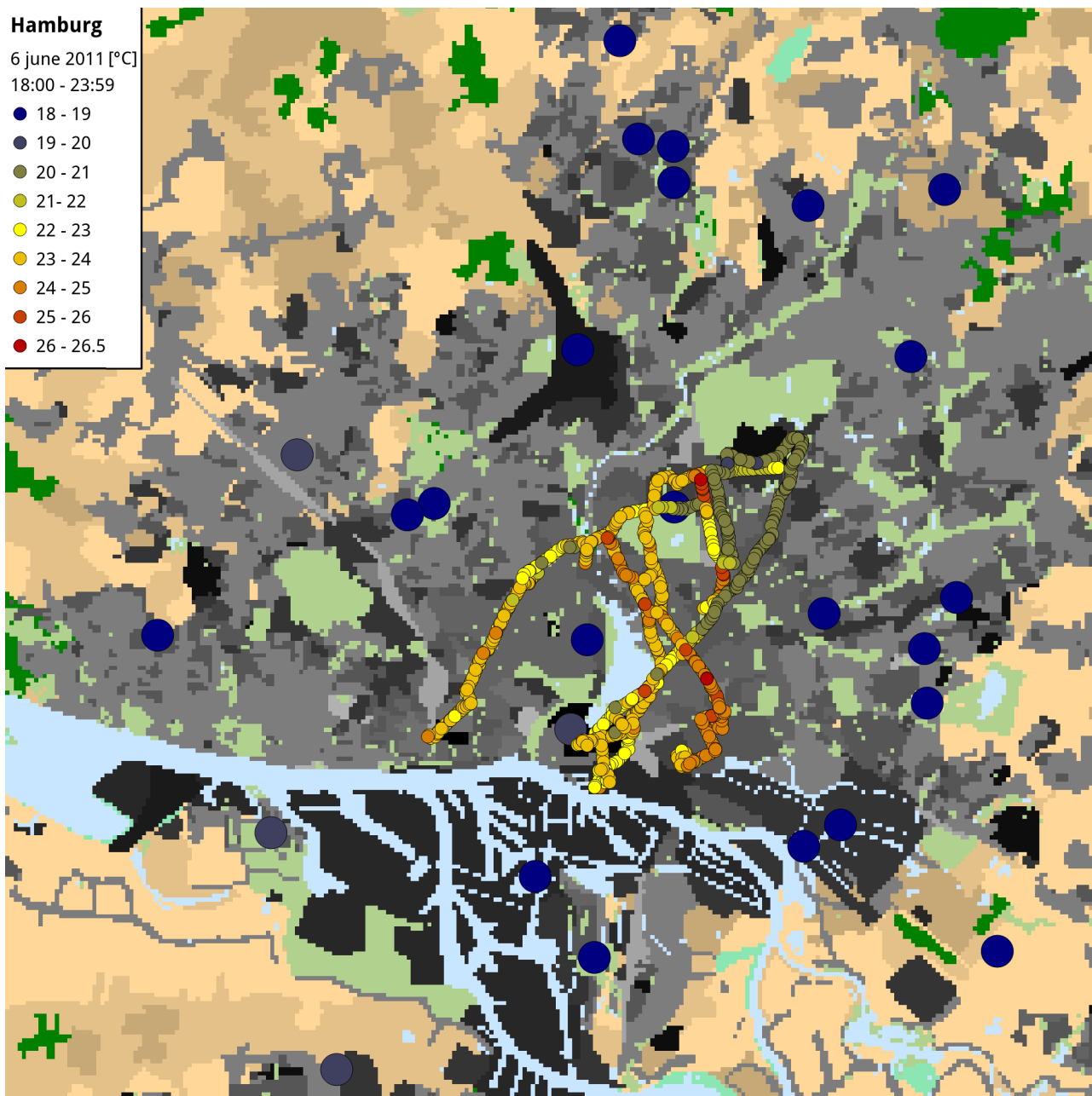


**Fig. 3.7.4** Absolute T of mobile and stationary measurements.

Most of the bus measurements here were taken in the evening, which can be seen at the much higher temperatures.

Besides the need and the possibility to continue the bus measurements in cooperation with the Hochbahn AG, the idea occurred, to also use garbage collection vehicles or cabs to carry the instrumentation. Those vehicles also drive through side streets and would cover further land use classes. In addition, the already collected data pool has to be evaluated further, as only the temperature data are exploited in this research. The urban climate, however, is determined by humidity and other, already discussed factors as well.

## 4 Parameterization of urban roughness

The WRF modeling goal of this research was to achieve a more detailed representation of the wind field impact on the urban air temperature distribution. To reach it, WRF was evaluated against the measurements (Chapter 6). Since the wind field at the urban surface is mainly affected by the roughness (Section 2.6), we improved this data, based on the airborne IFSAR DEM (Section 4.1) and the nLUC (Daneke, Bechtel, and Langkamp 2010; Section 4.2). In Sections 4.3 and 4.4 we evaluated statistical methods to derive the aerodynamic roughness ( $z_0$ ) in the form of urban morphology parameters from the DEM. Bechtel et al. (2011) proposed the method described in Section 4.3, without giving a specific implementation. Section 4.5 documents the implementation into WRF, of the similar but new method described in Section 4.4. The method of Bechtel et al. (2011) recognizes the impact of the wind **direction** on the roughness, the new one ignores it. Both are based on the morphology, isotropy, and texture of all roughness elements, contrary to 3D building data as demanded in Section 2.6.

### 4.1 The IFSAR based digital elevation model

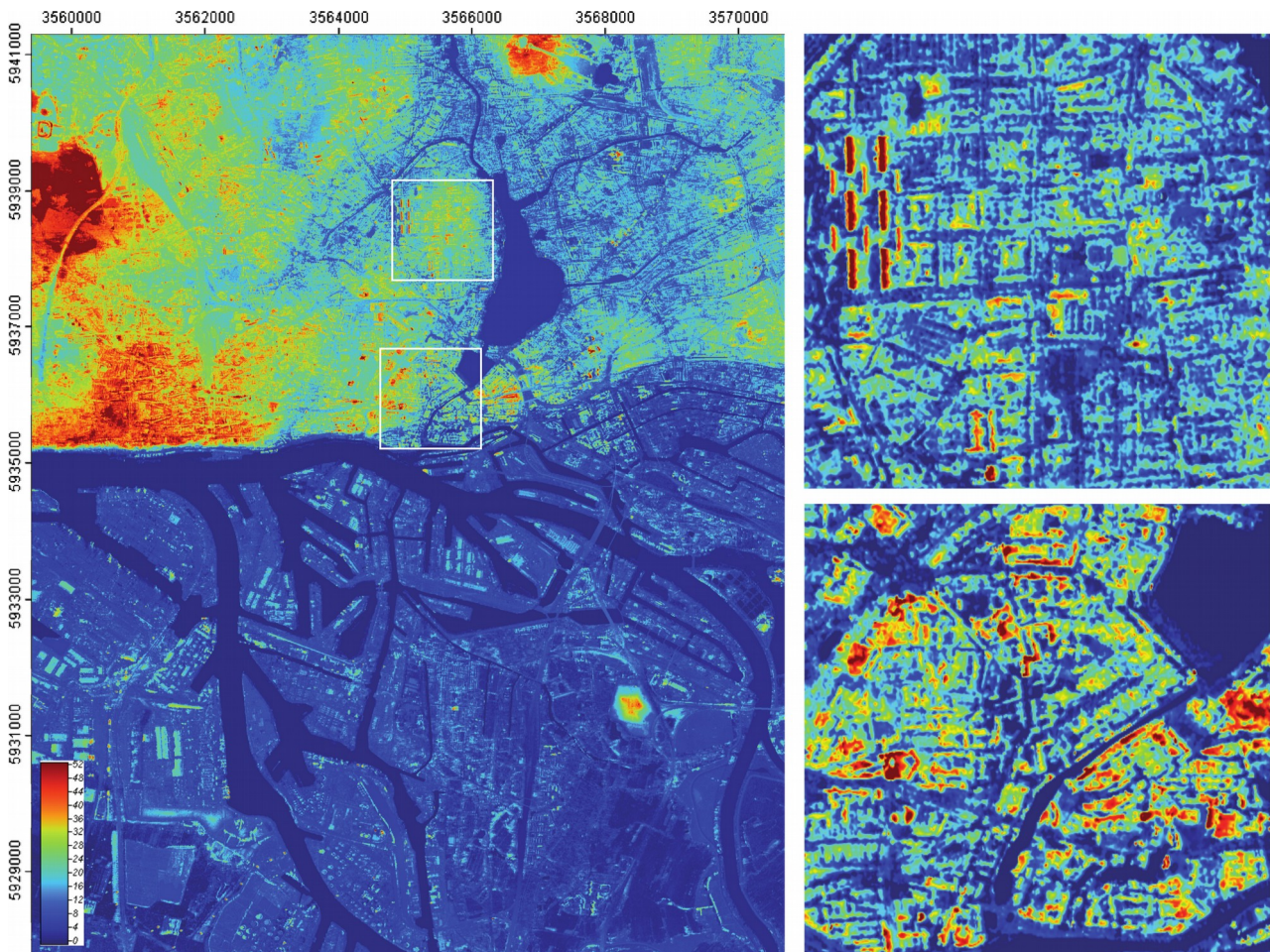


**Fig. 4.1.1** IFSAR derived DEM maps of different parts of Hamburg.

**Left** shows the urban morphology including the topography for a big part of Hamburg. Its lower half shows the Elbe estuary with its big river island, where large parts of the harbor are located. **Upper right:** The district Harvestehude is a Wilhelminian (Classical) period town expansion with a very regular ground plan and the six big and the six small Grindel high rise buildings (red). **Lower right:** The district Neustadt with no preferred orientation of the morphology visible. (modified Bechtel and Langkamp et al. 2009, data NEXTMap®.)

To derive an improved high resolution roughness layer for WRF modeling application we used airborne (8.5 km) side-looking IFSAR data of Hamburg (NEXTMap® Intermap Technologies, Fig. 4.1.1).

The IFSAR raw data products are a digital surface model (DSM) and a digital terrain model (DTM). They were transformed (with open source SAGA GIS) to a digital elevation model (DEM = DSM - DTM). The DEM delivers a high resolution map (3 to 5 m horizontally, 1 m vertically) of the urban morphology. It has the advantage that all types of obstacles, including trees, are taken into account (as discussed in Section 2.6). This is because the DSM represents the first reflective surface as illuminated by the radar and integrates over a square footprint, containing the effects of all scattering objects within it. Thus, it inherits the quantitative spatial information about the morphology-specific impact on the wind, which shall be unveiled.

All data products used for this research are of the NEXTMap® core product v3.3 and edit rule v2.0<sup>22</sup>. This means, they have a root mean square error (RMSE) of 2 m in areas of obstructed flat ground and a RMSE of 1 m or even lower in areas of unobstructed flat ground. The RMSEs increase with dense vegetation and increasing slope (double RMSEs for slopes > 20°).

## 4.2 Morphological land use and roughness classification

The goal of Stewart and Oke's (2009) LCZs was defining LUCs that combine climate sensitive descriptors, resulting in a unique urban climate per LUC (Section 2.5). Therefore, each LCZ was assigned with an:

- aerodynamic roughness class [1-8] with associated  $z_0$  values (Davenport et al. 2000, Wieringa et al. 2001);
- mean annual anthropogenic heat flux at the local scale [ $\text{W}/\text{m}^2$ ];
- thermal admittance of the construction materials [ $\text{Jm}^{-2}\text{s}^{0.5}\text{K}^{-1}$ ];
- built fraction [%]; sky view factor from ground level [0-1]; albedo [0-1].

Including these descriptors the 9 urban LCZs (Fig. 2.5.1) are well suited for urban climate applications, enabling a better representation of the IUHIs. The reclassification to the nLUC (Daneke, Bechtel, and Langkamp 2010) resulted in 14 urban classes. The classes Shantytown and Open Grounds were eliminated since they rarely exist in Hamburg, while the classes Old Core, Compact Housing, and Extensive Lowrise were subdivided into 7 new classes. The final classification is displayed in Fig. 4.2.2; the assigned class names and roughness classes are given in Table 4.2.1. Despite the reclassification both LUCs are still compatible and exchangeable.

One might question the assigned roughness classes of the final 21 nLUCs in two cases. First, Sealed Area had no direct expression within Stewart and Oke (2009) or Wieringa et al. (2001), but was assigned with class 7, reflecting its height-variance (Section 4.4) calculated with the IFSAR DEM. Second, Urban Green was connected to the LCZ Forest (roughness class 7.5), as the urban parks of Hamburg consist of trees to a large share. The assignment of the other classes was straight forward and followed the descriptions of Stewart and Oke (2009).

The nLUCs originated from the digitization of data from the European Environment Agency CORINE land cover of 2006 (EEA HP 2012). CORINE offers the best spatial resolution (100 m) but its classes are not suitable for urban climate application. Thus, it was adapted by removing its urban layer and replacing it, using several land cover data sources. Those comprise the official German topographic-cartographic information system of 2008 (ATKIS HP 2012), topographic maps 1:50,000 of 2005 ( $\pm 2$  years), and building outlines of 2005 (LGV HP 2012)<sup>23</sup>.

<sup>22</sup> Find details on Intermap's data processing methods in the product handbook: <http://www.intermap.com/images/handbook/producthandbook.pdf>

<sup>23</sup> Find details on the data processing and the reclassification of the LCZs in Daneke, Bechtel, and Langkamp (2010).



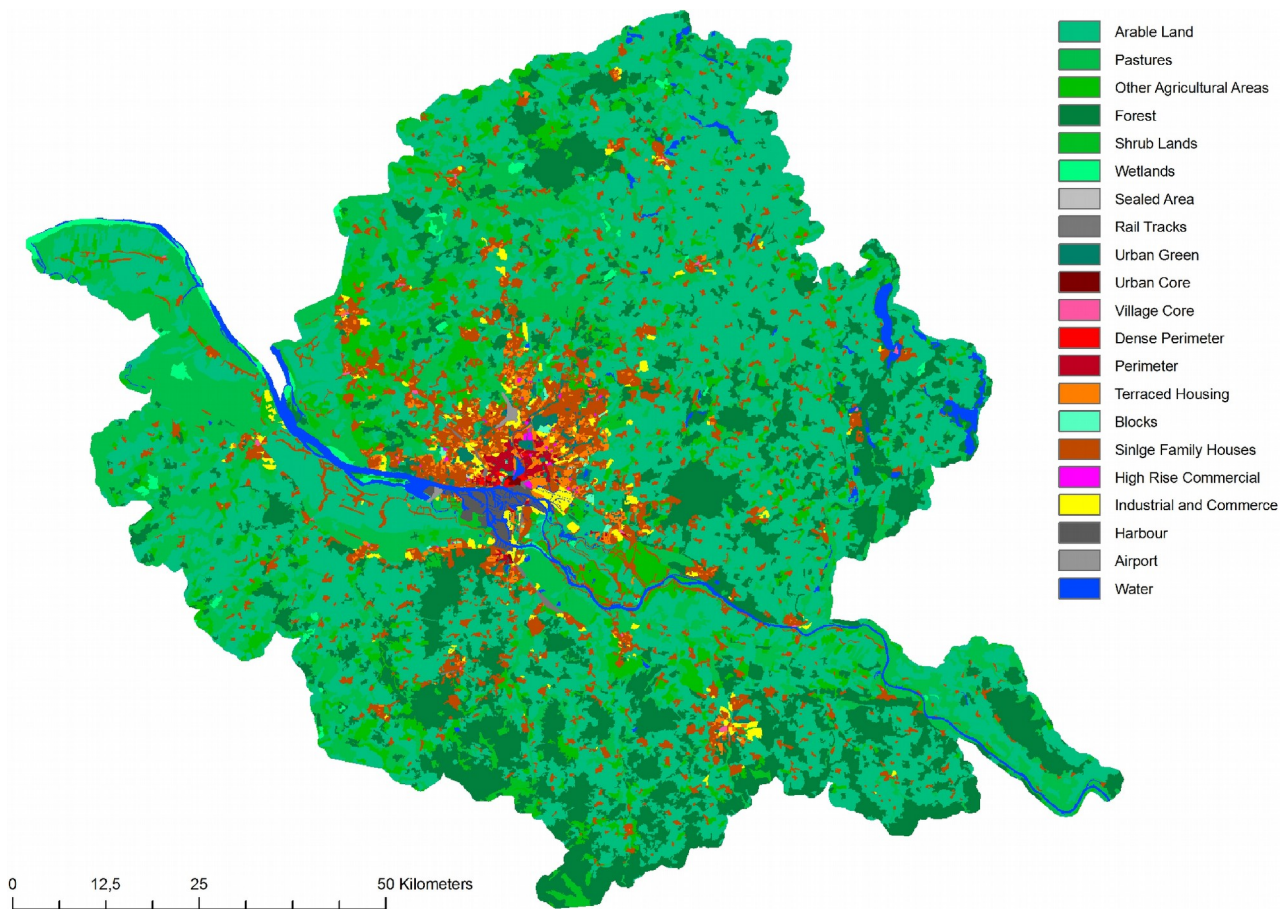


**Fig. 4.2.2** The nLUC over a part of the metropolitan area of Hamburg (Fig. 4.2.1).  
(Figure by C Daneke)

### 4.3 Improved roughness mapping by sector height statistics

This first method shows the correlation between the IFSAR DEM and empirical roughness data to find the functional relation as demanded in Section 2.6. The correlation demonstrates that the DEM is suitable for urban roughness applications.

The variance of sectors height (VSH) computes the height variance of the DEM for a circle's sector. The resulting variance is then given to the center grid cell of the circle. This computation is repeated for every grid cell, replacing the DEM by a variance grid. The size of the circle's sector is defined by direction, radius, and opening angle (Bechtel and Langkamp et al. 2011):

- **Direction:** The VSH is computed for one dominant wind direction at a time. Repeating it for different wind directions, results in different variance grids.
- **Radius:** It reflects the slowing of the wind through an obstacle's drag with increasing distance.
- **Opening angle:** It reflects the turbulent fluxes that smear the effect of obstacles to a certain downwind area. This is a simplification of the superposition of different turbulent footprints.

The final VSH grids – that can be computed with the new SAGA GIS module `Directional statistics for single grid` – were correlated with empirical  $z_0$  values. Therefore,  $z_0$  needed to be derived from wind measurements for the same dominant wind direction and opening angle as used in the VSH computation. The VSH grids were then compared with those  $z_0$  data for different wind directions.

Thanks to the research of Peek (2011) extensive empirical  $z_0$  data (Fig. 4.3.1) was available from the MI-station (Appendix A). The  $z_0$  calculation was based on a 3-year climatology of vertical wind speeds and directions measured at neutral atmospheric stability conditions. Therefore, the logarithmic wind speed profile was assumed to be valid for the urban canopy layer (Fig. 2.1.1).

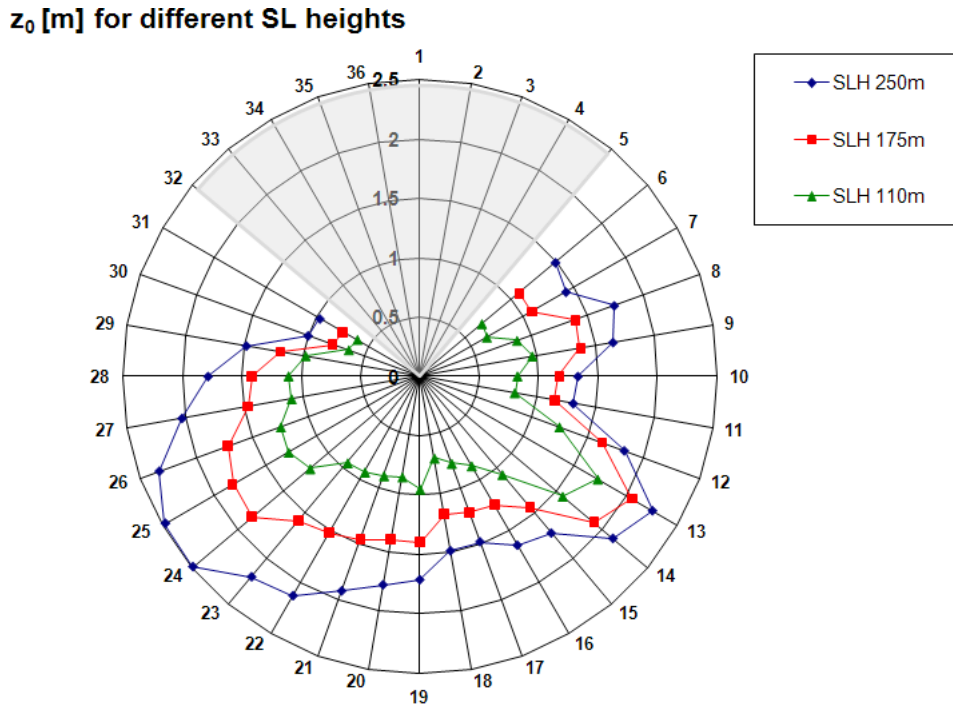


**Fig. 4.3.1**  $z_0$  derived from wind profile measurements at the MI-station.

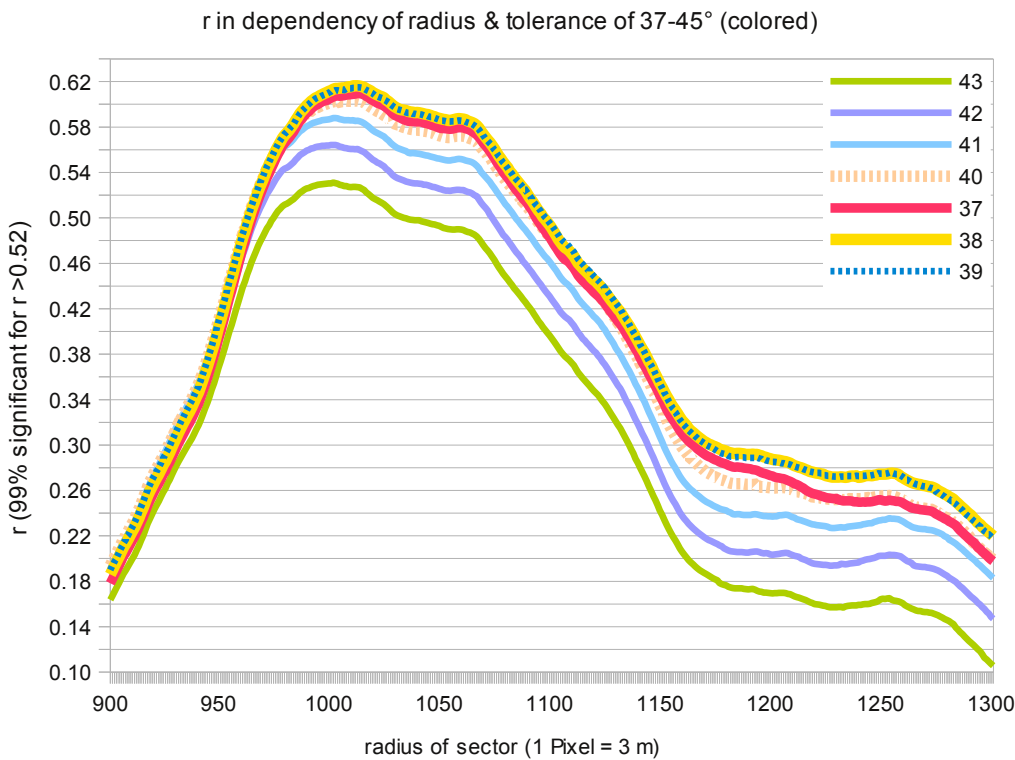
Values within the gray area are biased by local flow effects due to the presence of the mast and were discarded. The colors indicate three different surface layer heights (SLH). The SLH influences the magnitude, but not the general distribution characteristics of the directional  $z_0$  values. The later used data of SLH 250 m include all five vertical measuring points in contrary to the other SLH data, discarding the measurements above 110 or 175 m. (Peeck 2011)

Fig. 4.3.2 and 4.3.3 show the calculated VSH and its calibration for the DEM of Hamburg. Fig. 4.3.2 shows the shape of the sectors with an opening angle of  $60^\circ$  and a radius of 250 pixels (750 m) for an easterly wind. The lake Alster for example (black, top left corner) corresponds to a low height variance. The white sectors indicate pixels of high variance, correlating with high roughness, like the old city core south of the lake. However, to quantitatively use the VSH as a measure for roughness, appropriate values for the sector's radius and opening angle had to be calibrated. The result is shown in Fig. 4.3.3 for different wind directions, radii, and opening angles for the pixel of the MI-station. These VSH values were correlated with the 26  $z_0$ -means of  $10^\circ$  sectors (Fig. 4.3.1) at the SLH of 250 m (best correlation result), resulting in a maximum Pearson product-moment correlation coefficient ( $r$ ) of  $VSH^{0.5}$  to  $z_0$  of 0.62.

A second calibration attempt was made in the same way towards  $z_0$  values derived from boundary layer wind tunnel measurements from the city core model of Basel (Feddersen 2005). They delivered higher  $r$  of 0.8, but peaked at very different values of 150 pixels and an opening angle of  $6^\circ$ .



**Fig. 4.3.2** VSH for Hamburgs inner city, the Elbe estuary and the Elbe island. Wind direction is east, sector radius 250 pixel, sector opening angle 60°. The MI-station is located at the center (53° 31' 9" N and 10° 6' 10.3" E, district Billwerder).



**Fig. 4.3.3** Pearson's r of  $VSH^{0.5}$  to  $z_0$  in dependence of radius and tolerance for 250 m SLH (Fig. 4.3.1). The VSH and  $z_0$  were calculated for different wind directions at MI-station. Tolerance (half opening angle) is colored, the radius can be seen on the x-axis.

Summing up the VSH calibration: There is not yet a recommendation for the sector's radius and opening angle. The calibration towards  $z_0$  derived from field site measurements like the MI-station, on the one hand, turned out to be difficult. Many variables influence the original calculation of  $z_0$  and their representativeness is affected by the variability of wind, atmospheric stability, and SLH. Laboratory measurements in boundary layer wind tunnels, on the other hand, can be conducted under constant mean inflow and boundary conditions. Thus, the measured quantities have high statistical confidence levels. These differences in calculating  $z_0$  from wind tunnel or field site measurements explain the contradictory calibration result:

- **Opening angle:** The mean wind direction in the wind tunnel is steady while in atmosphere it is constantly changing. This explains the narrow opening angle of  $6^\circ$  vs.  $76^\circ$  for the MI-station calibration. The implementation of a sophisticated footprint concept like a source area model (Schmid 1994) may improve the measure.
- **Radius:** The measuring heights of the MI-station are higher than the one within the Basel wind tunnel experiment. This explains the higher radius of 1000 vs. 150 pixels. A distance weighting may improve the measure.

The calibration should continue with incorporating a source area model, a distance weighting, and more  $z_0$  data of other cities, to verify the conclusions and to find an appropriate compromise. However, to find further reliable  $z_0$  data is not trivial as discussed in Section 2.6 (paragraph empirical measures). It is even harder, when one is spatially limited, since Intermap provided us with the DEMs of Hamburg and Basel only.

However, we continued calibrating another method that delivered applicable results (Section 4.4), which neglects the wind direction dependence and thus results in an easier implementation and higher applicability. For a wind direction dependent roughness function in WRF, a huge intervention probably including the programming of a new LSM module would have been needed. This is not needed for the following simpler method, ignoring the wind direction and the inner class variability.

#### 4.4 Improved roughness mapping by class specific height statistics

As WRF needs rasterized LUC based input data it was logical to combine the IFSAR DEM with the  $z_0$  data of the LCZs. Accordingly, instead of calibrating the sectors' variance with  $z_0$  at single points, this method relates known values of  $z_0$  for predefined LUC from literature (Table 4.2.1) with the height-variance (HV) of the IFSAR DEM for the respective LUC. The result shows a close relation of HV to those  $z_0$  values from literature (Stewart and Oke 2009, Wieringa et al. 2001, Davenport et al. 2000).

At first, we tried rasterized versions of the HV at different resolutions. Fig. 4.4.1 shows the result for a 250 m raster including only cells of the urban nLUCs. The result is very sensitive to the resolution, but always showed qualitatively how the roughness distribution of Hamburg looks like. However, as the default WRF LSM does not support the input of an individual  $z_0$  value at every grid cell, but rather requires class based roughness values, HV was computed for the nLUC polygons (Fig 4.4.2).

To verify Fig. 4.4.2 quantitatively, it was correlated with the corresponding  $z_0$  values (Table 4.4.1 and Fig. 4.4.3). Since Stewart and Oke (2009) give roughness class ranges to their LCZs, means had to be calculated. For example Old Core has a roughness class range of 6 to 7, corresponding to a  $z_0$  of 0.5 to 1 m. As of the idealized character of the wind profile (Section 2.4) the means of the class ranges were interpolated using the formula:

$$z_0 = \exp \frac{\ln(0.5 \text{ m}) + \ln(1 \text{ m})}{2} = 0.707 \text{ m}$$

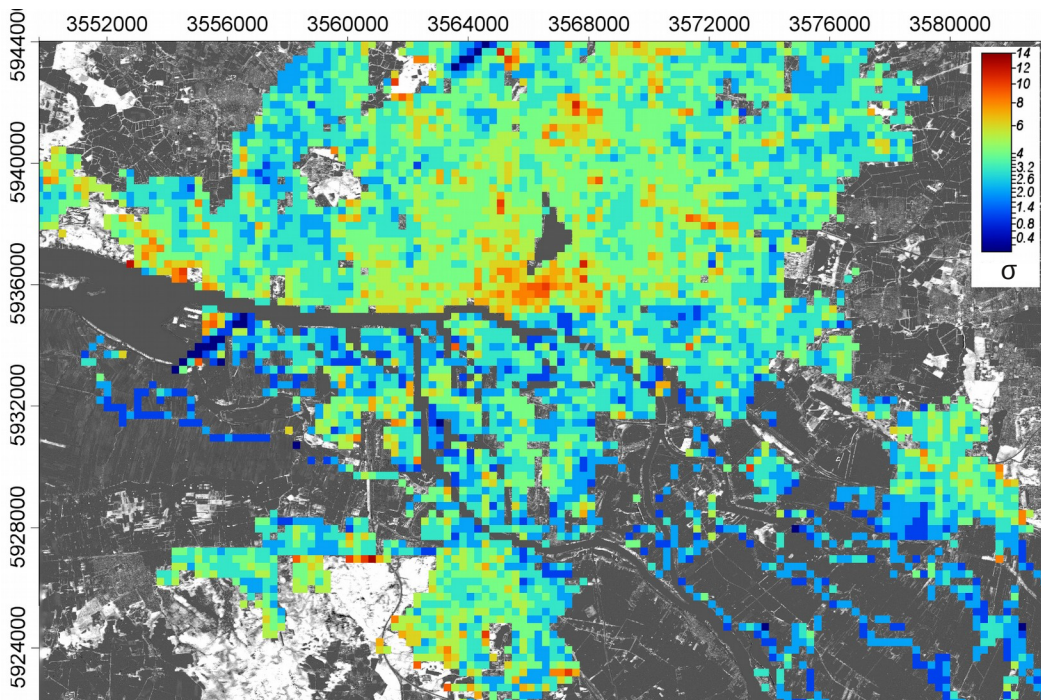


**Fig. 4.4.1**  $\sigma$  (colored) of the DEM (gray scale) for a raster of 250 m. Non-urban classes were cut out in this early version. As expected low HV (blue) is found for example over the airport runways (deep blue lines in the north and in the west) while high HV (red) is found over the central old core south of the lake Alster.

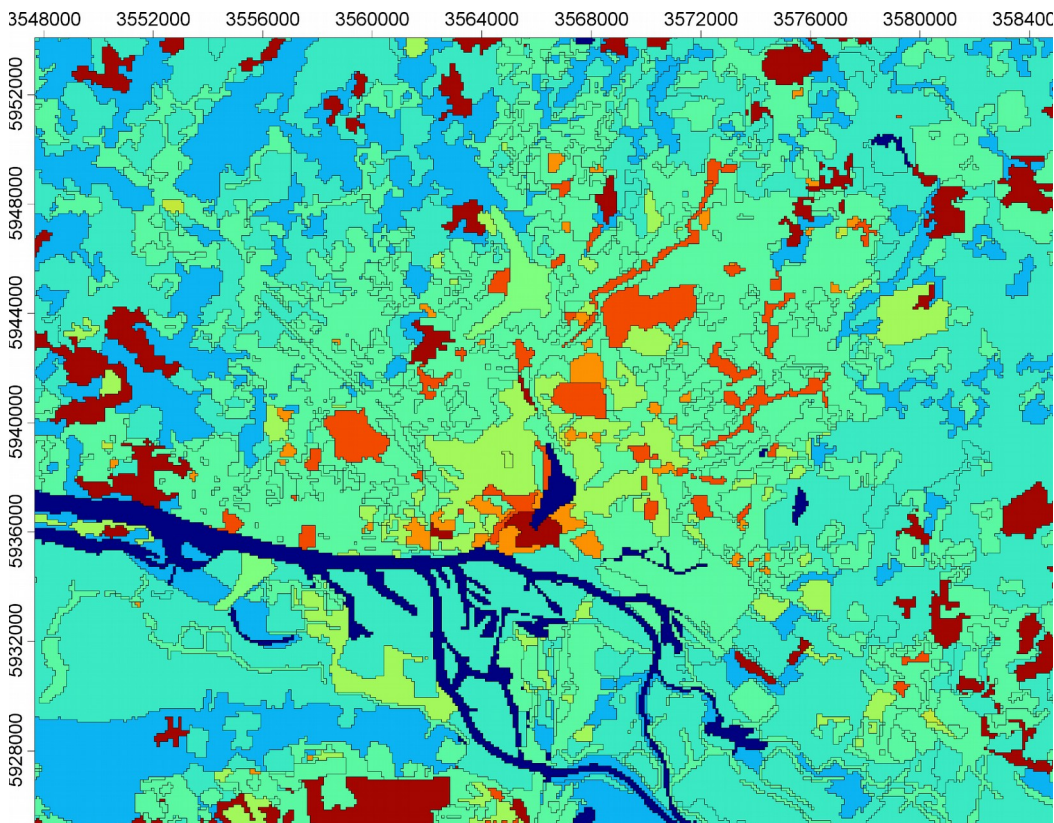


**Fig. 4.4.2** Mean class HV for the 100 m resolved LUC polygons. The northern parts without an overlap of the IFSAR DE area were excluded from the computation, but are assigned with the class based results afterward. This qualitative result already shows reasonable high HV (red) for old central districts, wooden area, and low HV (blue) for flat agricultural area and water.

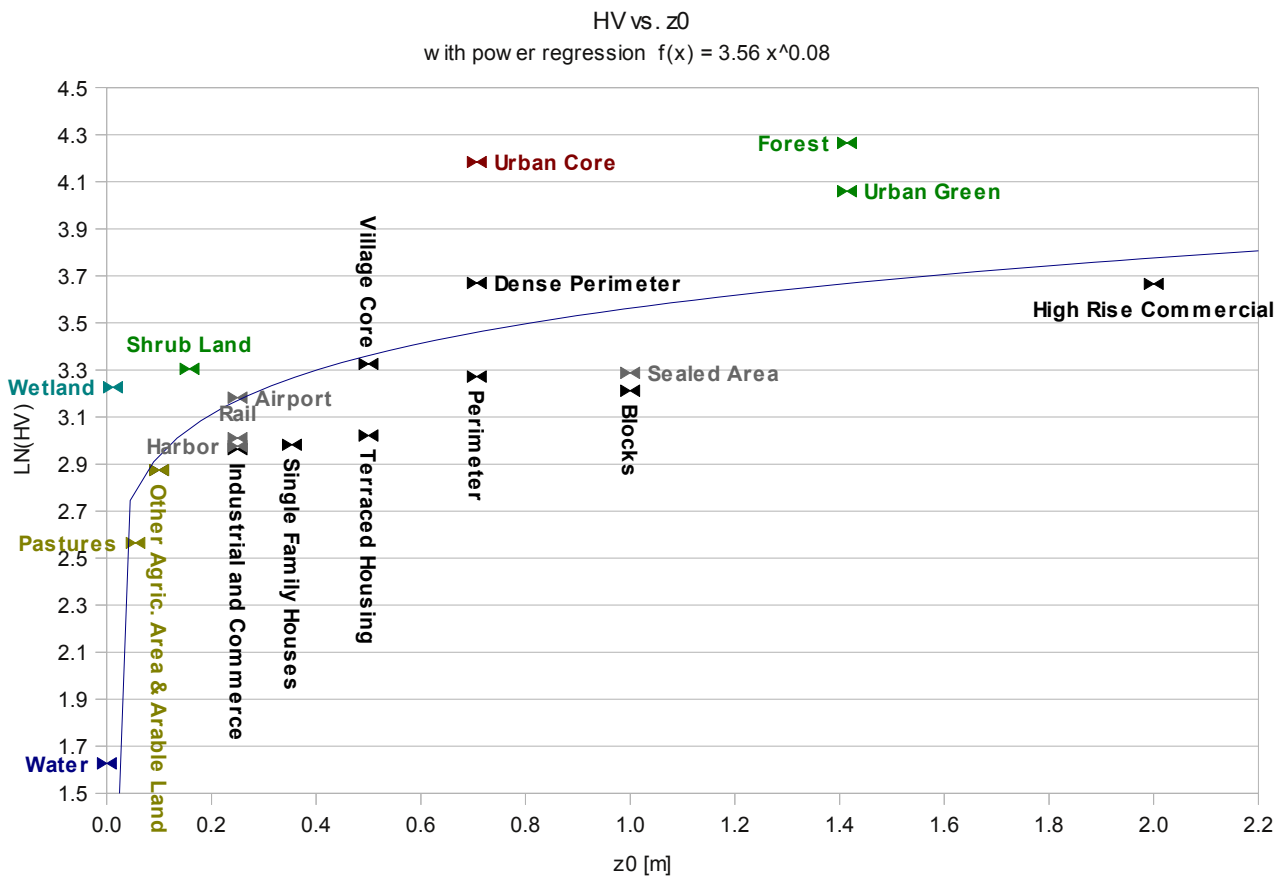


**Fig. 4.4.3** The logarithmized mean HVs of the nLUCs plotted towards their literature  $z_0$ -values. Colors are to highlight land use. The line shows the power regression that was used to interpolate new, individual  $z_0$  parameters for every LUC (Table 4.4.1).

The original  $z_0$  and HV have a Spearman rank correlation coefficient ( $\rho$ ) of 0.77 for all classes and 0.81 for urban classes only. To verify this result, the HVs were computed also based on smaller domains of the IFSAR DEM: with the eastern half, the western half, and a central domain (Fig. 4.4.4). Furthermore, because of the nLUC resolution of 100 m the margins of a class include neighboring classes with very different HVs. To eliminate those mixed class pixels a 100 m buffer was cut from the nLUC polygon margins for the four different DEM domains. See Table 4.4.2 for all  $\rho$  results.

To give a summary of the section (4.4): The 14 urban nLUCs (21 including the rural ones) are an improvement of the single urban class that comes with the original WRF land use data. They are also a refinement of the nine LCZs (Stewart and Oke 2009), but still backwards compatible. To improve the method, the class count could be raised further.

The Hamburg optimized nLUC (Daneke, Bechtel, and Langkamp 2010) was complemented with a reasonable roughness measure computed from a DEM's HV. It was highly correlated with the original  $z_0$  values and could be translated to new  $z_0$  values. Advantages of the method are the easy availability of the IFSAR DEM, the inclusion of all obstacles, and the potential for wind direction dependence with the VSH method. Further calibration of HV with IFSAR and nLUC data of other cities is desirable. This would confirm the worldwide applicability despite of cultural differences in city morphology.

Section 4.5 comprises the implementation of the new roughness values into WRF. Chapters 5.3 and 6 will then give an estimate on how the new roughness data improves the WRF temperature output, utilizing the collected T measurements.

nLUC names for Hamburg	orig. $z_0$ [m]	HV	new $z_0$ [m]
Arable Land	0.100	17.71	0.106
Pastures	0.055	13.00	0.039
Other Agricultural Area	0.100	17.71	0.106
Forest	1.414	71.20	3.234
Shrub Land	0.158	27.25	0.354
Wetland	0.012	25.19	0.288
Sealed Area	1.000	26.78	0.339
Rail Track	0.250	20.29	0.158
<b>Urban Green</b>	1.414	57.98	2.109
<b>Urban Core</b>	0.707	65.65	2.739
<b>Village Core</b>	0.500	27.81	0.374
<b>Dense Perimeter</b>	0.707	39.25	0.878
<b>Perimeter</b>	0.707	26.36	0.325
<b>Terraced Housing</b>	0.500	20.51	0.163
<b>Blocks</b>	1.000	24.83	0.277
<b>Single Family Houses</b>	0.354	19.72	0.145
<b>High Rise Commercial</b>	2.000	39.10	0.871
Industrial and Commerce	0.250	19.35	0.137
Harbor	0.250	19.61	0.143
Airport	0.250	24.10	0.255
Water	0.0002 <sup>24</sup>	5.09	0.0008
$\rho$ of original $z_0$ and HV		0.77	
$\rho$ of original $z_0$ and HV urban only		0.81	

**Table 4.4.1** HV and new  $z_0$  for the nLUC, plus Spearman ( $\rho$ ) between HV and original  $z_0$ . Bold faced nLUCs are urban classes, colors indicate land use. The HV of the DEM was computed for the nLUC shapes in Fig. 4.4.2. The new  $z_0$  was calculated from a power regression between the original  $z_0$  and the HV, see Fig. 4.4.3.

domains	[ $\rho$ ] classes:	without buffer		with 100 m buffer	
		all	urban	all	urban
full IFSAR DEM		<b>0,89</b>	0,73	0,72	<b>0,74</b>
east half		0,55	<b>0,63</b>	0,53	0,57
west half		0,83	<b>0,88</b>	0,71	0,75
central domain		0,48	<b>0,88</b>	0,88	0,84

**Table 4.4.2**  $\rho$  of mean HV for different LUCs correlated with the original  $z_0$  (Table 4.4.1).  $\rho$  was calculated for different domains, different class sets (all or urban), and excluding a 100 m buffer zone along the class margins. The correlation is higher for the unbuffered domain (green) and for the urban class subset (bold green). The highest  $\rho$  overall (0.89) is computed from all classes over the full and unbuffered DEM, the lowest (red) is found with the central domain over all unbuffered classes. For the central domain the buffer helped significantly, demonstrating that the resolution of 100 m is not sufficient for Hamburgs center, which contains a fine grained land use mixture (Fig. 4.2.2).

<sup>24</sup> A zero got lost during the process. Consequently,  $Water = 0.002$  m instead of 0.0002 was used within the power regression. Thus, the roughness values fed into WRF were different from Table 4.4.1 and had an overall lower roughness. The effect of the error is limited and discussed with the results in Chapters 5.3, 6, and Appendix I, listing all roughness values.

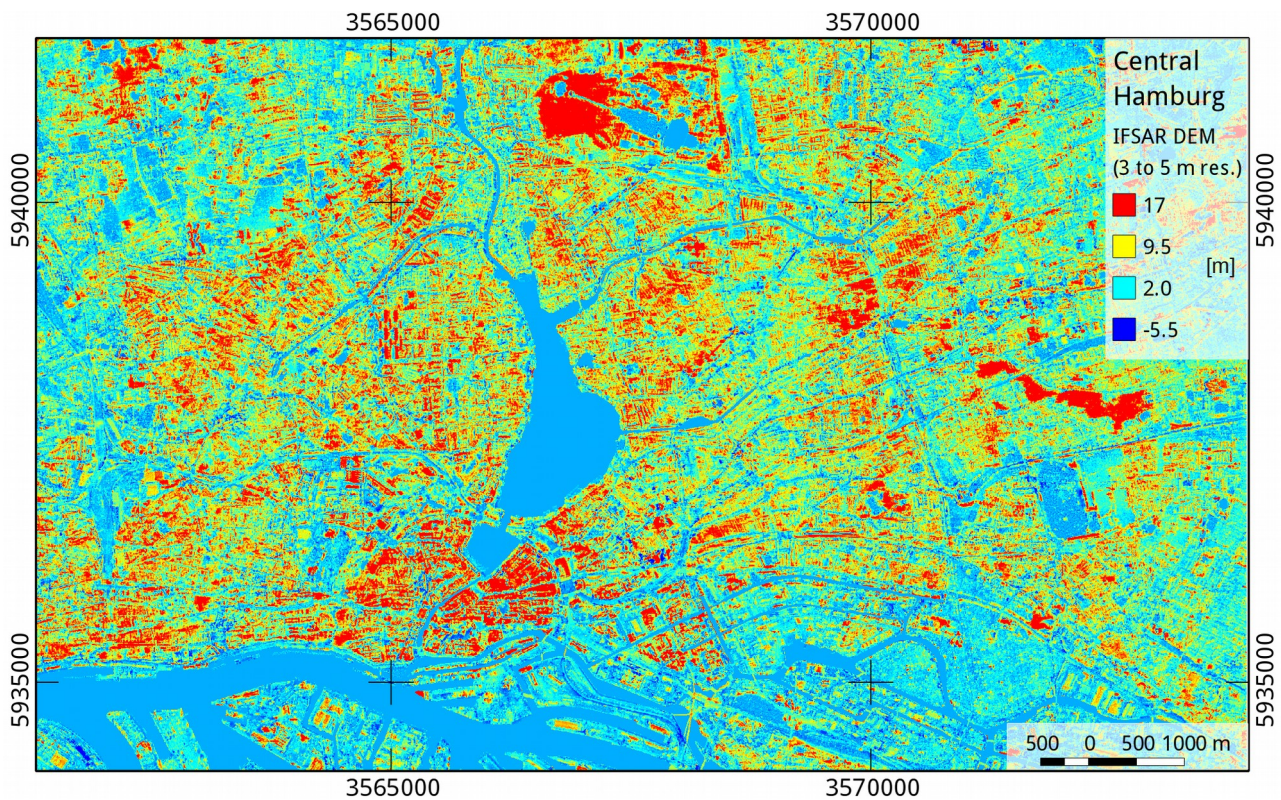


Fig. 4.4.4 The IFSAR DEM for a central part of Hamburg, used in the evaluation of Table 4.4.2.

## 4.5 Implementation of the new roughness data into WRF

The new roughness data was implemented by replacing parts of WRFs original LUC (WRF oLUC 2009, Fig. 4.5.1). The oLUC (Appendix G) includes the parameters  $z_0$ , albedo, emissivity, soil moisture availability, and snow albedo effect<sup>25</sup>. The data comes as a binary grid and defines the parameter values in the file `LANDUSE.TBL` (Appendix I), used by WRFs default 5-layer thermal diffusion LSM. To implement the nLUC its names and  $z_0$  values were added to the `LANDUSE.TBL`, then the oLUC binary grid of 30" was modified (Appendix H), as the `index` file of the binary grids, and the WRF configuration file `namelist.input`. After the integration the inner WRF domain looks like in Fig. 4.5.2.

<sup>25</sup> The also included parameter surface heat capacity (`SFHC`) is not used by WRF (Wang et al. 2011).

### WRF ARW Surface - USGS LUCs

OUTPUT FROM WRF V3.3 MODEL

WE = 121 ; SN = 121 ; Levels = 60 ; Dis = 1km ; Phys Opt = 8 ; PBL Opt = 2 ; Cu Opt = 0

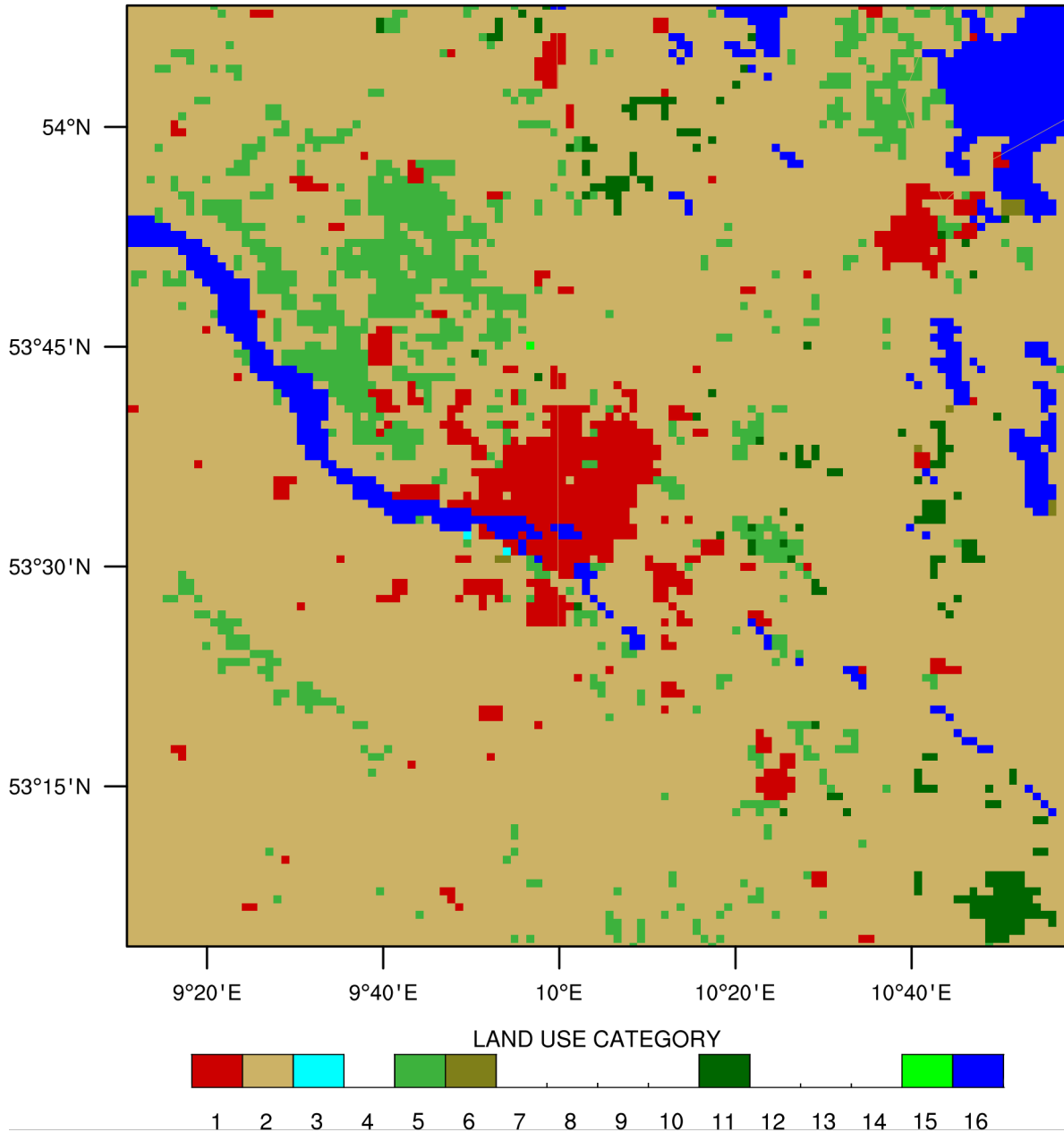


**Fig. 4.5.1** WRFs original LUC (oLUC) for the inner 1 km domain.

The domain comprises Hamburg and the surrounding counties (Fig. 4.2.1). It contains only one urban (red) and 7 natural classes (see Appendix I for class names). The blank classes are missing in this region. The data is freely available via the U. S. Geological Survey (USGS).

## WRF ARW Surface - nLUCs

OUTPUT FROM WRF V3.3 MODEL

WE = 121 ; SN = 121 ; Levels = 60 ; Dis = 1km ; Phys Opt = 8 ; PBL Opt = 2 ; Cu Opt = 0

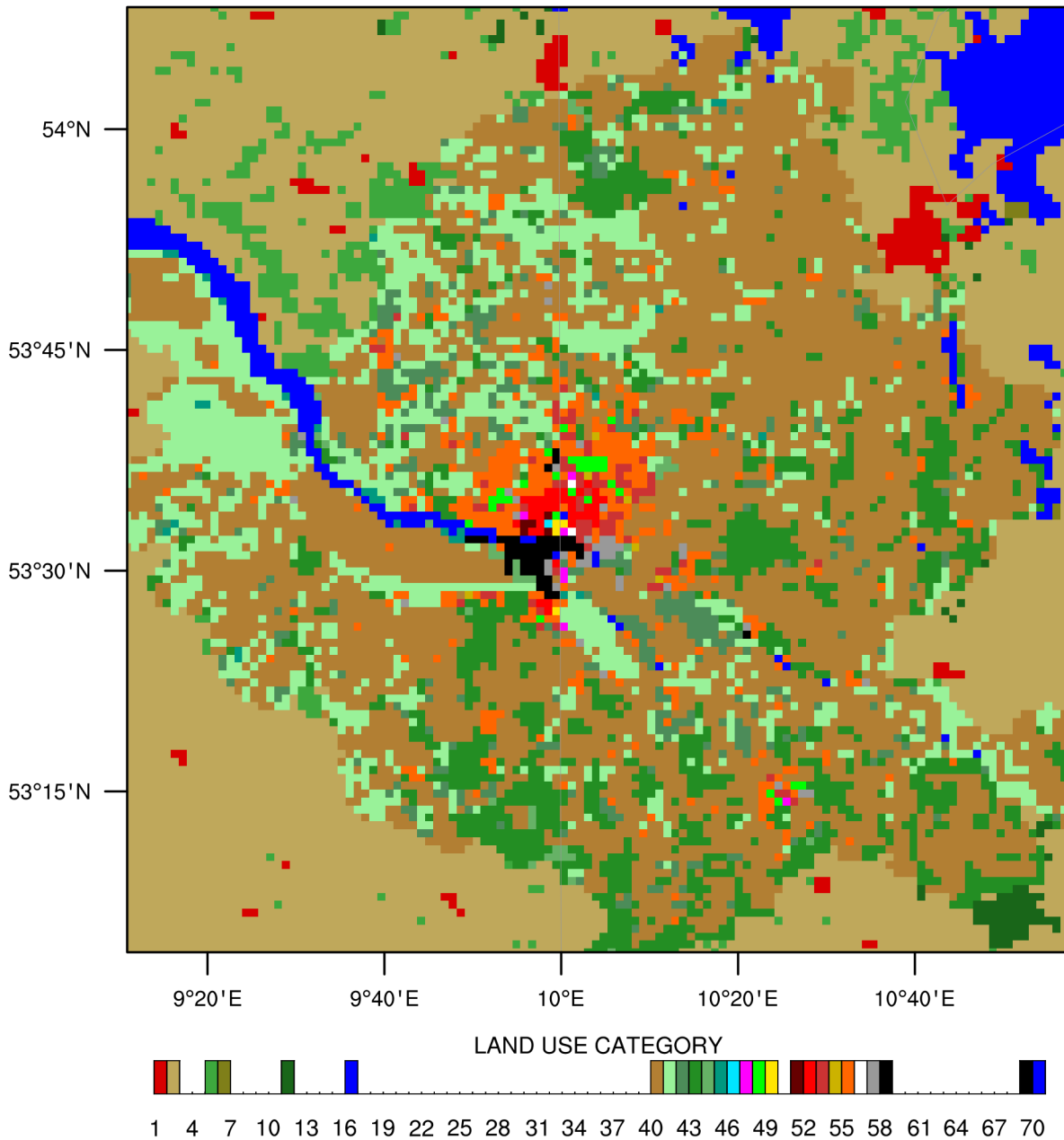


**Fig. 4.5.2** The nLUC after its integration in the inner 1 km domain of WRF.

One can recognize the extent of the new data by the darker brown (agricultural class). The many missing LUCs in the legend originate from missing classes in this region like the *Tundra* or from old classes replaced by new ones. Also the class *Village Core* got lost due to the upscaling from 100 m to 1 km. Find the classes' names and IDs in Appendix I.

# 5 Dynamical downscaling

## 5.1 Optimizing WRF performance for a HPC

In numerical weather modeling limited computing capacity is a crucial problem. Therefore, the performance of WRF was evaluated in Langkamp and Böhner (2011) running on the high performance cluster (HPC) Tornado (Fig. 5.1.1) of the German climate computing center (DKRZ). The benchmark study analyzed the impact of different compilers and message passing interface (MPI) libraries on WRF to save computing time.

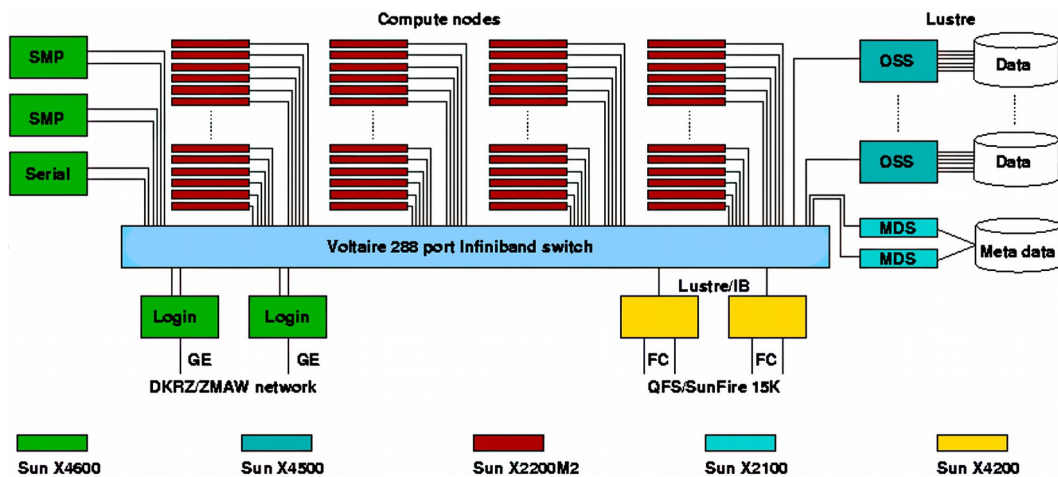


Fig. 5.1.1 The 2048 core HPC Tornado of the DKRZ.

Tornado operated under Debian GNU / Linux, Kernel v2.6.16. Its main part (red) was a 256 node compute server (2 AMD Opteron quad-core CPUs per node) with 4 GB RAM per core (8 TB total). The nodes were connected via Gigabit Ethernet and low latency Infiniband DDR network. The cluster was decommissioned on 19 July 2012. (Tornado HP 2012)

The compiler is the most important performance critical software. The compilation process translates the source code written in a programming language into a machine-readable binary format, opening various possibilities of performance optimizations for different hardware. Langkamp and Böhner (2011) determined that the costly and proprietary PGI and Intel compilers were the best choice<sup>26</sup> for Tornado, while the free and open source GCC caught up when using many cores. Owing to network related problems our relatively small domain for Hamburg performed efficiently for only up to eight cores (for details see Langkamp and Böhner 2011).

Besides the compiler, the MPI library is the second important software on HPCs. It is responsible for the efficient communication between CPUs, which is often a bottleneck due to a limited network bandwidth. However, only one MPI implementation was available for Tornado and the different tested versions turned out to be fairly equal in performance. A third performance parameter is set in `configure.wrf` (Appendix J), a file that is generated right before WRF's compilation. In this file, one of three different multi-CPU modes are configured:

- `smpar`: an OpenMP shared memory thread paradigm, not to be confused with MPI;
- `dmpar`: a MPI task distributed memory paradigm;
- `hybrid`: each MPI task spawns a number of OpenMP threads to utilize the node's shared memory.

<sup>26</sup> We chose the PGI compiler v11.1, since it produced the fewest compilation problems.

Most times `dmpar` outperforms `hybrid` and `smpar` clearly, while it is only sometimes "slightly" slower than the `hybrid` approach (Morton et al. 2009, HPC Advisory Council 2010). Thus, `dmpar` is generally recommended and was used in this research<sup>27</sup>.

An optional performance parameter selectable after WRFs compilation is `numtile` (Appendix M). WRF decomposes the domain into tasks or patches each assigned to a core via a MPI process. Each patch can be further decomposed into tiles that are processed separately, but by default there is only one tile. If this is too large to fit into the CPU cache it slows down computation due to WRFs memory bandwidth sensitivity (Roman 2009). In order to reduce the size of the tiles, it is possible to increase their number via `numtile = x`. The best value found was six tiles for the used eight cores. However, the optimal value depends on the cache sizes of core and CPU, the number of assigned cores, and the size of the domain. Thus, six is only a rough guide.

## 5.2 ERA Interim preprocessing and domain setup

WRF was configured using the ERA-Interim Reanalysis (ERA-I) as its forcing. Implementing ERA-I is not straight forward, because there is no standard output of it. To avoid complications we downloaded ERA-I in GRIB format at full resolution and with model levels<sup>28</sup>. All used parameters and grid transformations are documented in Appendix K.

The model domain was set up with a two-way nesting of a 1:5 ratio. The three nests had a horizontal resolution of 25, 5, and 1 km and a vertical resolution of 60 model levels each (Fig. 5.2.1). The 1:5 ratio saves computing time in comparison with the alternative 1:3 ratio (27, 9, 3, and 1 km). A sensitivity study by Liu et al. (2012) on different ratios revealed that the ratios 1:5 and 1:7 can also perform as well as the generally recommended 1:3 ratio. The size of the nests were determined by the goal to include all nLUC data within the inner domain of 1 km. Some details on the inner domain are given in Fig. 5.2.2. The distances between the nests were automatically set by Domain Wizard (DW HP 2011).

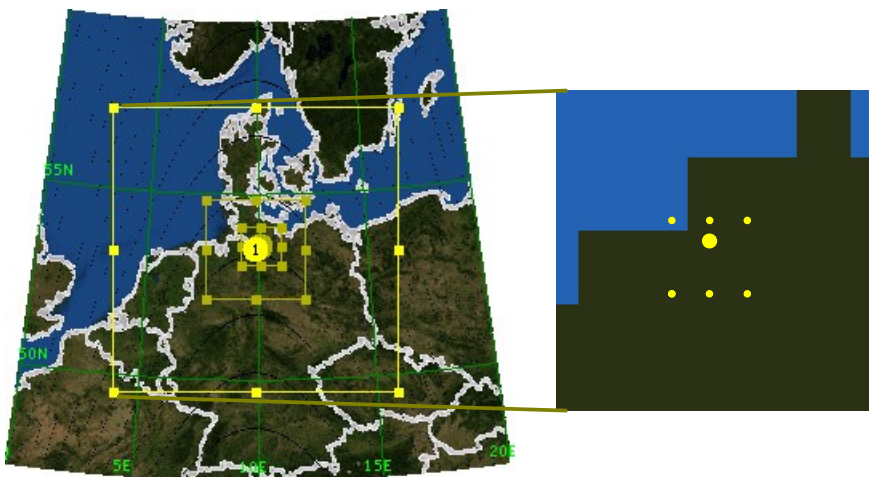


**Fig. 5.2.1** The WRF domains with three nests and the ERA-I land-sea mask.

Consider the nest configuration (left) and the ERA-I land-sea mask (right) for the extent of WRFs outer domain of 25 km. It consists of the North Sea to about one fifth. The Baltic fills the small part of the north east corner. The big yellow dot marks the center position of all collected measurements.. The small yellow dots mark the grid points of ERA-I, that were interpolated on the measurements coordinates (cf. Chapter 6).

<sup>27</sup> Another prerequisite to compile WRF is the network Common Data Format (netCDF, here v4.01). A specialized version of netCDF that affects the performance in combination with domains containing several hundred million cells is parallel netCDF (pNetCDF HP 2012). More WRF performance and compilation hints are available in Langkamp and Böhner (2011) and the WRF online tutorial (2012).

<sup>28</sup> The European Centre for Medium-Range Weather Forecasts (ECMWF HP 2011) offers the fully resolved (T255, N128, L60) ERA-I version for free since 2012. In 2011 we received ERA-I from DKRZs Climate and Environmental Retrieval and Archive (CERA HP 2011). The surface pressure (ID 134) was received by a separate file server.

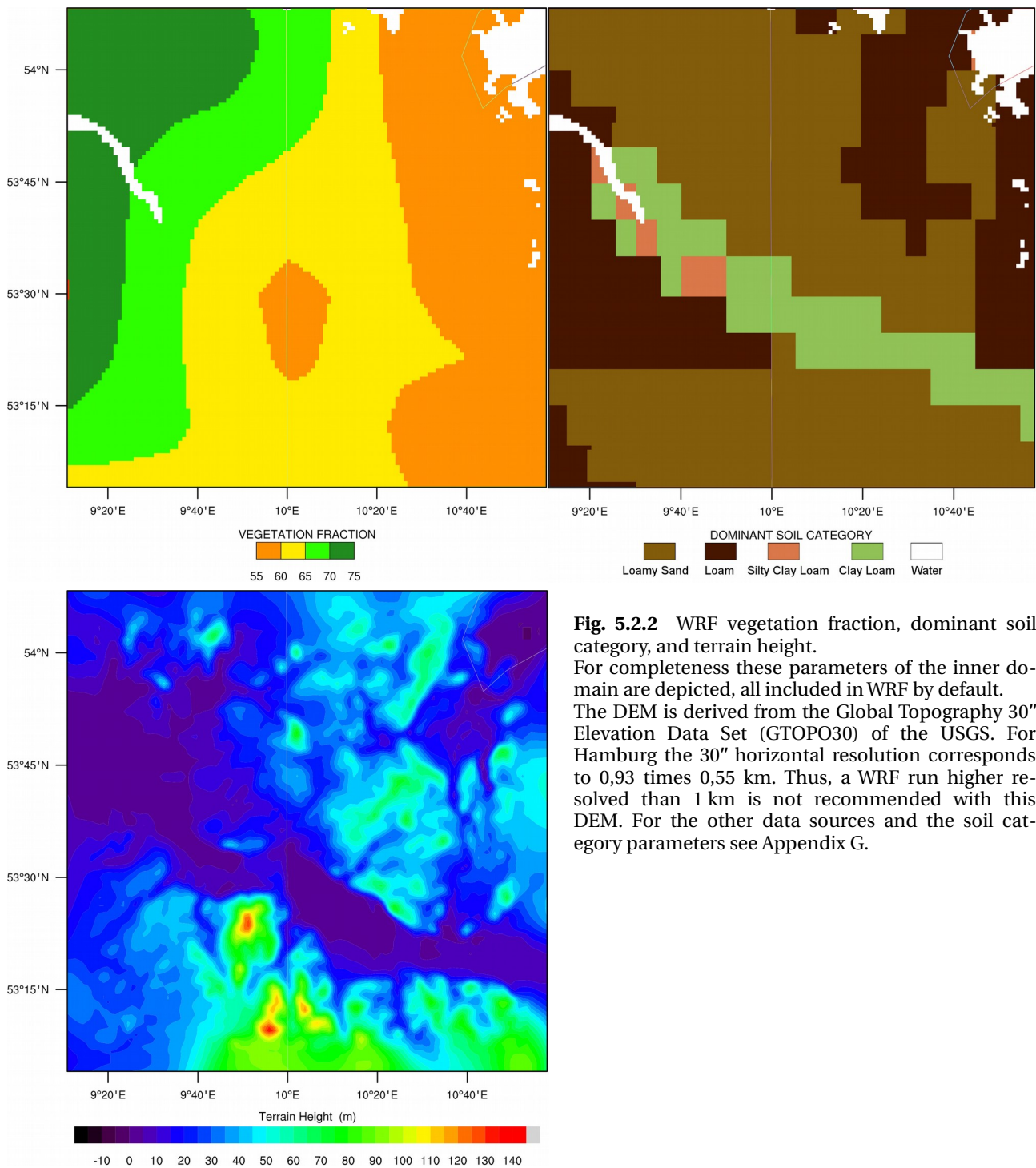


**Fig. 5.2.2** WRF vegetation fraction, dominant soil category, and terrain height. For completeness these parameters of the inner domain are depicted, all included in WRF by default. The DEM is derived from the Global Topography 30" Elevation Data Set (GTOPO30) of the USGS. For Hamburg the 30" horizontal resolution corresponds to 0,93 times 0,55 km. Thus, a WRF run higher resolved than 1 km is not recommended with this DEM. For the other data sources and the soil category parameters see Appendix G.

The set of used WRF physic modules was chosen following the recommendations of Wang et al. (2012) for high resolution and regional climate runs (for the configuration files `namelist.input` and `namelist.wps`, and the correct use of ERA-I with model levels see Appendix L, M, and N). To run WRF on a HPC a jobscript is needed (Appendix O), that starts the selected number of processes, each at one core<sup>29</sup>.

<sup>29</sup> For very large domains it is advisable to compile WPS with multi-core support. In this way the preprocessors `geogrid` and `metgrid` can run on multiple cores via the jobscript; `ungrib` can run at a single core only.

### 5.3 WRF roughness sensitivity tests

To test the WRF embedded nLUC, including the spatially differentiated roughness data, and compare it with WRFs original LUC (oLUC) a sensitivity study with ERA-I forcing was accomplished. It analyzed the effect of altered roughness on modeled 2 m air Temperature (T2) and the wind pattern qualitatively. The hottest week in 2003 in Hamburg was chosen, to cover an extreme temperature signal: 6 till 12 August. Three runs with the following modeling setups were performed.

A: modified oLUC: urban  $z_0 = 0.0001$  m (set in `LANDUSE.TBL`, Appendix I)

B: unmodified oLUC: urban  $z_0 = 0.8$  m

C: spatially differentiated nLUC: 14 urban classes with different  $z_0$  values<sup>30</sup>.

Exemplary results from all 3 runs are shown in Fig. 5.3.1. In general, all runs show a similar wind direction pattern and low wind speeds, with an exception for the Baltic Sea in the northeast corner. However, the wind speed overall is slightly lower in A.

It is conspicuous that WRF models too high T2 above the river Elbe (Fig. 5.3.1) for all three runs, except for the nLUC area of C. This is caused by the oLUCs low  $z_0$  of the class `Water`, generating a reduced vertical momentum flux, when combined with general low wind speeds. Regarding the river Elbe, this effect was only observed for one further day, also during noon. The Baltic Sea, however, stays always cool because of its high heat capacity. Like the river Elbe, A reveals a much higher T2 above the smoothed surface, due to the reduced vertical momentum flux. Accordingly, the vertical temperature gradient of the lower troposphere is significantly higher in A. In contrast B and C reveal an increased eddy activity, lifting up the warm air (Fig. 5.3.3 left). The cross-section plots on the right side also show significant differences in RH, negatively correlated to the temperature.

The observed more differentiated T2 in C corresponds to the differentiated representation of the nLUC. This is primarily caused by the increased spatial accuracy and resolution of the data on which the nLUC is based. Comparing the results of B and C, land use features like big parks or suburbs are missing or underrepresented in B. Additionally, the higher number of classes of the nLUC leads to a better T2 differentiation of C (cf. Chapter 6). Many small suburbs of Hamburg show their own small UHIs in C, but not in B. This can be seen best in Fig. 5.3.2 with highlighted contours, without the wind, and supplementary as a difference plot. The increased T2 differentiation is not restricted to the suburbs, but can also be seen for big areas of the class `Urban green`, like the biggest city park (Volkspark), the woods Niendorfer Gehege, and the Ohlsdorfer cemetery (all three marked with black circles in Fig. 5.3.1). They are spatially better represented with the nLUC than with the oLUC and show cool islands.

The following runs for the summer 2011 will quantitatively show if the higher T2 differentiation of the nLUC run is actually more realistic (Chapter 6). These runs are compared with the temperature measurements presented in Chapter 3.

<sup>30</sup> The actually used values (Appendix I) were different from those in Table 4.4.1, due to an early nLUC version. Since the roughness rank was the same, this does not affect the results of this qualitative analysis.

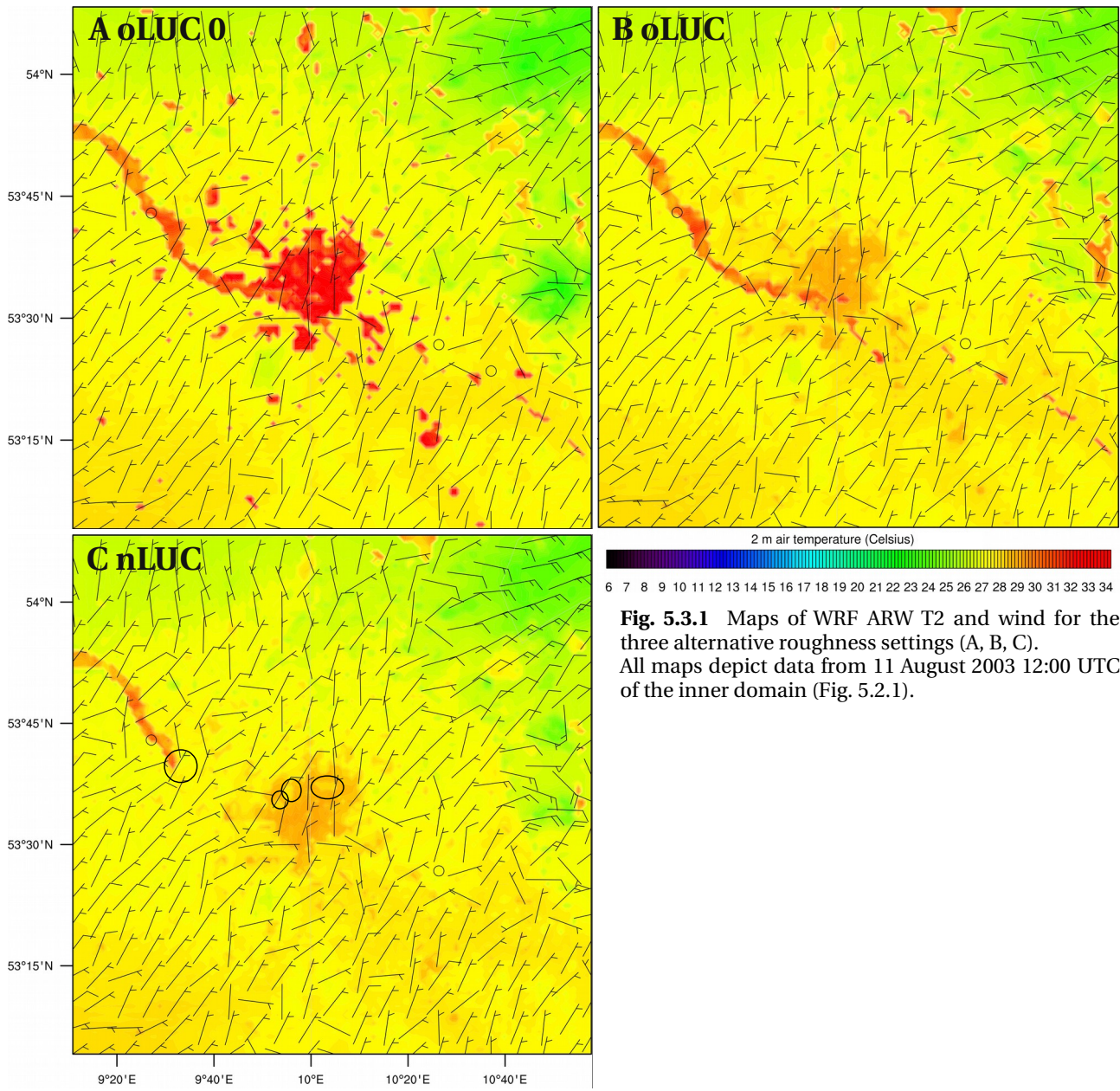


**Fig. 5.3.1** Maps of WRF ARW T2 and wind for the three alternative roughness settings (A, B, C). All maps depict data from 11 August 2003 12:00 UTC of the inner domain (Fig. 5.2.1).

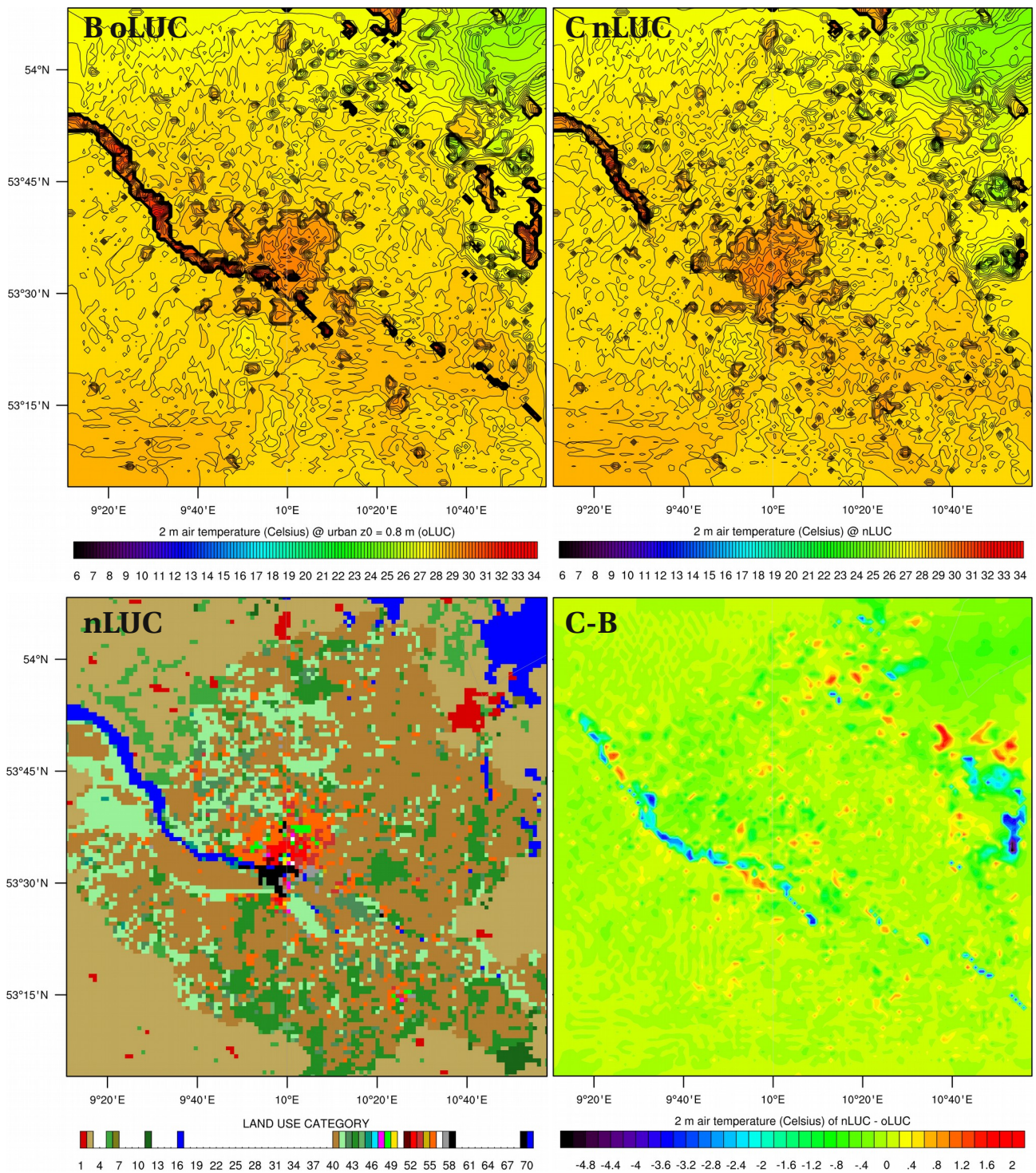


**Fig. 5.3.2** 0.2 K contours of B and C, the nLUC, and the C-B difference.

The WRF maps depict data from 11 August 2003 12:00 UTC. All maps show the area of the inner domain of 1 km resolution (Fig. 5.2.1).

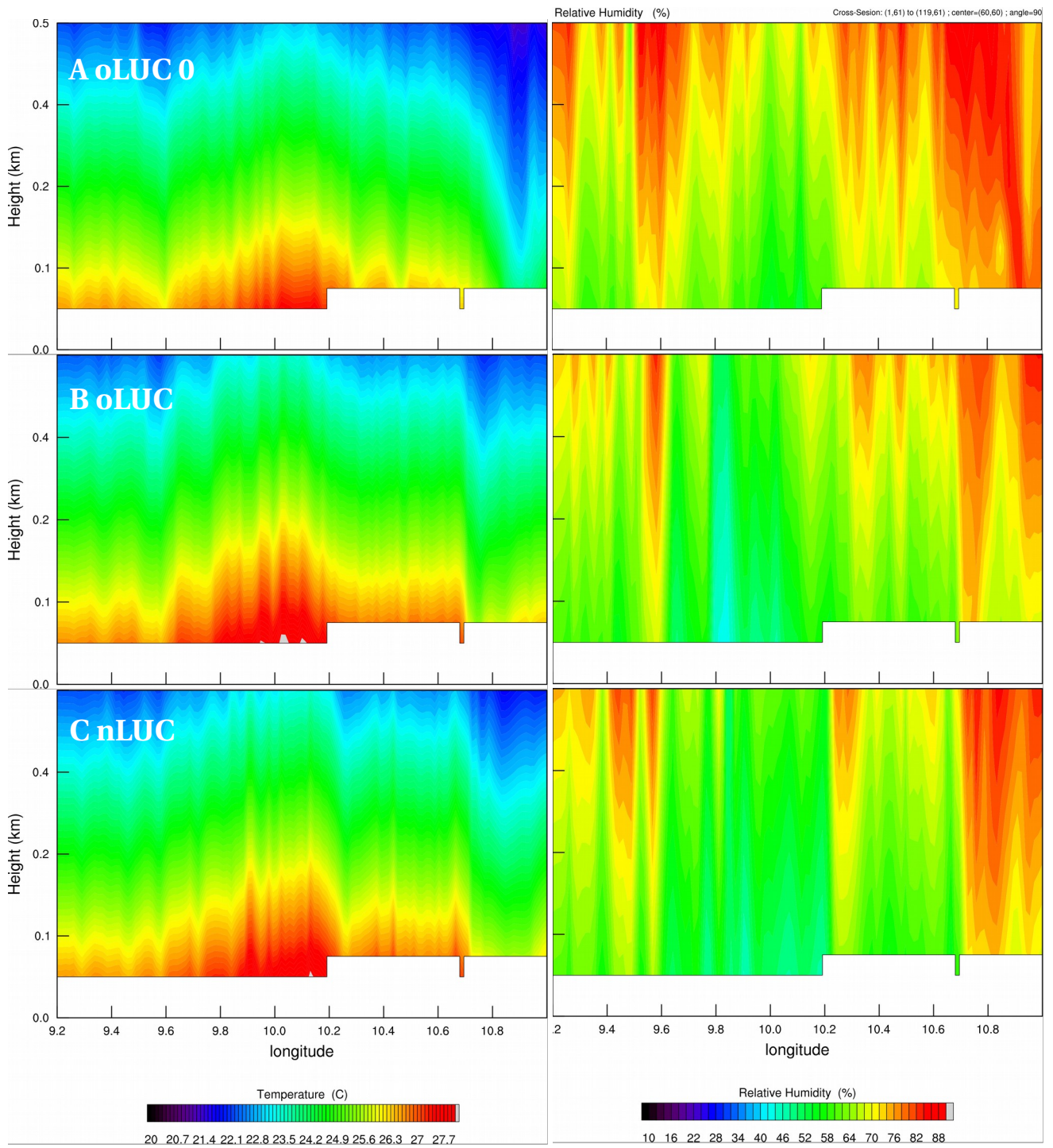


**Fig. 5.3.3** Vertical temperature and RH for a 90° cross-section of the plots in Fig. 5.3.1. The bottom white space results from the terrain height above NN, see Fig. 5.2.2 bottom right.

# 6 Sensitivity study results of the improved LSM

For Chapter 6 the WRF **configurations B and C** (Section 5.3) **are referred to as the oLUC and nLUC runs**, the name highlighting their different roughness layers. Both were modeled for the period of 1 May till 25 June 2011<sup>31</sup>. The period was not extended to October (the end of the bus measurement campaign), because of the relatively cold late summer. Also the warmest months in 2011 – May and June – were not nearly as warm as the summer 2010. In May and June 2011 there were only three days with a daily mean above 20 °C (Fig. 6.1.1). Thus, it is desirable to continue the mobile measurement campaign, until a year with a heat wave like 2003 or 2010 is covered.

The WRF output files were written at a high temporal resolution (30 min). An even higher resolution would improve the comparison with the discontinuous bus measurements – which have been aggregated into 1 min means (Section 3.6). However, an increased WRF output frequency was not possible due to limitations in data storage capacity. Thus, for the comparison with the model only bus measurements of  $\pm 2.5$  min around the 30 min WRF time stamp were included in the sensitivity study. To compare the gridded WRF output with the tabular empirical data, multiple postprocessing steps were necessary: The empirical data was exported to point shape files, synced with WRFs UTC time zone, and projected onto WRFs grid. The T2 and other grids of every time step were then B-spline interpolated<sup>32</sup> onto the DB exported measurements' point shapes. A full documentation of the postprocessing is given in Appendix P.

In this manner, the runs oLUC, nLUC, and the ERA-I forcing could be compared with the **combined** stationary and mobile measurements. Rather than just simply averaging ERA-I, oLUC, and nLUC data over the whole inner domain, the gridded data were **B-spline interpolated onto the measurements' point data for the selection that had measurement neighbors in space and time**. This interpolated selection of model data was then averaged and compared with the measured data. All displayed data averaged this way, is marked with the prefix "**Mean**" in the following figures. Graphs with the prefix "**Point**" are representing data from the single DWD station Fuhlsbüttel or the neighboring model grid point.

To clarify: All **figures** of Chapter 6 present the spatial means, of the **interpolated spatial selection of T2** (model) or the **non-interpolated spatial selection of T** (measurements) and further meteorological variables. The **tables** present also results from the same spatial data selection, but not necessarily temporal means.

## 6.1 Temperature

In focus is the evaluation of temperature data, since the modeling goal was a better representation of the UHI. Table 6.1.1 present statistics that show a cold bias for ERA-I, that is equated by WRF to some degree. The reason of ERA-I's cold bias is seen in Fig. 5.2.1, where the ERA-I grid points are marked, which were interpolated onto the measurement coordinates and, also, were forcing WRF. The grid point on the North Sea introduces an overestimated T2 damping affect. This is quite strong, because the actual North Sea is scattered and shallow and accordingly has a lower heat capacity compared to its model in ERA-I. Thus, the oLUC run is about 0.5 K and the nLUC run about 0.9 K warmer. The measurement data is even 2.9 K warmer than ERA-I and shows a higher standard deviation ( $\sigma$ ). To model such a variability and such a measurements' range, WRF would need to be run in much higher resolution than 1 km.

The nLUC run, however, shows a small improvement compared to the oLUC run in mean and  $\sigma$  and a big improvement compared to ERA-I. Fig. 6.1.1 shows the temporal course of the daily data. The model data shows the biggest cold bias for the warmest days, which is consistent with the previous argumentation. The nLUC run shows the biggest improvements also for the warmest situations.

31 Each run was splitted in 5 parallel runs, one using 8 cores. Altogether the 80 cores needed almost 2 weeks to compute the results. The last and the first 24 h of each part were computed overlapping to enable deletion of the parts where the model needed time to transient.

32 Note that every interpolation introduces a new source of error. About the pros and cons of different interpolation methods like the B-Spline see Meijering (2002) and Mitas and Mitasova (1999).

Table 6.1.2 presents Pearson's  $r$  for the measurements correlated with WRF and ERA-I data. The low coefficients represent the missing temperature variance in the model data, because of the dampening character of the North Sea's overestimated heat capacity.

[°C]	T	T2 oLUC	T2 nLUC	T2 ERA-I
Min	-1.30	5.00	5.00	4.80
Max	31.40	24.90	24.90	18.80
Mean	15.77	13.39	13.80	12.92
$\sigma$	4.93	3.25	3.46	2.40

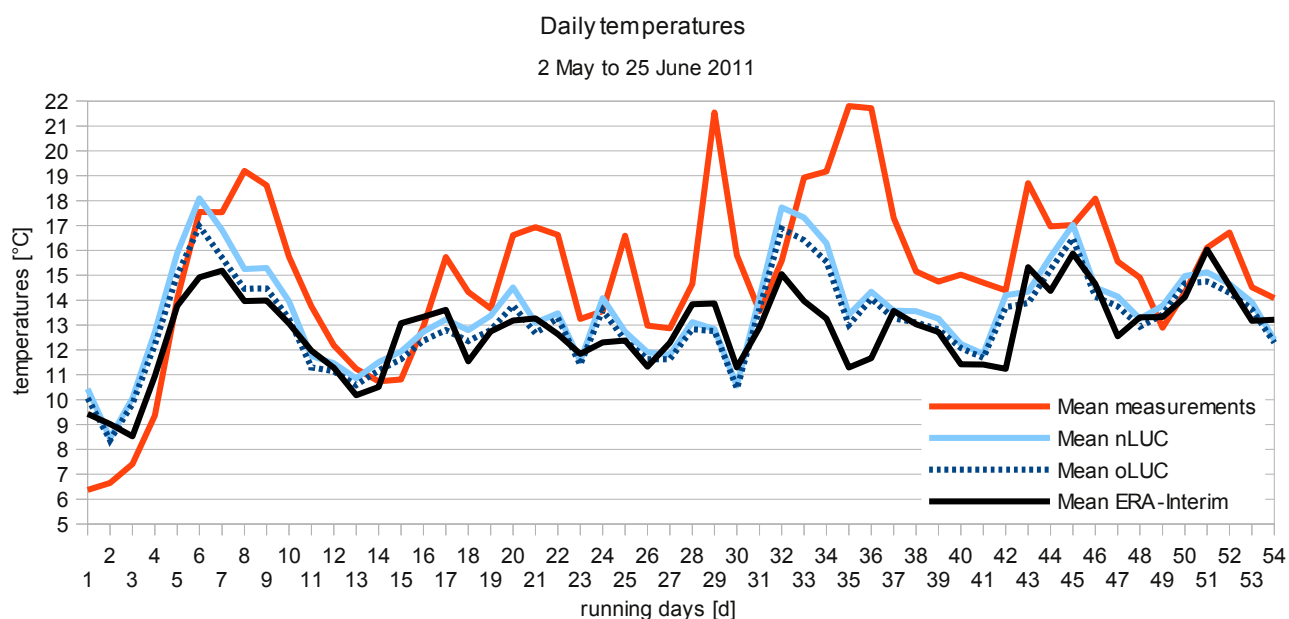
**Table 6.1.1** Some statistics on the 6 hourly data.

Extreme low and high temperatures are not modeled by WRF or ERA-I, the standard deviation ( $\sigma$ ) is also much smaller. ERA-I shows an overall cold bias and a lower  $\sigma$  which consequently influences WRF. The cause is seen in Fig. 5.2.1 within ERA-I's bad spatial representation of the North Sea shore line.

[r]	T to T2 oLUC	T to T2 nLUC	T to T2 ERA-I
0 UTC	0.53	0.53	0.44
6 UTC	0.15	0.10	0.33
12 UTC	0.52	0.54	0.43
18 UTC	0.46	0.45	0.27

**Table 6.1.2** Pearson's  $r$  on the data that was available for ERA-I's temporal resolution (6 h).

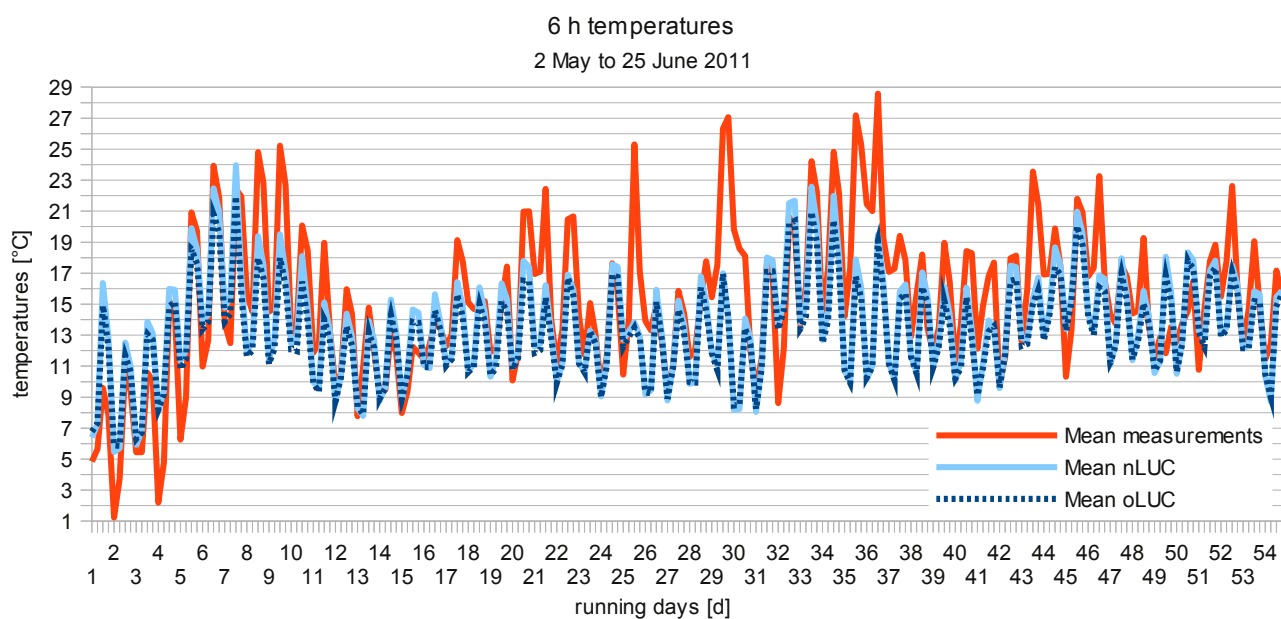
Pearson's  $r$  of T to WRF is higher than for T to ERA-I except for 6 UTC. There is no significant difference between the oLUC and the nLUC run.



**Fig. 6.1.1** Daily means of T2 from measurements and WRF runs.

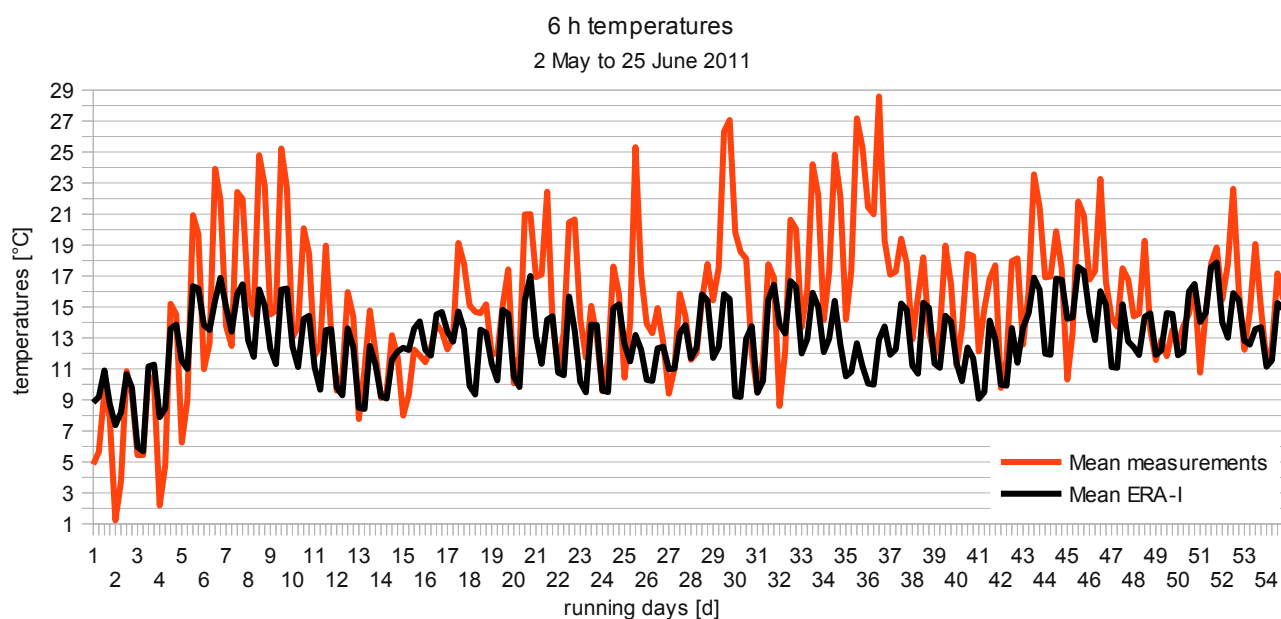
On some days the measurements are much warmer than the model data. This can be attributed to the far too cold ERA-I forcing.

Fig. 6.1.2 and 6.1.3 basically display the same data as Fig. 6.1.1, but at 6 hourly resolution. The higher resolution reveals that the general diurnal pattern and its amplitude is captured well by WRF, while the amplitude is much too low for ERA-I.



**Fig. 6.1.2** 6 hourly data of temperatures from measurements and WRF runs.

This is the same data as in Fig. 6.1.1 but 6 hourly and the ERA-I data is displayed in Fig. 6.1.3 for better legibility.



**Fig. 6.1.3** 6 hourly data of temperatures from measurements and ERA-I.

This is the same data as in Fig. 6.1.1 but 6 hourly and without the WRF data, displayed in Fig. 6.1.2.

Fig. 6.1.4 and 6.1.5 show the diurnal pattern and its bias in hourly resolution and, additionally, the pattern for met stations only. The latter shows that the bus measurements are not warm biased compared to the met station data. This could be suspected, since the buses basically collected data in potentially warmer street canyons. However, the met station curve is almost identical to the combined measurements.

The added value of the nLUC run during noon can be explained by the influence of the warmer river Elbe, due to its higher nLUC roughness. This is not affected by stronger near surface vertical momentum flux here – which would have a cooling effect – since the stronger advection covers its effect (Fig. 6.1.6).

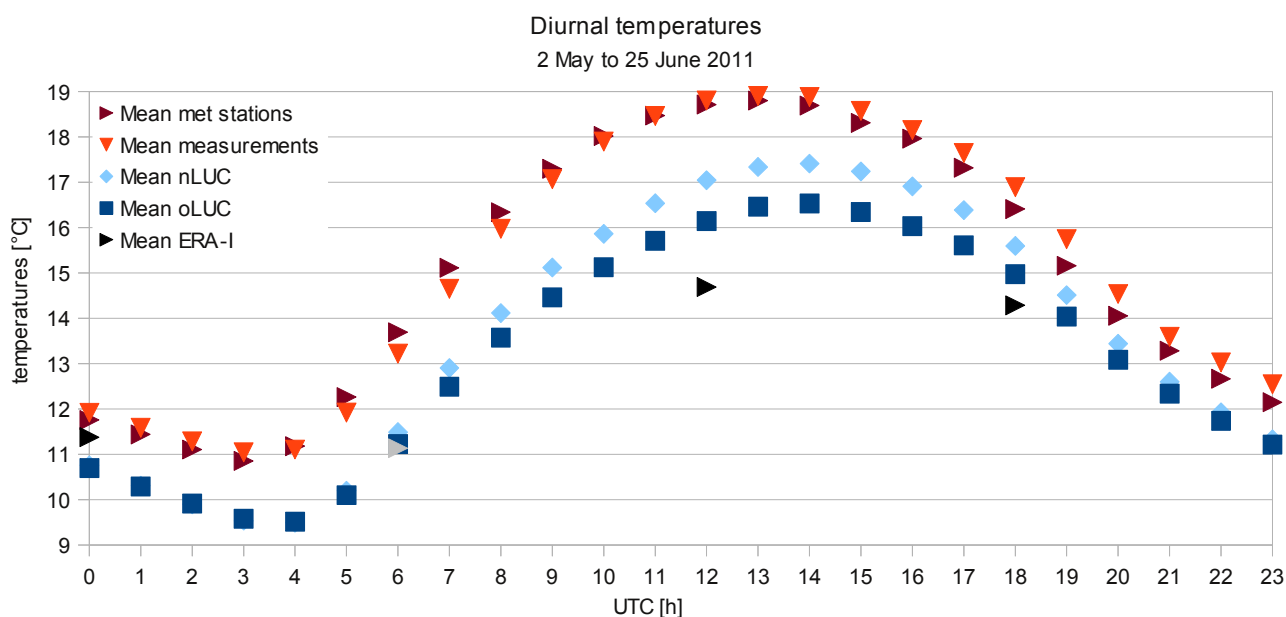


**Fig. 6.1.4** Diurnal hourly temperature for measurements, WRF, and ERA-I.

To further analyze the bus measurements for a warm bias compared to the met station data, the graph also shows the mean for met stations only. The other curves illustrate Fig. 6.1.2 in more detail: The nLUC run is warmer than the oLUC run mainly during noon, WRF is cold biased, and the measurements higher in temperature than all model data.

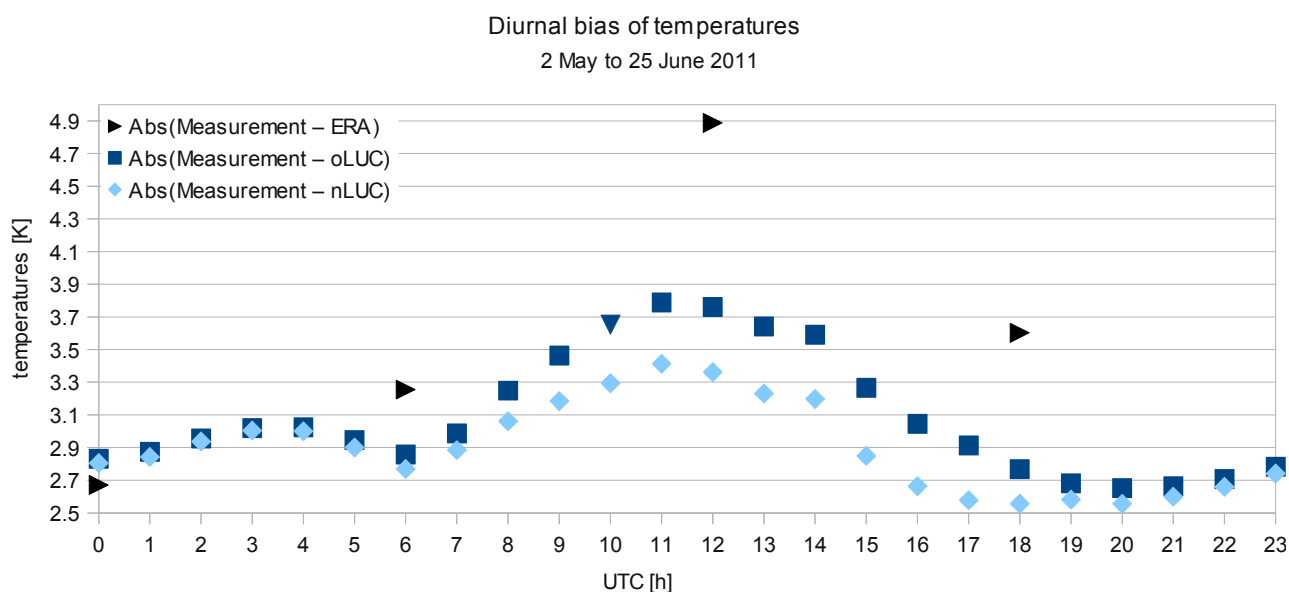


**Fig. 6.1.5** Diurnal hourly bias of temperature.

The spatial T2 pattern (Fig. 6.1.6) shows the same added value as already seen in the sensitivity test (Section 5.3), even though it was run with a newer nLUC version with small roughness differences (Table 7.2). For example, the roughness of the class *Water* was higher (0.0031 vs. 0.0025 m), introducing more near surface vertical momentum flux – and thus cooling – as found in the sensitivity test. Besides, throughout the whole modeling period, no situation with warm biased air over the Elbe could be observed (Fig. 5.3.1) in the oLUC area. This can be explained with the general higher wind speeds during that period.

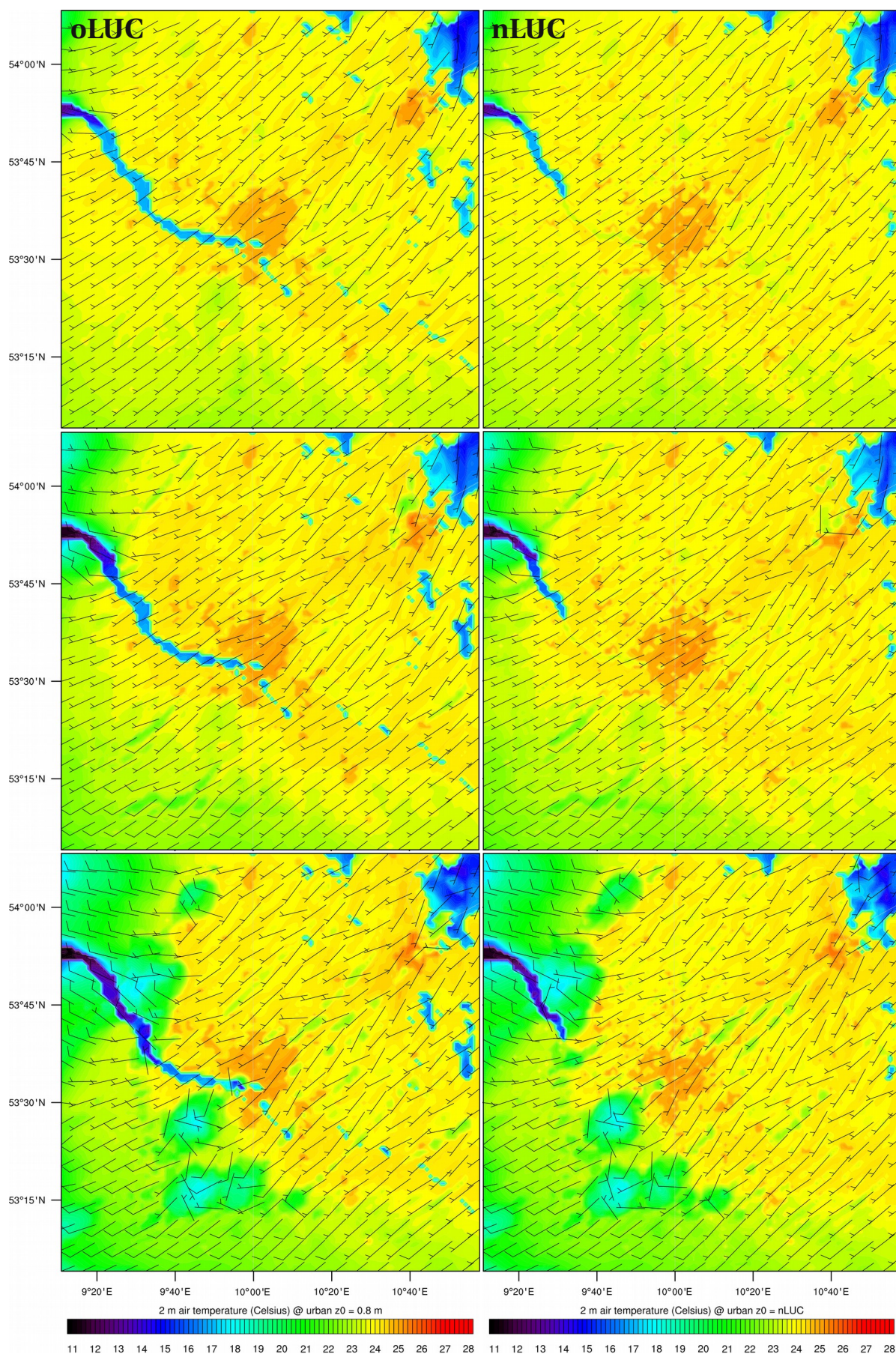


**Fig. 6.1.6** WRF oLUC and nLUC T2 and wind for 8 May 2011, 12:00 to 13:00 UTC. This day has the highest T2 peak within the modeling period (peak of measurements: 6 June 2011, Fig. 6.1.2).

## 6.2 Surface wind field

Additionally the WRF runs were evaluated versus 10 m wind velocity and surface pressure at the single point of the DWD airport station Fuhlsbüttel. The following table depicts statistical characteristics of hourly values for the modeling period 2 May and 25 June 2011 are given in the following table.

	Measured	oLUC	nLUC
Min [m/s]	0.30	0.04	0.03
Max [m/s]	9.00	16.70	15.44
Mean [m/s]	3.81	4.70	4.35
$\sigma$ [m/s]	1.94	2.61	2.36
r		0.44	0.46

**Table 6.2.1** Statistics of the hourly 10 m mean wind velocities.

Extreme low and high wind velocities modeled by WRF are not recorded by the point measurement. Mean and standard deviation ( $\sigma$ ) are also smaller. Pearson's  $r$  of the measurements to the nLUC is slightly higher than those to the oLUC mean velocities.

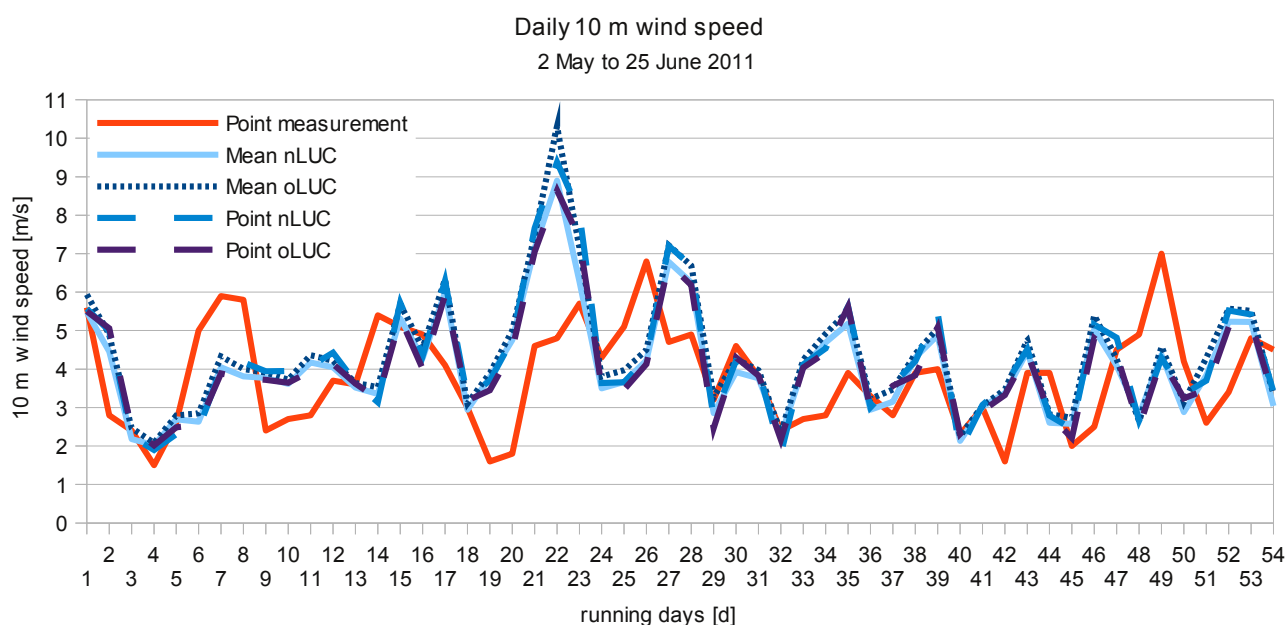


**Fig. 6.2.1** Daily 10 m wind speed of WRF and measurements.

The solid and fine dashed blue lines are the spatial means averaged over the whole domain, similar to Fig. 6.1.1. The rough dashed drawn lines are only for the WRF grid point neighbor of the DWD airport station Fuhlsbüttel (Table 7.1). The Point oLUC and nLUC patterns are very similar to the spatial mean patterns.

In general, the WRF wind speed is higher compared with the DWD measurement. The point nLUC has higher wind speeds than the point oLUC, while it is the opposite for the mean values. This is caused by the lower roughness of the nLUC run class *Airport* (0.25 m), compared with the oLUC run and its single urban class (0.8 m). The lower roughness reduces the near surface vertical momentum flux. This effect is inverse when advection is dominant due to higher horizontal wind speeds. The phenomenon can also be seen at the not overheated river Elbe (Fig. 6.1.6). The mean oLUC has higher wind velocity overall, which implies that the overall area weighted roughness of oLUC is lower than of nLUC.

The diurnal analysis (Fig. 6.2.2) shows higher model wind velocities especially during the night and general lower wind speeds for the measurements. The nLUC run shows a small added value over the oLUC run also during night. The diurnal pattern in general is well reproduced.

The almost identical surface pressure pattern (Fig. 6.2.3) of the two WRF runs match the measurement pattern but is about 5 hPa lower, due to the limited vertical resolution of WRF.

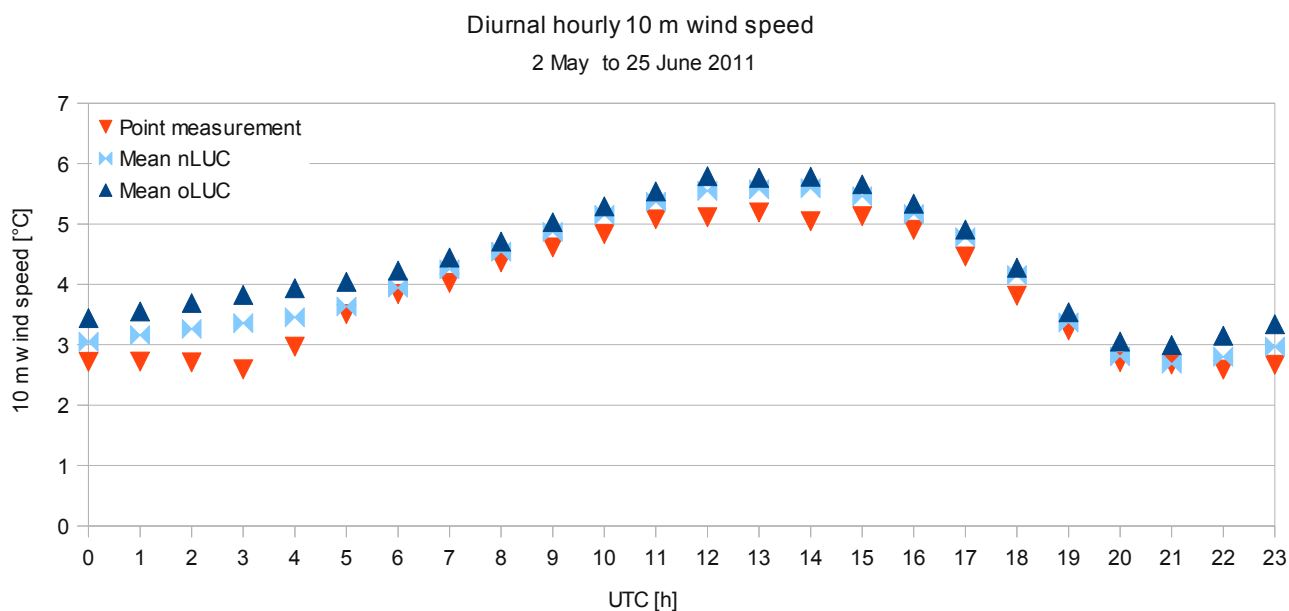


**Fig. 6.2.2** The diurnal hourly 10 m wind speed for measurements and WRF

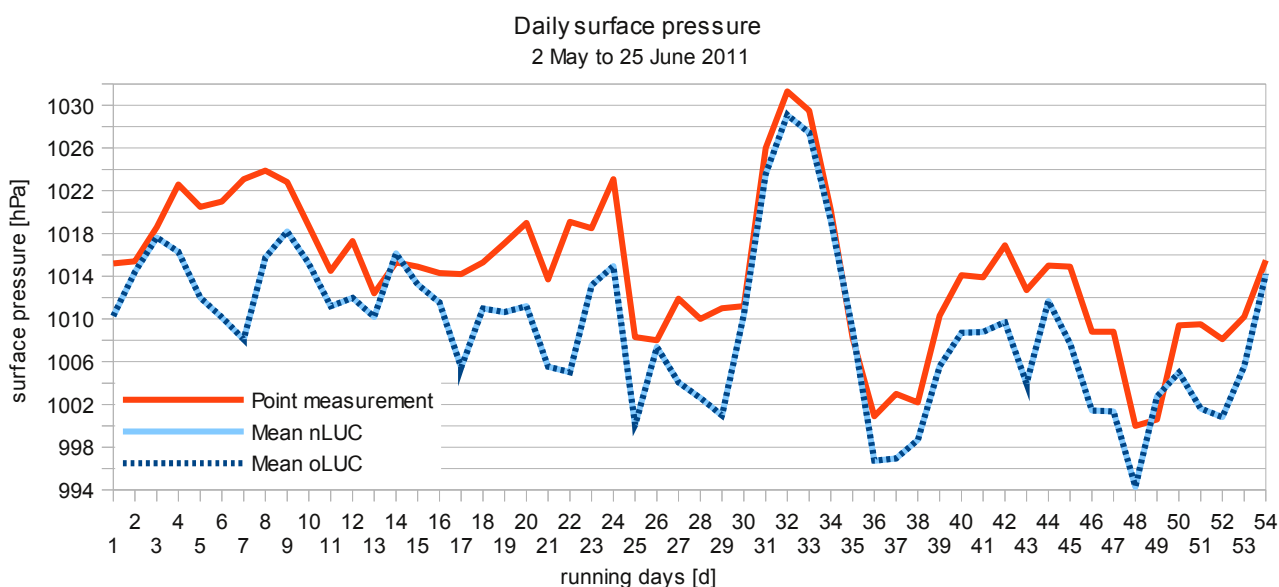


**Fig. 6.2.3** Daily surface pressure of WRF and measurements.

### 6.3 Circulation types

WRF was also analyzed regarding an objective circulation type classification (i. e. the objective “Wetterlagenklassifikation”) by the DWD (Table 6.3.1):

ID	Acronym	Wind direction	Cyclonicity at 950 hPa	Cyclonicity at 500 hPa	Humidity
1	XXAAT	not defined	anticyclonic	anticyclonic	arid
2	NOAAT	northeast	anticyclonic	anticyclonic	arid
3	SOAAT	southeast	anticyclonic	anticyclonic	arid
4	SWAAT	southwest	anticyclonic	anticyclonic	arid
5	NWAAT	northwest	anticyclonic	anticyclonic	arid
6	XXAAF	not defined	anticyclonic	anticyclonic	humid
7	NOAAF	northeast	anticyclonic	anticyclonic	humid
8	SOAAF	southeast	anticyclonic	anticyclonic	humid
9	SWAAF	southwest	anticyclonic	anticyclonic	humid
10	NWAAF	northwest	anticyclonic	anticyclonic	humid
11	XXAZT	not defined	anticyclonic	cyclonic	arid
12	NOAZT	northeast	anticyclonic	cyclonic	arid
13	SOAZT	southeast	anticyclonic	cyclonic	arid
14	SWAZT	southwest	anticyclonic	cyclonic	arid
15	NWAZT	northwest	anticyclonic	cyclonic	arid
16	XXAZF	not defined	anticyclonic	cyclonic	humid
17	NOAZF	northeast	anticyclonic	cyclonic	humid
18	SOAZF	southeast	anticyclonic	cyclonic	humid
19	SWAZF	southwest	anticyclonic	cyclonic	humid
20	NWAZF	northwest	anticyclonic	cyclonic	humid
21	XXZAT	not defined	cyclonic	anticyclonic	arid
22	NOZAT	northeast	cyclonic	anticyclonic	arid
23	SOZAT	southeast	cyclonic	anticyclonic	arid
24	SWZAT	southwest	cyclonic	anticyclonic	arid
25	NWZAT	northwest	cyclonic	anticyclonic	arid
26	XXZAF	not defined	cyclonic	anticyclonic	humid
27	NOZAF	northeast	cyclonic	anticyclonic	humid
28	SOZAF	southeast	cyclonic	anticyclonic	humid
29	SWZAF	southwest	cyclonic	anticyclonic	humid
30	NWZAF	northwest	cyclonic	anticyclonic	humid
31	XXZZT	not defined	cyclonic	cyclonic	arid
32	NOZZT	northeast	cyclonic	cyclonic	arid
33	SOZZT	southeast	cyclonic	cyclonic	arid
34	SWZZT	southwest	cyclonic	cyclonic	arid
35	NWZZT	northwest	cyclonic	cyclonic	arid
36	XXZZF	not defined	cyclonic	cyclonic	humid
37	NOZZF	northeast	cyclonic	cyclonic	humid
38	SOZZF	southeast	cyclonic	cyclonic	humid
39	SWZZF	southwest	cyclonic	cyclonic	humid
40	NWZZF	northwest	cyclonic	cyclonic	humid

**Table 6.3.1** The objective circulation type classification by the DWD. The colors explain the acronyms. See DWD HP (2012b) for the current data archive. (DWD HP 2012a)

The circulation type specific analysis of the WRF daily mean temperature differences clearly reveal a distinct sensitivity of modeled temperatures towards the synoptic conditions. The classified daily means show that the average deviations between the two WRF runs and the measurements are exceptionally cold biased for the circulation types 28 and 29 with their southern wind direction (Fig. 6.3.1). This is because WRF did not reproduce these circulation types at all. Instead WRF produced north-west winds at the days the types 28 and 29 occurred, most likely due to a too small WRF domain and already wrong ERA-I input.

The difference between oLUC and nLUC run reflect the overall higher temperature of the nLUC run, with the main improvement for class 1 (anticyclonic, arid), while class 2 is even warmer.

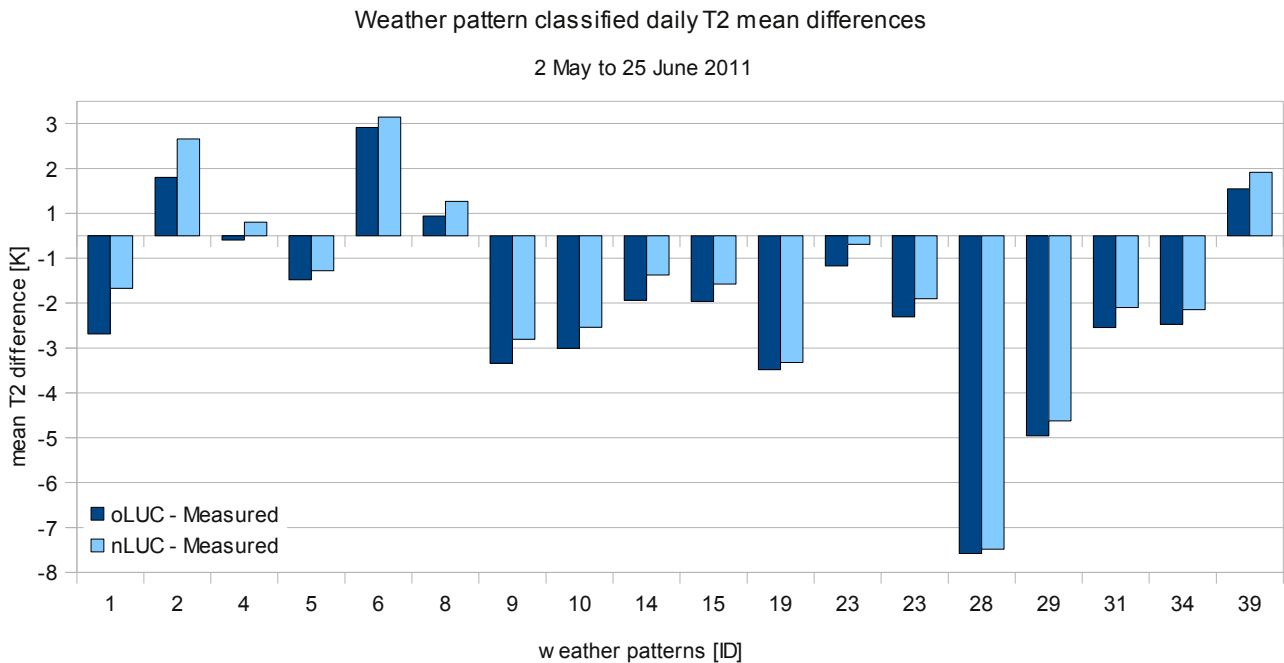


**Fig. 6.3.1** Average T2 deviation of daily data for objective DWD circulation types (DWD HP 2012a). The circulation types 28 and 29 jut out with their cold bias. Both differ in the wind direction only (Table 6.3.1).

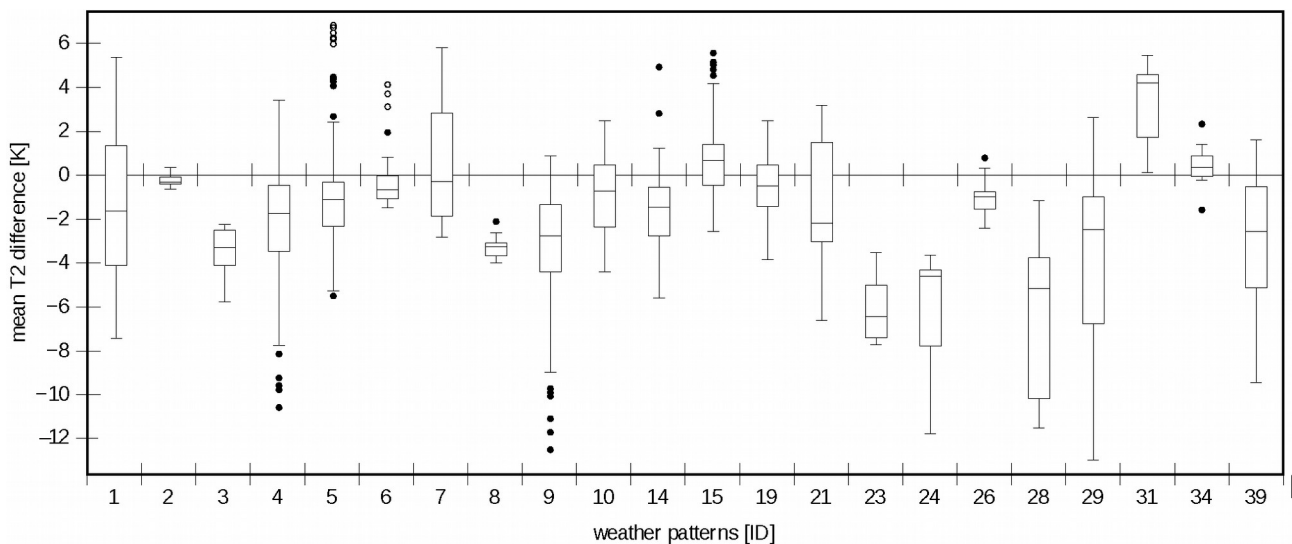


**Fig. 6.3.2** Average T2 deviation of the oLUC hourly data

When extending the analysis to hourly modeled and measured data, classified with either 00:00 UTC circulation types and additionally 12:00 UTC forecasts (DWD HP 2012c), the results reveal further details. Now the mean differences of the types 9, 23, 24, 28, 29, and 39 are very pronounced (Fig. 6.3.2, 6.3.3). All have a southern wind direction, most have humid conditions, and same cyclonicities.

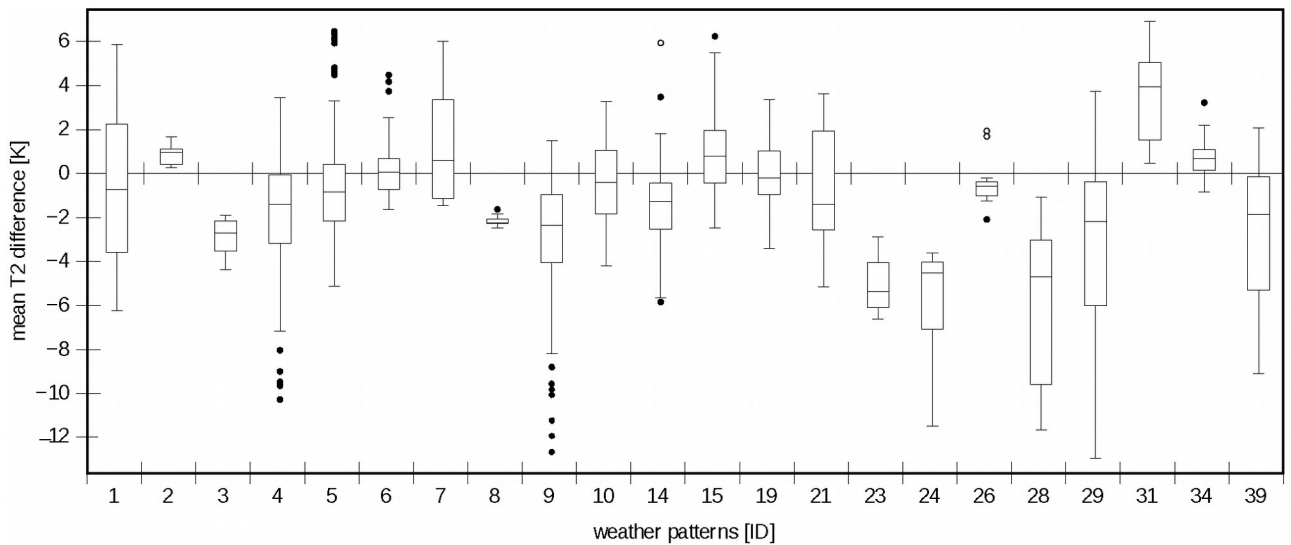


Fig. 6.3.3 Average T2 deviation of the nLUC hourly data

The warm biased circulation types are 2, 6, 8, and 39 from the daily analysis (Fig. 6.3.1) and 2, 6, 7, 15, 31, and 34, for the hourly analysis (Fig. 6.3.2 and 6.3.3). They have a northern or undefined wind direction (except 34) with mostly anticyclonic curvature on the 950 hPa level (except 31 and 34). Those warm biased types mostly occur during cold cut-off situations especially for circulation type 7, 15, and 31 (Wetterzentrale.de HP 2012). As ERA-I has a too low resolution to reproduce cold cut-off situations and as the outer WRF domain does not match the area of upper troposphere cold air formation, this phenomenon is missing in the WRF simulations.

Variance analysis of the weather pattern classified temperatures

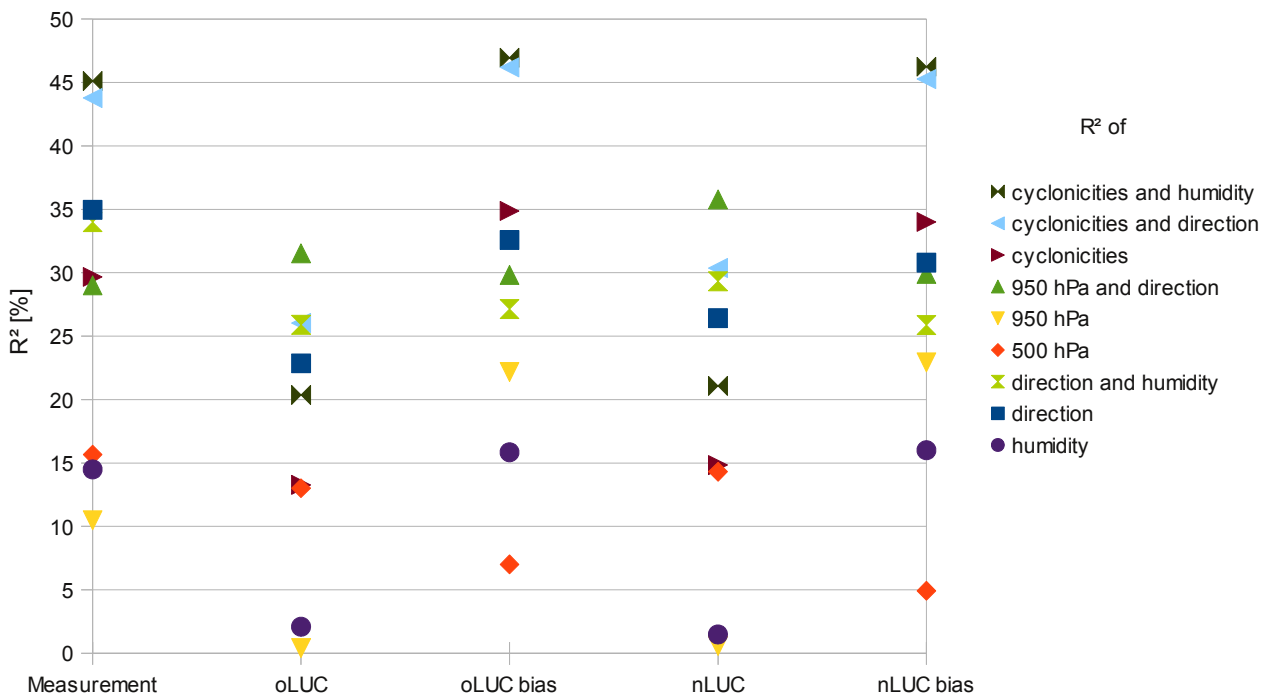


Fig. 6.3.4 ANOVA with given R<sup>2</sup> of different circulation type combinations (colored).

An analysis of variance (ANOVA) was used to identify parameter combinations of lowest and highest  $R^2$  when classifying the temperature data. This is useful for later statistical downscaling (SD) approaches of the WRF output as explained in Section 2.2. The parameters with the lowest  $R^2$  will likely yield the highest added value from SD using a circulation type approach. The results from the variance analysis also explain the preceding figures in more detail. The nLUC run yield overall higher explained variance than the oLUC run as expected from the previous results. The parameter combination 950 hPa cyclonicity and wind direction (light green), has the highest coefficient of determination ( $R^2$ ) for both WRF runs. This means, that circulation types with these parameters are modeled best by WRF. In contrast, the higher the  $R^2$  of the bias, the worse is WRF modeling the measured circulation types and the more the dynamically downscaled WRF results will benefit of SD, utilizing the circulation type classification.

The combination of the cyclonicities and the humidity (dark green) gives the highest  $R^2$  of above 45% for the measurements and the model biases. The WRF runs only yield 27% here. The combination of cyclonicity and wind direction (light blue) is similar, but with 5 to 10% higher  $R^2$  for the WRF runs.

To give a summary of Chapter 6: Pressure and wind are modeled accurate in comparison to temperature, due to a cold biased ERA-I forcing. The diurnal temperature analysis showed, that the added value for the nLUC run is highest during noon and on warm days. This temperature error decrease for the nLUC run during noon, with its faster winds, can be explained by the increased influence of the roughness: At higher wind velocities the improved roughness layer shows its benefits.

The circulation type analysis showed that cold air troughs or types with southern wind directions are not captured by ERA-I or WRF. The result was a warm bias for the cold air trough types and a extreme cold bias for the southern wind direction types. In addition an ANOVA identified cyclonicity in combination with humidity as the most important parameters to utilize in the SD.

## 6.4 Discussion

The spatial heterogeneity of the urban climate with its constant changes in vertical momentum flux could be modeled more accurately through introducing a spatial improved roughness layer. At the same time a significant bias still needs to be attributed in further research. The bias consists of errors introduced by ERA-I input data and of errors that originate in the still missing urban climate features like modified radiation patterns etc. as only  $z_0$  was modified. Other urban climate studies that used urbanized LSMs partly show similar temperature bias (Chen 2010, Flagg 2012, Holt 2007, Kusaka 2009, Lo 2007, Loridan 2010, Miao 2009, Oleson 2008, Otte 2004, Pedro 2012, Smolarkiewicz 2007, Taha 2007, Tewari 2010), but are not directly comparable to the results shown in this study as they used different models and / or setups (domain, resolution, time, evaluated parameters etc.). Hence, there is a need for runs on the same domain but with different RCMs and / or LSMs to complete this research; and for runs on another domain with the same setup.

However, the concentration on one model and the single parameter  $z_0$  was needed for this research and yielded results that compare the added value of WRFs default LSM and its improved version.

# 7 Conclusions and Outlook

This research stated these questions in Chapter 1:

- Are remotely sensed raster topographies suitable to parameterize the heterogeneous urban surface roughness and its influence on the surface wind field?
- How can the parameterization be linked to a new LUC – optimized on use in urban climate studies – to implement it into RCMs, enabling RCM scenario runs also including scenarios of urban development?
- Leads such a surface roughness parameterization to an added value in a RCM?
- Which systematic biases of RCM results compared to measurements can be identified in dependence to circulation types to develop SD methods?
- Can spatiotemporal highly resolved mobile measurements be suitable to enlarge the data basis needed for SD and are they suitable to evaluate RCMs? Which conceptual requirements are needed to make them suitable?

These questions are answered as in the following:

We demonstrated the feasibility of parameterizing sub-grid scale processes in urban climate modeling, using digital surface models obtained from remote sensing data (IFSAR, Bechtel and Langkamp et al. 2011) within the RCM WRF ARW v3.3 at 1 km horizontal resolution. The sensitivity studies identified the added value of a new surface roughness parameterization, influencing the urban wind- and temperature-field. The higher differentiated  $z_0$  data includes the information on the overall morphology, isotropy, and texture of all obstacles instead of the individual building geometry like expensive 3D data. Given the vast and ubiquitous availability of this new generation of remote sensing geodata, our approach opens new options for modeling urban climates in developing countries despite poor geodata infrastructures, since the roughness parameterization is easily transferable and remains operational for scenario simulations due to a new LUC (Daneke, Bechtel, and Langkamp 2010). The nLUC is a more detailed classification of urban morphologies optimized for climate use and derived from Stewart and Oke's (2009, 2012) local climate zones.

Although there are already different approaches available to model the urban canopy more precisely since WRF ARW v3.1 (Chen et al. 2010), they are all computationally too demanding for urban planning relevant resolutions and time spans. In this respect, our approach integrates the nLUCs with the computationally less demanding default land surface model of WRF, which is a simple 5-layer thermal diffusion (soil temperature only) scheme.

Referring to Burian et al. (2004:6) there is a lack of adequate methods which "efficiently and accurately produce gridded coverage of roughness parameters". Also our new roughness data is still not gridded but class based. Thus, it can be easily exchanged, to incorporate land use scenarios for WRF climate scenario runs, depicting the dynamic urban system. The land use scenarios origin is a separate, already operational urban land use model, set up by C Daneke. With it, changes of the constant evolving city are implementable in WRF or any other RCM using the new LUC. Other available RCMs and their urban canopy modules still do not take changes of the city's morphology into account. One disadvantage of the class based data is the limitation in the number of classes. This results in a loss of variability and a homogenization of the actually heterogeneous roughness in the urban boundary layer.

To evaluate the new land use data with its differentiated roughness values a vast amount of data was collected incorporating mobile and stationary measurements into a climate data base that is available for the scientific community. The mobile measurement campaign was carried out with buses of a local public transportation company and yielded results of the required minimum travel speed due to the sensors' sensitivity and the ideal logger position on the bus roof. Due to the concentration on a few bus lines, the data was spatially not as extensive as anticipated. However, the possible suggestion, that the mobile measurements may reflect mainly the temperature from warmer street canyons, or might be warm biased due to other influences could be refuted by comparing it to the met station collective. The campaign yielded new and spatial explicit results, but has to be continued to cover years with heat waves like 2003 or 2010 and further weather conditions.

The sensitivity study of the WRF runs showed qualitative and quantitative added values especially during noon and on warm days, despite a cold biased ERA-I forcing. The spatial pattern appeared qualitatively more differentiated and reasonable as big urban greens were modeled cooler than the surrounding land use. The correlation, however, was not significantly higher for the new LUC. A variance analysis identified potential for further improvements through SD for specific circulation types that are not modeled well by WRF.

Climate research and in particular urban climate modeling initiatives targeted in CliSAP-2 and other future research projects will increasingly utilize the extensively available remotely sensed geodata and delineated land use information. This will lead to a distinctly improved digital representation of orographic and topographic settings, improved in terms of spatial and temporal resolution, thematic differentiation, and reliability. State of the art numerical modeling approaches will be able to increasingly exploit their potential through focussing on the near surface small scale processes, that represent the heterogeneous urban surface. In addition, contemporary GIS and data base integration will enable the statistical downscaling to high, urban planning relevant, resolutions. This enables the adaption of the city and can mitigate the impacts of problematic climate change.

The main enhancement of the new LUC presented in this research lies in providing more classes of urban roughness. The number of roughness classes and other parameters, however, will be increased further within RCMs and statistical methods to capture the heterogeneous urban canopy even better. As the proposed roughness parameterization is transferable to other cities in the world utilizing the LUC, its correlation with land use data of other cities should be evaluated. Afterwards the transfer of the model to cities that suffer from fast changing climate conditions can be approached. In addition, further steps such as advanced radiation schemes, improved layers of soil sealing, albedo, vegetation fraction, or heat storage and emissivity have to be added to the classification and thus to RCMs. To fill the gap of spatial resolution, the biggest opportunity for improvement is seen in the combination of SD and DD. Although the parameterization of topographically determined processes is an emerging field in SD and DD (Böhner & Antonic 2008) to refine climate model outputs for environmental modeling applications, the parameter-definition from remotely sensed raster topographies in urban climate modeling is apparently new and its development will continue.

In the long run the goal is to create an integrated operational urban climate modeling chain, which uses consistent parameterizations in DD and SD combined with an online running dynamic land use model. Such model coupling is a precondition to foresee urban climate in terms of changing temperatures, reflecting both independent drivers: global climate change and changes of the urban built environment. Based on the empirical results of this operation it becomes possible to define urban vulnerabilities from the perspective of physical expositions. These expositions will be linked to urban social area analysis which allows an identification of the affected population groups for an integrative climate related risk and impact assessment (cf. Oßenbrügge et al. 2012).

As soon as we understand these factors better, we can efficiently mitigate and adapt the cities according to climate change impacts. Thus the urban model development also has to be translated into urban planning applications and policy measures on a broad scale.

# Appendix

## A Met station data sources and details

- 4 DWD stations: The German weather service once had six stations within Hamburg, today only three are operative. The 4th station we used (in Quickborn) is outside of Hamburg (DWD WebWerdis HP 2012).
- 3 HaLm stations: The ambient air pollution network of Hamburg has ten stations, of which only four are still measuring, one on the roof of a high building, the data of which was not used (HaLm HP 2012).
- 6 HUSCO stations: The Hamburg urban soil climate observatory of the university of Hamburg has five stations that started measuring during September 2010, one in august 2011 (HUSCO HP 2012).
- 1 MI-station: The meteorological institute of the university of Hamburg runs instruments at two so called weather-masts. From its origin the tall mast is a radio transmission tower. It is 300 m high and measures at 50, 70, 110, 175, 250 and 280 m, and another in a distance of 170 m that is 12 m high and measures at 10 and 2 m (MI HP 2012).
- 18 school stations: The school measurement network is run by Frank Böttcher, founder of the wetterspiegel.de GmbH, in cooperation with schools in Hamburg and other cities. It has 25 stations that started measuring between 2009 and 2012. Two of them are placed on high buildings, one was not operative in 2011 and three are in cities over 100 km away from Hamburg (Wetterspiegel HP 2012).
- 7 SRHH stations: The winter road clearance service of the Hamburg city cleaning service (SRHH) has nine stations, two of them on the Köhlbrand bridge, that crosses the river Elbe at a height of 55 m and is heated by a waste incineration plant at the shore beneath (SRHH HP 2012).
- In cooperation with the DWD the KLIMZUG NORD project also collected and provided us with data from many stations of North Germany. In the end those could not be utilized, as they were too far away from Hamburg. (KLIMZUG NORD HP 2012)

Source	Name	start date	end date	lon	lat	height over NN [m]	height over terrain [m]	coordinate / location quality	frequency
DWD	Fuhlsbüttel 3	2000-01-01	2011-10-31	53.63500	9.99000	11	2	certain	60 min
DWD	Mittelnkirchen-Hohenfelde	2004-09-01	2011-10-31	53.55280	9.60940	1	2	certain	60 min
DWD	Neuwiedenthal	2003-03-01	2011-10-31	53.47940	9.89860	3	2	certain	60 min
DWD	Quickborn	1988-11-01	2011-10-31	53.73470	9.87860	13	2	certain	60 min
HaLm	Billbrook Pinkertweg am Industriekanal	1987-01-01	2011-10-31	53.53098	10.08339	5	3.5	certain	10 min
HaLm	Bramfeld Umweltzentrum Karlshöhe	2000-01-01	2011-10-31	53.63246	53.63246	30	3.5	certain	10 min
HaLm	Finkenwerder West Neßkatenweg 1a	2004-01-01	2010-10-27	53.53777	9.84542	0	3.5	certain	10 min
HUSCO	HafenCity Vattenfall Am Dalmannkai 1	2011-08-31	2011-10-23	53.54240	9.99640	8	2	certain / low (near power station)	5 min
HUSCO	Innenhof Schulbehoerde An der Stadthausbruecke 1	2010-09-06	2011-10-23	53.55263	9.98552	9	2	certain	5 min
HUSCO	Langenhorn Grünfläche Tweeltenmoor 11	2010-09-22	2011-10-23	53.67889	10.02604	23	2	certain	5 min
HUSCO	Langenhorn Wohngebiet Foßberger Moor 31	2010-09-08	2011-10-23	53.68061	10.01333	26	2	certain	5 min
HUSCO	Stellingen Grünfläche Gazelenkamp 138	2010-09-24	2011-10-23	53.60206	9.93682	14	2	certain	5 min
HUSCO	Stellingen Wohngebiet Wördemanns Weg 48	2010-09-06	2011-10-23	53.59966	9.92698	21	2	certain	5 min
MI	Wettermast	2004-12-31	2011-10-31	53.51990	10.10510	0	2	certain	1 min
Schools	Ahrensburg	2009-01-30	2011-07-03	53.67985	10.21780	48	2	uncertain height over NN (source google-earth)	5 min
Schools	Blankenese	2009-02-04	2011-11-13	53.56482	9.82545	39	2	see above	5 min
Schools	Bramfeld	2011-09-15	2011-11-19	53.46026	9.97371	20	2	see above	5 min
Schools	Buxtehude	2009-01-30	2011-11-19	53.47620	9.69267	5	2	see above	5 min
Schools	Finkenwerder	2009-03-05	2011-11-19	53.53139	9.87573	4	2	see above	5 min
Schools	Heidberg	2009-01-30	2011-11-19	53.67156	10.02699	28	2	see above	5 min
Schools	Jenfeld	2010-07-07	2011-11-19	53.58004	10.12741	20	2	see above	5 min
Schools	Norderstedt	2009-01-30	2011-11-19	53.70223	10.00741	33	2	see above	5 min
Schools	Poppenbüttel	2009-02-09	2011-11-19	53.66561	10.07505	32	2	see above	5 min
Schools	Rahlstedt	2009-01-30	2011-11-19	53.60086	10.14503	31	2	see above	5 min
Schools	Rotherbaum	2009-01-30	2011-11-19	53.57208	9.99227	20	2	see above	5 min
Schools	Sasel	2009-02-09	2011-11-19	53.65947	10.11529	30	2	see above	5 min
Schools	Sinstorf	2009-01-30	2011-11-19	53.43071	9.96943	43	2	see above	5 min
Schools	Süderelbe	2009-01-30	2011-11-19	53.47041	9.86581	29	2	see above	5 min
Schools	Wandsbek	2009-12-16	2011-11-19	53.57772	10.07860	15	2	see above	5 min
Schools	Wilhelmsburg	2009-01-30	2011-11-17	53.50355	9.99378	4	2	see above	5 min
Schools	Winsen/Luhe	2009-08-13	2011-11-19	53.36452	10.22010	7	2	see above	5 min
Schools	Eidelstedt	2009-01-30	2011-11-11	53.61344	9.88799	22	2	see above / low (near bad isolated building)	5 min
SRHH	Alte Schmiede	2006-11-30	2011-12-20	53.66863	10.12501	28	2	certain	5 min
SRHH	Am Botterberg	2006-11-28	2011-12-20	53.57419	9.83524	27	2	certain	5 min
SRHH	Ausschläger Allee	2005-11-09	2011-12-20	53.52648	10.06989	5	2	certain	5 min
SRHH	Billwerder Billteich	2006-11-27	2011-12-20	53.50303	10.13983	0	2	certain	5 min
SRHH	Jahnring	2005-10-28	2011-12-20	53.60056	10.02448	12	2	certain	5 min
SRHH	Rossdamm	2005-10-28	2011-12-20	53.52077	9.97184	2	2	certain	5 min
SRHH	Schiffbeker Weg	2005-11-08	2011-12-20	53.55716	10.11571	17	2	certain	5 min

**Table 7.1** Detailed station meta data for evaluated stations only.

Some stations are placed on high buildings<sup>33</sup> or were not operative for the desired period. The school station Eidelstedt is located near a poorly insulated building, but could be used, since the heat from the building impacts measurement only during winter (Fischer 2010).

<sup>33</sup> Two are placed on the Köhlbrand bridge, that crosses the river Elbe at a height of 55 m and is heated by a waste incineration plant at the shore beneath

## B Bus data processing R-script with hints and comments

If you never ran R before I recommend this GUI: <http://rstudio.org>.

The following R-script reads ASCII (.txt, .asc, .csv) T or RH data from files named only after the logger number (for our case 1 to 15; for example 1.csv), while it is not important, if a number is missing, or if there are more than 15. The GPS data to merge comes from a different folder, because of the same file-naming scheme. The folders are named wXgps, wXtemp, wXrf (w = week, X = running number of week). T and RH data are then linearly interpolated to 1 s and merged with the GPS data with the timestamp as the merging ID (be aware of identical timezones!). The data is also cut off for GPS measured speeds below 12 and above 100 km/h, then it corrects the logger-offsets, and writes the result into the folder wboth as file wX.

Note the following points:

- The script can be run from anywhere, when the path given with `setwd` is altered appropriately. As the measure campaign goes forward the DRAFT of the script has to be copied to the bottom of BODY and filled with the new weeks number (just search and replace the ??? and delete the leading #).
- It is not important, that the data in the folder w3temp is really of week 3. It can also be from week two. It is only important that w3temp and w3gps contain data from the same week.
- You will have to fill in your own logger-offset values at `korrrtemp` and `korrrrf`!
- To run the script for RH instead of T just search and replace `temp` with `RH`.
- If you do use different loggers, remember to adapt the script to their output format (e.g. different column-order etc.).
- If the script produces strange T or RH values it is normally because of mixing up `.` and `,`. When the raw data uses `.` for as the floating point, the file must be read in with `read.delim`, otherwise with `read.delim2`.

Below follows the DRAFT and a step by step commented "ready to go" example for week 1.

```
##### DRAFT start #####
# setwd("./w???temp")
# filenames <- list.files(path=getwd())
# numfiles <- length(filenames)
# for (bus in c(1:numfiles)) {
# assign(gsub("[.]ASC$", "", filenames[bus]), read.delim2(filenames[bus], fileEncoding="ISO-8859-15", skip = 4))
# }
# temp = sapply(ls(), get)
# temp = temp[sapply(temp, is.data.frame)]
# temp <- lapply(temp, function(x){names(x) <- c("date", "time", "temp", "");
# x <- zoo(x$temp, as.POSIXct(paste(x$date, x$time), format="%d.%m.%y%H:%M:%S"));
# x <- merge(x, zoo(order.by=seq(start(x), end(x), by=1)));
# x <- na.approx(x);
# x <- data.frame(date=format(index(x), "%y%m%d"),
# time=format(index(x), "%H:%M:%S"), temp=coredata(x));x})
# setwd("./w???gps")
# filenames <- list.files(path=getwd())
# numfiles <- length(filenames)
# for (bus in c(1:numfiles)) {
# assign(gsub("[.]csv$", "", filenames[bus]), read.csv(filenames[bus]))
# }
# gps = sapply(ls(), get)
# gps = gps[sapply(gps, is.data.frame)]
# gps <- lapply(gps, function(x) {x <- x[,c(6,7,9,11,13,14,15)];
# names(x) <- c("date", "time", "lat", "lon", "alt", "spe", "hea");
# x <- x[x$spe > 12,];
# x <- x[x$spe < 100,];
# x <- zoo(x[,c(3,4,5,6,7)], as.POSIXct(paste(x$date, x$time), format="%Y/%m/%d%H:%M:%S"));
# x <- data.frame(date=format(index(x), "%y%m%d"),
# time=format(index(x), "%H:%M:%S"), x=coredata(x));x})
```

```

# w??? <- Map(merge, gps, temp)
# korrtemp <- list("1"=-
0.0677690903,"2"=0.10277464,"3"=0.2722224798,"4"=0.0116334387,"5"=-
0.0277553916,"6"=0.0349158412,"7"=-0.0028280998,"8"=0.1009495609,"9"=-
0.1331905866,"10"=0.1331592554,"11"=-0.1200578152,"12"=-0.2911220934,"13"=-
0.0227859501,"14"=0.0336250088,"15"=-0.0237711978)
# korrRH <- list("1"=-0.3668802007,"2"=-
0.0444436644,"3"=0.3250458892,"4"=0.2882650833,"5"=-0.0471502382,"6"=0.3110665003,"7"=-
0.3325128242,"8"=-0.0731869114,"9"=0.4660252378,"10"=0.3356343921,"11"=-
0.1480803135,"12"=-0.0011558338,"13"=0.0926787542,"14"=-0.896215936,"15"=0.0909100653)
# for(nam in names(w???)) {w???[nam][['temp']] <- w???[nam][['temp']] + korrtemp[[nam]]}
# for(nam in names(w???)) {w???[nam][['RH']] <- w???[nam][['RH']] + korrRH[[nam]]}
# df??? <- ldply(w???)
# write.csv(df???,file="./wboth/w???.csv")
# rm(list = ls())
# gc(TRUE)
##### DRAFT end #####

#####
# Commented example script for week 1
#####

# HEADER -- only needed once
#####
library(zoo) # loads a necessary library to handle timestamps
library(plyr) # loads a necessary library to convert lists to dataframes (both are
special R data formats)

# BODY -- WEEK 1
#####
setwd("./wtemp") # set the path / working directory to the temperature data
filenames <- list.files(path=getwd()) # reads all data in this folder (make sure there
are NO other files in there)
numfiles <- length(filenames) # counts the number of the files in the working directory
# a for loop follows to read and number the files after their name but without the ending
(.ASC); in addition the loop cuts of the first 4 rows with irrelevant informations
(change if your files do not have those)
for (bus in c(1:numfiles)) {
assign(gsub("[.]ASC$", "", filenames[bus]), read.delim2(filenames[bus], fileEncoding="ISO-
8859-15", skip = 4))
}
temp = sapply(ls(), get) # get all objects that are now loaded and write them to one list
called "temp"
temp = temp[sapply(temp, is.data.frame)] # keep only data.frames in "temp" (throws out
"numfiles" etc.)
temp <- lapply(temp, function(x){names(x) <- c("date", "time", "temp", ""); # give
reasonable names for the columns (change if needed!)
x <- zoo(x$temp, as.POSIXct(paste(x$date, x$time), format="%d.%m.%y%H:%M:%S")); # reads
the timestamp (time zone MEST) and converts it into an index
x <- merge(x, zoo(order.by=seq(start(x), end(x), by=1))); # interpolates the timestamp
from 5 to 1 s and fills the new T cells with NA
x <- na.approx(x); # interpolates T lineary to replace the NAs
x <- data.frame(date=format(index(x), "%y%m%d"), # convert the timestamp back to a
readable form
time=format(index(x), "%H:%M:%S"), temp=coredata(x));x})

setwd("./wlgps") # everything from the start, but now for the GPS data; further comments
only if new
filenames <- list.files(path=getwd())
numfiles <- length(filenames)
# instead of .ASC .csv and no header info to skip
for (bus in c(1:numfiles)) {
assign(gsub("[.]csv$", "", filenames[bus]), read.csv(filenames[bus]))
}
gps = sapply(ls(), get)
gps = gps[sapply(gps, is.data.frame)]

```

```

gps <- lapply(gps, function(x) {x <- x[,c(6,7,9,11,13,14,15)]; # keep only relevant
columns to keep the memory footprint low (you should have at least 2 GB RAM, if it was a
"good" week (data of all 15 loggers) 4 GB are better)
names(x) <- c("date", "time", "lat", "lon", "alt", "spe", "hea"); # give reasonable names
for the left columns
x <- x[x$spe > 12,];
x <- x[x$spe < 100,]; # keep only speeds between 12 and 100 km/h
x <- zoo(x[,c(3,4,5,6,7)],as.POSIXct(paste(x$date, x$time), format="%Y/%m/%d%H:%M:%S"));
x <- data.frame(date=format(index(x), "%y%m%d"), time=format(index(x), "%H:%M:%S"),
x=coredata(x));
x})

# T and GPS are ready now to be merged!
w1 <- Map(merge, gps, temp) # keeps only the intersection
# make lists of the logger-offsets including the logger numbers (temp in °C ; RH in %)
korrtemp <- list("1"=-0.0677690903,"2"=0.10277464,"3"=0.2722224798,"4"=0.0116334387,"5"=-
0.0277553916,"6"=0.0349158412,"7"=-0.0028280998,"8"=0.1009495609,"9"=-
0.1331905866,"10"=0.1331592554,"11"=-0.1200578152,"12"=-0.2911220934,"13"=-
0.0227859501,"14"=0.0336250088,"15"=-0.0237711978)
korrRH <- list("1"=-0.3668802007,"2"=-
0.0444436644,"3"=0.3250458892,"4"=0.2882650833,"5"=-0.0471502382,"6"=0.3110665003,"7"=-
0.3325128242,"8"=-0.0731869114,"9"=0.4660252378,"10"=0.3356343921,"11"=-
0.1480803135,"12"=-0.0011558338,"13"=0.0926787542,"14"=-0.896215936,"15"=0.0909100653)
# now subtract the offset for all loggers available in this week
for(nam in names(w1)) {
w1[[nam]]['temp'] <- w1[[nam]]['temp'] + korrtemp[[nam]]
}
df1 <- ldply(w1) # convert the final file back to a better readable dataframe
write.csv(df1,file="./wboth/w1.csv") # save it as a .csv
rm(list = ls()) # clear workspace to process the next week
gc(TRUE) # free RAM

```

## C Python script to find non-unique GPS values

If the above R-script complains about non-unique values, check the raw data file for doubled timestamps. That appeared in rare cases and is a GPS logger error. To check you may use this handy python script by Alexander Czech (thank you!):

```

import os, csv
files_in_folder = os.listdir("./")
for name in files_in_folder:
if name[-4:] == '.csv':
f_f = open(name)
f_f2 = open(name)
data = csv.reader(f_f)
data2 = csv.reader(f_f2)

list = []
row1list = []
row2list = []
for row in data:
rowparts = row[0],row[3],row[4]
row1list.append(rowparts)
row2list.append(rowparts)

for row in row1list:
for row2 in row2list:
if not row2[0] == row[0] and row2[1] ==
row[1] and row2[2] == row[2]:
list.append(row)
list.append(row2)

print "Dopplungen in Datei: " +str(name)
leerzeilen = 4
i_f = 1
for row in list:
print row
if i_f == leerzeilen:
print " "
leerzeilen = leerzeilen + 4
i_f = i_f + 1

else:
print "skipped " +str(name)
raw_input("press enter to exit")

```

## D SAGA GIS manuals to aggregate the bus measurements

The spatial aggregation was done via an irregular grid of route following, virtual measurement stations. The irregular grid was derived from the measurement-density-center of a regular 100 m grid laid over all original measurements.

First install SAGA GIS in the 64 bit version (<http://sourceforge.net/projects/saga-gis/>) and make sure you have at least 16 GB RAM<sup>34</sup>. If you are on Linux you have the choice of just running the binary (as under windows) or (for performance reasons) you may want to compile the recent 2.1 beta (choice 1.) that can use multiple cores. At the time you read this it may even be already released in the stable branch (choice 2.). To compile, first install the dependencies mentioned here: <http://sourceforge.net/apps/trac/saga-gis/wiki/Compiling%20a%20Linux%20Unicode%20version>

Copy and paste the whole command to your favorite terminal and press thumbs!

### 1. unstable beta:

```
svn co https://saga-gis.svn.sourceforge.net/svnroot/saga-gis/trunk && cd trunk/saga-gis/
&& autoreconf -i && ./configure --enable-unicode && make && sudo make install
```

### 2. stable version:

```
svn co https://saga-gis.svn.sourceforge.net/svnroot/saga-gis/branches/release-2-1 && cd
release-2-1/saga-gis/ && autoreconf -i && ./configure --enable-unicode && make && sudo
make install
```

### Start SAGA:

```
env LANG=C saga_gui &
```

SAGA GIS manual of aggregating the bus coordinates to an irregular 100 m grid:

- after processing the raw data with the R-script, cut out all coordinates; at Linux just use this shell script utilizing `awk` and a `for` loop:

```
for week in w*; do
  awk -v FS="," '{ print $5 "\t" $6 ; }' $week >> wAllcoords.csv ;
done
```

- double click on the final `.csv` from within SAGA GIS to import it
- use the module `convert table to points` on the imported `.csv`; you can easily find modules within SAGA by a right click on modules in the left panel and a left click on search.
- project the point shape from LAT / LON to UTM and add the UTM coordinates to the table using the following modules
- set coordinate system
- coordinate transformation
- add coordinates to points
- use the module `shapes to grid` first for the x then for the y coordinate with the settings value aggregation: mean and grid system cellsize 100m
- use the module `grid values to points` on the new x/y-mean-grids
- use the module `convert table to points` on the table with the new points with the x/y-means as coordinates (not on the original x/y coordinates)
- save as `new-network.shp`

---

<sup>34</sup> If you have 8 GB RAM you can process about 4 to 5 weeks at once and you have to repeat the procedure, construct - ing slightly different measurement networks. To merge them, calculate 100 m buffers around the point shapes of the first network and cut out all points of the other networks that are within those buffer zones. Merge the left stations with the first network.

SAGA GIS manual of mapping the measurements onto the new virtual station network

- import the data of the first week (`w1.csv`) by double click from within SAGA; if you have enough RAM, you can combine some weeks. On Linux use `cat` to put combine the files.  

```
cat w1.csv >> wALL.csv && cat w2.csv >> wALL.csv ...
```
- open the `new-network.shp` and project it back to LAT / LON
- module change time format of the `.csv` with default options
- module aggregate point observations; this uses the `.shp` and the `.csv` and calculates the means of all measurements in a custom bufferzone (for example 100 m) and within 60 s window around every station. If the 60 s window is reached, the next measurements are again averaged and saved as another 1 min measurement of that station. You have to repeat this for speed, heading, temp, **time**, and every week.
- convert the time back from s to `hh:mm:ss`.
- combine the single processed columns back to one file.

## E Data formats and constraints handled by the DBMS

A DBMS sets constraints to guarantee data integrity and automatically handles all logical dependencies. For our purpose the open source relational DBMS PostgreSQL was chosen as it can be extended with PostGIS which adds support for geographic objects. Thus, it enables an easy way of communicating and connecting a DB with GIS like SAGA or Quantum (QGIS), both open source. Those GIS can directly access the DB and visualize the desired part of the data as a map with few clicks. This makes exporting and importing the data in the right format unnecessary. The data handling can further be simplified by graphical tools like pgAdmin. The stationary data came in the following formats:

- `.csv`, `.xlsx`, `.xls`, `.xml` format;
- UNIX-timestamp, regular timestamp, only start and end timestamp;
- Coordinated Universal Time (UTC), Central European Time (CET), Central European Summer Time (CEST);
- at multiple measurement frequencies (1 min, 10 min, 20 min, 30 min, hourly, daily), averaged differently;
- from stations that moved over the years to slightly or totally different locations;
- with different coordinate formats (UTM, GK3, LAT / LON);
- measured by low or high tech equipment, coming with or without a quality flag, or a location quality flag;
- measured at different heights (2 m, 10 m, at high buildings);
- different measurands / climate factors (T, RF, wind, surface pressure, precipitation, etc.);
- different constraints in terms of who is allowed to see or use the data.

## F SQL queries to calculate the UHI

a) Calculate all temperature differences between the mobile measurements and the MI-station:

```
CREATE TABLE tom_uhi_all AS
SELECT c.id_messwerte, c.messgroesse_fk, c.zeitstempel, c.station_fk, c.logger_id,
c.speed, c.altitude, c.heading, c.messwert, c.uhi FROM
(SELECT a.id_messwerte, a.messgroesse_fk, a.zeitstempel, a.station_fk, a.logger_id,
a.speed, a.altitude, a.heading, a.messwert, a.messwert - b.messwert as UHI from
(SELECT * from messwerte where station_fk > 0 AND messgroesse_fk = 1) as a
JOIN (SELECT * from messwerte where station_fk = 0) as b
```

```

ON ((EXTRACT (YEAR FROM a.zeitstempel) = EXTRACT (YEAR FROM b.zeitstempel))
AND (EXTRACT (MONTH FROM a.zeitstempel) = EXTRACT (MONTH FROM b.zeitstempel))
AND (EXTRACT (DAY FROM a.zeitstempel) = EXTRACT (DAY FROM b.zeitstempel))
AND (EXTRACT (HOUR FROM a.zeitstempel) = EXTRACT (HOUR FROM b.zeitstempel))
AND (EXTRACT (MINUTE FROM a.zeitstempel) = EXTRACT (MINUTE FROM b.zeitstempel))))
as c
ORDER BY c.uhi ASC

```

**b) Average temperature differences, if multiple are at one station, count them and add coordinates**

```

CREATE TABLE tom_uhi_all_mean AS
SELECT * from (
SELECT count(zeitstempel) as count_measurements, avg(messwert) as ABS_temp, station_fk as
Station_ID, avg(speed) as speed, avg(altitude) as NN_altitude, avg(heading) as heading,
avg(UHI) as UHI_ref_NDR from tom_uhi_all
GROUP BY station_fk)
as a
JOIN (SELECT the_geom, stations_id from stationsnetz)
as d ON a.Station_ID = d.stations_id
ORDER BY UHI_ref_NDR ASC

```

**c) To average a specific period, skip b) and select the period from a)**

```

CREATE TABLE tom_uhi_0300_0559 AS
SELECT * from tom_uhi_all where
EXTRACT (HOUR FROM zeitstempel) >= 03
AND EXTRACT (HOUR FROM zeitstempel) <= 05
ORDER BY zeitstempel ASC

```

**d) Then go on and average as in b) for c):**

```

CREATE TABLE tom_uhi_0300_0559mean AS
SELECT * from (
SELECT count(zeitstempel) as count_measurements, avg(messwert) as ABS_temp, station_fk as
Station_ID, avg(speed) as speed, avg(altitude) as NN_altitude, avg(heading) as heading,
avg(UHI) as UHI_ref_NDR from tom_uhi_0300_0559
GROUP BY station_fk)
as a
JOIN (SELECT the_geom, stations_id from stationsnetz)
as d ON a.Station_ID = d.stations_id
ORDER BY UHI_ref_NDR ASC

```

## G Sources and contents of the default WRF surface data

The following list is summarized from the index files of the surface data itself, from Wang et al. (2012), and from Dudhia et al. (2005, Chapter 4):

- The oLUC originated from the 30" USGS data which itself originated from the global land cover characteristics database (v2.0). This database was build upon satellite data of NOAAs advanced very high resolution radiometer.
- The DEM is derived from the Global Topography 30" Elevation Data Set (GTOPO30) of the U. S. Geological Survey (USGS). For Hamburg the 30" resolution corresponds to about 0,93 times 0,55 km.
- Albedo and vegetation data are based on NOAAs National Environmental Satellite Data Field.
- An alternative LUC since WRF ARW version 3.1 is MODIS. It has 4 classes less but is more current and based on a NASA satellite analysis of the International Geosphere-Biosphere Program with the Moderate Resolution Imaging Spectroradiometer.
- The soil temperature and humidity comes from the Land and Water Development Division of the UN Food and Agriculture Organization.
- For the slope inclination data the only mentioned dates on the source is NCEP.

Soiltype (top layer 0-30 cm; bottom layer 30-90 cm), each with FAO / WMO 16-category soil texture (Wang et al. 2012 and UCAR 2002: Data Format Handbook)

Code	Description	Wilting Point	Porosity
1	Sand	0,010	0,339
2	Loamy Sand	0,028	0,421
3	Sandy Loam	0,047	0,434
4	Silt Loam	0,084	0,476
5	Silt	0,084	0,476
6	Loam	0,066	0,439
7	Sandy Clay Loam	0,067	0,404
8	Silty Clay Loam	0,120	0,464
9	Clay Loam	0,103	0,465
10	Sandy Clay	0,100	0,406
11	Silty Clay	0,126	0,468
12	Clay	0,138	0,468
13	Organic Materials	0,066	0,439
14	Water	0,000	1,000
15	Bedrock	0,006	0,200
16	Other (land-ice)	0,028	0,421

## H How to edit WRFs land surface with SAGA GIS

The nLUC data:

- Import the nLUC as a grid to SAGA GIS and project it to LAT / LON.
- With the `Grid Calculator` add 33 (this is the highest ID value of the oLUCs in `LANDUSE.TBL`) to the nLUC, so that their IDs do not overlap with the oLUCs.

The oLUC data:

- Download and unpack the whole WRF surface descriptors v3.1 (not v3.4) including the oLUCs: [http://www.mmm.ucar.edu/wrf/src/wps\\_files/geog\\_v3.1.tar.gz](http://www.mmm.ucar.edu/wrf/src/wps_files/geog_v3.1.tar.gz)
- In the `index` file from `/geog/landuse_30s` you need to increase the category value to the new class ID maximum you created in the nLUC data.
- Wang et al. (2012) mentions the files `read_geogrid.c` and `write_geogrid.c` (at `/WPSversion/geogrid/src`) to handle the binary grid format, but SAGA GIS developer O. Conrad of our working group implemented the following more comfortable SAGA GIS module for this purpose. With `Import WRF Geogrid Binary Format` open the oLUC tiles you want to modify from `/geog/landuse_30s`. Only modify the oLUC at 30" resolution. The grids at the lower resolutions contain percentages of land use per tile, which is unnecessary complicated to handle. For Hamburg the tiles are 21601–22800.16801–18000 and 22801–24000.16801–18000. One tile consists of 1200 times 1200 cells and has a little endian integer format written from bottom to top (Wang et al. 2012:3-37).

Resample and merge them:

- Resample the nLUC to the same resolution as the oLUC (30"); therefore the module `resampling` has to be applied with the `target grid system` onto the oLUC and the option `majority` as interpolation method. This overwrites the oLUC with the nLUC.

- With the grid calculator set the nodata ID of the nLUC to the same value as the nodata ID of the oLUC. Use this formula replacing the nodata ID: `ifelse((a=old-nodata-value),new-nodata-value,a)`
- Load the oLUC tiles again from `/geog/landuse_30s`.
- Merge the just loaded oLUC with the oLUC (that you have partly overwritten with the nLUC three steps before); use this formula and variable definitions: `a = nLUC, b = oLUC, ifelse(eq(a,common-nodata-value),b,a)`
- With the module `convert data storage type` set the data format back to unsigned 1byte integer.
- Save the result as a default `.sgrd` but remove this extension from the filename afterwards. Make sure that the filename is identical to the oLUC tiles (make a backup of the originals) and replace them in `/geog/landuse_30s`.
- in `/WRFversion/run/namelist.input`, section physics, set `num_land_cat = new maximum LUC ID` (in our case 70, Appendix I)
- Add the new classes to `/WRFversion/run/LANDUSE.TBL`, section USGS, with a running ID (see below) and also set the new maximum ID in the header of the table (in our case 70, marked bold); only summer values were modified as we did only WRF runs for summer; the bold faced classes are new.

## I The new LANDUSE.TBL

Find this file in `/WRFversion/run/`. `LANDUSE.TBL` is also used by WRFs other LSM modules, but they overwrite values of `LANDUSE.TBL` if they use further table files with overlapping values. The Noah LSM for example uses `VEG-PARM.TBL` and three more tables since WRF ARW v3.1 (WRF basics 2012).

The nLUCs are marked bold. The following includes the "correct" `z0`, named **SFZ0 and is in cm!** However, we accidentally did not use these values. See the discussion and the table below for the values used.

```
USGS
70,2, 'ALBD SLMO SFEM SFZ0 THERIN SCFX SFHC '
SUMMER
1, 15., .10, .88, 80., 3., 1.67, 18.9e5, 'Urban and Built-Up Land'
2, 17., .30, .985, 15., 4., 2.71, 25.0e5, 'Dryland Cropland and Pasture'
3, 18., .50, .985, 10., 4., 2.20, 25.0e5, 'Irrigated Cropland and Pasture'
4, 18., .25, .985, 15., 4., 2.56, 25.0e5, 'Mixed Dryland/Irrigated Cropland and Pasture'
5, 18., .25, .98, 14., 4., 2.56, 25.0e5, 'Cropland/Grassland Mosaic'
6, 16., .35, .985, 20., 4., 3.19, 25.0e5, 'Cropland/Woodland Mosaic'
7, 19., .15, .96, 12., 3., 2.37, 20.8e5, 'Grassland'
8, 22., .10, .93, 5., 3., 1.56, 20.8e5, 'Shrubland'
9, 20., .15, .95, 6., 3., 2.14, 20.8e5, 'Mixed Shrubland/Grassland'
10, 20., .15, .92, 15., 3., 2.00, 25.0e5, 'Savanna'
11, 16., .30, .93, 50., 4., 2.63, 25.0e5, 'Deciduous Broadleaf Forest'
12, 14., .30, .94, 50., 4., 2.86, 25.0e5, 'Deciduous Needleleaf Forest'
13, 12., .50, .95, 50., 5., 1.67, 29.2e5, 'Evergreen Broadleaf Forest'
14, 12., .30, .95, 50., 4., 3.33, 29.2e5, 'Evergreen Needleleaf Forest'
15, 13., .30, .97, 50., 4., 2.11, 41.8e5, 'Mixed Forest'
16, 8., 1.0, .98, 0.01, 6., 0., 9.0e25, 'Water Bodies'
17, 14., .60, .95, 20., 6., 1.50, 29.2e5, 'Herbaceous Wetland'
18, 14., .35, .95, 40., 5., 1.14, 41.8e5, 'Wooded Wetland'
19, 25., .02, .90, 1., 2., 0.81, 12.0e5, 'Barren or Sparsely Vegetated'
20, 15., .50, .92, 10., 5., 2.87, 9.0e25, 'Herbaceous Tundra'
21, 15., .50, .93, 30., 5., 2.67, 9.0e25, 'Wooded Tundra'
22, 15., .50, .92, 15., 5., 2.67, 9.0e25, 'Mixed Tundra'
23, 25., .02, .90, 10., 2., 1.60, 12.0e5, 'Bare Ground Tundra'
24, 55., .95, .95, 0.1, 5., 0., 9.0e25, 'Snow or Ice'
```

```

25, 30., .40, .90, 1., 5., .62, 12.0E5, 'Playa'
26, 18., .50, .95, 15., 6., .62, 12.0E5, 'Lava'
27, 70., .40, .90, 1., 5., 0., 12.0E5, 'White Sand'
28, 15., .02, .88, 80., 3., 1.67, 18.9e5, 'Unassigned'
29, 15., .02, .88, 80., 3., 1.67, 18.9e5, 'Unassigned'
30, 15., .10, .88, 80., 3., 1.67, 18.9e5, 'Unassigned'
31, 10., .10, .97, 80., 3., 1.67, 18.9e5, 'Low Intensity Residential'
32, 10., .10, .97, 80., 3., 1.67, 18.9e5, 'High Intensity Residential'
33, 10., .10, .97, 80., 3., 1.67, 18.9e5, 'Industrial or Commercial'
34, 15., .02, .88, 80., 3., 1.67, 18.9e5, 'Unassigned'
35, 15., .02, .88, 80., 3., 1.67, 18.9e5, 'Unassigned'
36, 15., .02, .88, 80., 3., 1.67, 18.9e5, 'Unassigned'
37, 15., .02, .88, 80., 3., 1.67, 18.9e5, 'Unassigned'
38, 15., .02, .88, 80., 3., 1.67, 18.9e5, 'Unassigned'
39, 15., .02, .88, 80., 3., 1.67, 18.9e5, 'Unassigned'
40, 18., .25, .985, 10.56, 4., 2.56, 25.0e5, 'Arable Land'
41, 17., .30, .985, 3.94, 4., 2.71, 25.0e5, 'Pastures'
42, 18., .25, .985, 10.56, 4., 2.56, 25.0e5, 'Other Agricultural Areas'
43, 15., .50, .92, 323.44., 5., 2.67, 9.0e25, 'Forest'
44, 22., .10, .93, 35.44, 3., 1.56, 20.8e5, 'Shrub Lands'
45, 14., .60, .95, 28.76, 6., 1.50, 29.2e5, 'Wetlands'
46, 15., .10, .88, 33.86, 3., 1.67, 18.9e5, 'Sealed area'
47, 15., .10, .88, 15.77, 3., 1.67, 18.9e5, 'Rail-Tracks'
48, 15., .50, .92, 210.93, 5., 2.67, 9.0e25, 'Green Urban'
49, 15., .10, .88, 273.88., 3., 1.67, 18.9e5, 'Urban Core'
50, 15., .10, .88, 37.38, 3., 1.67, 18.9e5, 'Village Core'
51, 15., .10, .88, 87.84, 3., 1.67, 18.9e5, 'Dense Multistory Tenements'
52, 15., .10, .88, 32.47, 3., 1.67, 18.9e5, 'Perimeter Block Building'
53, 15., .10, .88, 16.26, 3., 1.67, 18.9e5, 'Terrace housing'
54, 15., .10, .88, 27.68, 3., 1.67, 18.9e5, 'Blocks'
55, 15., .10, .88, 14.52, 3., 1.67, 18.9e5, 'Regular Housing'
56, 15., .10, .88, 87.05, 3., 1.67, 18.9e5, 'High Rise Commercial'
57, 15., .10, .88, 13.74, 3., 1.67, 18.9e5, 'Industry Commerce'
58, 15., .10, .88, 14.29, 3., 1.67, 18.9e5, 'Port'
59, 15., .02, .88, 80., 3., 1.67, 18.9e5, 'Unassigned'
60, 15., .02, .88, 80., 3., 1.67, 18.9e5, 'Unassigned'
61, 15., .02, .88, 80., 3., 1.67, 18.9e5, 'Unassigned'
62, 15., .02, .88, 80., 3., 1.67, 18.9e5, 'Unassigned'
63, 15., .02, .88, 80., 3., 1.67, 18.9e5, 'Unassigned'
64, 15., .02, .88, 80., 3., 1.67, 18.9e5, 'Unassigned'
65, 15., .02, .88, 80., 3., 1.67, 18.9e5, 'Unassigned'
66, 15., .02, .88, 80., 3., 1.67, 18.9e5, 'Unassigned'
67, 15., .02, .88, 80., 3., 1.67, 18.9e5, 'Unassigned'
68, 15., .02, .88, 80., 3., 1.67, 18.9e5, 'Unassigned'
69, 15., .10, .88, 25.53, 3., 1.67, 18.9e5, 'Airport'
70, 8., 1.0, .98, .08, 6., 0., 9.0e25, 'Waterbody'

```

The Table below shows all the different  $z_0$  values not used and used. The column early LUC shows the values used in the WRF sensitivity study in Section 5.3. They originated from an early version of the nLUC, that was not that accurate in terms of Water and Urban Green. The column missing 0, shows the values used for the final WRF runs (Chapter 6). They originated from the final version of the nLUC, but include a calculation error due to a lost zero (Footnote 24). The differences column shows that the missing zero had a big effect on the class Water (+300%) compared to the desired  $z_0$  (not used). However, missing 0 Water compared to early LUC Water is only +24% different. The cause: As the final LUC was explicitly improved in terms of Water and Urban Green, especially cells that were classified as Wetland in the early version, got classified as Water in the final one. Hence, if one sees the classes Water and Wetland in combination, both, the early LUC and the missing 0 LUC have a similar error of too high roughness over those two classes (+298% and +314%). Other classes strongly affected by the missing 0 error are the agricultural ones (+40 to +70%). The classes Urban Green and Forest have a lower roughness (about -30%), the urban classes overall (without Urban Green) have a higher roughness (5%). The sensitivity study in general showed lower T2 for higher roughness and higher T2 for lower roughness. So the used missing 0 version is expected to show lower temperature differences between Urban Green + Forest

and the other urban classes; and lower temperatures for Water both compared to not used (Table 4.4.1). The higher roughness for Water improved WRF, as it had problems with very low roughness combined with slow winds (unrealistically warm biased T2 of river Elbe). However, all differences between not used and missing 0, did not influence the roughness ranks. Thus, the correlation results shown in Tables 4.4.1, 4.4.2, and Chapter 6 are not affected.

LUC names for Hamburg	z <sub>0</sub> [cm]			differences [%]	
	not used final (Table 4.4.1)	missing 0 used in 6	early LUC used in 5.3	6 to 5.3	6 to 4.4.1
Arable Land	10.56	14.84	16.23	-8.57	40.55
Pastures	3.94	6.82	7.10	-3.95	73.34
Other Agricultural Area	10.56	14.84	13.95	6.39	40.55
Forest	323.44	219.65	304.15	-27.78	-32.09
Shrub Land	35.44	38.51	36.01	6.95	8.66
Wetland	28.76	32.67	8.74	273.77	13.59
Sealed Area	33.86	37.15	39.98	-7.08	9.71
Rail Track	15.77	20.36	20.60	-1.17	29.06
<b>Urban Green</b>	<b>210.93</b>	<b>156.87</b>	<b>154.94</b>	<b>1.24</b>	<b>-25.63</b>
<b>Urban Core</b>	<b>273.88</b>	<b>192.69</b>	<b>245.71</b>	<b>-21.58</b>	<b>-29.65</b>
Village Core	37.38	40.16	43.23	-7.09	7.43
Dense Perimeter	87.84	78.69	94.81	-17.00	-10.41
Perimeter	32.47	35.94	40.04	-10.23	10.70
Terraced Housing	16.26	20.85	22.20	-6.10	28.23
Blocks	27.68	31.69	39.29	-19.33	14.52
Single Family Houses	14.52	19.07	22.44	-15.03	31.35
High Rise Commercial	87.05	78.14	90.79	-13.94	-10.24
Industrial and Commerce	13.74	18.26	19.37	-5.74	32.90
Harbor	14.29	18.83	16.26	15.77	31.80
Airport	25.53	29.74	30.41	-2.20	16.50
Water	0.08	0.31	0.25	24.24	300.73
<b>Means</b>	<b>62.09</b>	<b>52.67</b>	<b>60.31</b>		

**Table 7.2** Table of z<sub>0</sub> values in centimeter from different LUC versions.

WRF needs centimeter values instead of meter. Bold classes are urban, colors indicate land use. The means are not area weighted and hence give a rough estimate of the mean roughness.

## J Configure.wrf for PGI compiler

[...]

```
#### Architecture specific settings ####

# Settings for Linux x86_64, PGI compiler with gcc (dmpar)
#
DMPARALLEL = 1 # 1 for dmpar and hybrid mode, 0 for smpar and serial (single-CPU)
OMP_CPP = # -D_OPENMP # like the next two only for smpar mode
```

```

OMP = # -mp -Minfo=mp -Mrecursive
OMPCC = # -mp
SFC = pgf90
SCC = gcc
CCOMP = pgcc
DM_FC = mpif90
DM_CC = mpicc -DMPI2-SUPPORT
FC = $(DM_FC)
CC = $(DM_CC) -DFSEEK064_OK
LD = $(FC)
RWORDSIZE = $(NATIVE_RWORDSIZE)
PROMOTION = -r$(RWORDSIZE) -i4
ARCH_LOCAL = -DNONSTANDARD_SYSTEM_SUBR
CFLAGS_LOCAL = -w -O3
LDFLAGS_LOCAL =
CPLUSPLUSLIB =
ESMF_LDFLAG = $(CPLUSPLUSLIB)
FCOPTIM = -fastsse -Mvect=noaltcode -Msmartalloc -Mprefetch=distance:8 -Mfprelaxed #
-Minfo=all =Mneginfo=all
FCREDUCEDOPT = $(FCOPTIM)
FCNOOPT = -O0
FCDEBUG = # -g $(FCNOOPT)
FORMAT_FIXED = -Mfixed
FORMAT_FREE = -Mfree
FCSUFFIX =
BYTESWAPIO = -byteswapio
FCBASEOPTS_NO_G = -w $(FORMAT_FREE) $(BYTESWAPIO) $(OMP)
FCBASEOPTS = $(FCBASEOPTS_NO_G) $(FCDEBUG)
MODULE_SRCH_FLAG = -module $(WRF_SRC_ROOT_DIR)/main
TRADFLAG = -traditional
CPP = /lib/cpp -C -P
AR = ar
ARFLAGS = ru
M4 = m4 -B 14000
RANLIB = ranlib
CC_TOOLS = $(SCC)
[...]
```

Note: the compile flags `-ip` (with Intel compiler), `-f90=$(SFC)` and `-cc=$(SCC)` (with Open MPI) had to be manually erased from `configure.wrf`; `-DMPI2_SUPPORT` had to be added to the line `DM_CC`).

## K ERA-Interim grid transformation scripts utilizing CDO

Find the `Vtable` file for the parameter list in `/WPSversion/ungrib/Variable_Tables/Vtable.ERA-interim.ml`

Some parameters had to be transformed to another grid before the preprocessing was successful: Transformation from reduced to normal Gaussian grid, needed for all surface layer parameters and the model layer parameter `Q`:

```

for f in EIsf00_6H_* ; do
    cdo -R copy "$f" "$f.gauss" ;
done
```

Transformation from spherical harmonics to normal Gaussian grid, needed for all model layer parameters except `Q`:

```

for f in ERAIN_ML00_6H_* ; do
    cdo sp2gp "$f" "$f.gauss" ;
done
```

## L WPS' runtime configuration file namelist.wps

```
&share
wrf_core = 'ARW',
max_dom = 3,
start_date = '2011-05-01_00:00:00', '2011-
05-01_00:00:00', '2011-05-01_00:00:00',
end_date = '2011-06-25_00:00:00', '2011-06-
25_00:00:00', '2011-06-25_00:00:00',
interval_seconds = 21600,
io_form_geogrid = 2,
debug_level = 0,
/
&geogrid
parent_id = 1,1,2,
parent_grid_ratio = 1,5,5,
i_parent_start = 1,12,22,
j_parent_start = 1,12,21,
e_we = 35,61,121,
e_sn = 35,61,121,
geog_data_res = '30s','30s','30s',
dx = 25000,
dy = 25000,
map_proj = 'lambert',
ref_lat = 53.515,
ref_lon = 9.848,
truelat1 = 53.515,
truelat2 = 53.515,
stand_lon = 9.848,
geog_data_path = './username/geog', # there
were different geog-copies / folders for
the different LUC implementations
ref_x = 17.5,
ref_y = 17.5,
/
&ungrib
out_format = 'WPS',
prefix = 'FILE',
/
&metgrid
fg_name = 'FILE','PRES',
io_form_metgrid = 2,
/
&domain_wizard
grib_data_path = 'null',
grib_vtable = 'Vtable.ERA-interim.ml',
dwiz_name = hh
dwiz_desc =
dwiz_user_rect_x1 =4121
dwiz_user_rect_y1 =738
dwiz_user_rect_x2 =4423
dwiz_user_rect_y2 =905
dwiz_show_political =true
dwiz_center_over_gmt =true
dwiz_latlon_space_in_deg =10
dwiz_latlon_linecolor =-8355712
dwiz_map_scale_pct =100
dwiz_map_vert_scrollbar_pos =0
dwiz_map_horiz_scrollbar_pos =0
dwiz_gridpt_dist_km =25.0
dwiz_mpi_command =
dwiz_tcvitals =null
/
```

## M WRFs runtime configuration file namelist.input

The file is displayed for the first period of the temporal splitted 2011 run. Find the file in /WRFversion/run/namelist.input

```
&time_control
run_days = 12,
run_hours = 0,
run_minutes = 0,
run_seconds = 0,
start_year = 2011, 2011, 2011,
start_month = 05, 05, 05,
start_day = 01, 01, 01,
start_hour = 00, 00, 00,
start_minute = 00, 00, 00,
start_second = 00, 00, 00,
end_year = 2011, 2011, 2011,
end_month = 05, 05, 05,
end_day = 13, 13, 13,
end_hour = 00, 00, 00,
end_minute = 00, 00, 00,
end_second = 00, 00, 00,
interval_seconds = 21600,
input_from_file = .true., .true., .true.,
history_interval = 30, 30, 30,
frames_per_outfile = 1, 1, 1,
restart = .true.,
restart_interval = 2500,
io_form_history = 2,
io_form_restart = 2,
io_form_input = 2,
io_form_boundary = 2,
debug_level = 0,
/
&domains
time_step = 150,
time_step_fract_num = 0,
time_step_fract_den = 1,
max_dom = 3,
e_we = 35, 61, 121,
e_sn = 35, 61, 121,
e_vert = 60, 60, 60,
p_top_requested = 1000,
num_metgrid_levels = 61,
num_metgrid_soil_levels = 4,
dx = 25000, 5000, 1000,
dy = 25000, 5000, 1000,
grid_id = 1, 2, 3,
parent_id = 1, 1, 2,
i_parent_start = 1, 12, 22,
j_parent_start = 1, 12, 21,
parent_grid_ratio = 1, 5, 5,
parent_time_step_ratio = 1, 5, 5,
```

```

feedback = 1,
smooth_option = 0,
numtiles = 6,
/
&physics
mp_physics = 8, 8, 8,
ra_lw_physics = 1, 1, 1,
ra_sw_physics = 2, 2, 2,
slope_rad = 0, 0, 1,
radt = 10, 10, 10,
sf_sfclay_physics = 2, 2, 2,
sf_surface_physics = 1, 1, 1,
bl_pbl_physics = 2, 2, 2,
bldt = 0, 0, 0,
cu_physics = 5, 5, 0,
cudt = 5, 5, 5,
isfflx = 1,
ifsnow = 1,
icloud = 0,
surface_input_source = 1,
num_soil_layers = 5,
sf_urban_physics = 0, 0, 0,
maxiens = 1,
maxens = 3,
maxens2 = 3,
maxens3 = 16,
ensdim = 144,
num_land_cat = 70, # to use the original
WRF USGS land use switch back to 24; for
more differentiated land use set to your
maximum LUC ID of your LANDUSE.TBL
(Appendix I)
tmn_update = 1,
sst_skin = 0,

bucket_mm = 100.0,
/
&fdda
/
&dynamics
w_damping = 0,
diff_opt = 1,
km_opt = 4,
diff_6th_opt = 0, 0, 0,
diff_6th_factor = 0.12, 0.12, 0.12,
base_temp = 290.,
damp_opt = 0,
zdamp = 5000., 5000., 5000.,
dampcoef = 0.2, 0.2, 0.2,
khdif = 0, 0, 0,
kvdif = 0, 0, 0,
non_hydrostatic = .true., .true., .true.,
moist_adv_opt = 1, 1, 1,
scalar_adv_opt = 1, 1, 1,
/
&bdy_control
spec_bdy_width = 5,
spec_zone = 1,
relax_zone = 4,
specified = .true., .false., .false.,
nested = .false., .true., .true.,
spec_exp = 0.33,
/
&grib2
/
&namelist_quilt
nio_tasks_per_group = 0,
nio_groups = 1,
/

```

## N How-To execute ecmwf\_calc\_p.exe for ERA-I with model levels

To create the namelist files and configure size and location of the nests the java-application Domain Wizard (DW HP 2011) was used to the point where one has to start the preprocessing. The WRF preprocessing system (WPS) normally consists of the three programs geogrid, ungrib, and metgrid (WRF online tutorial 2012). To use ERA-I model levels, however, one has to execute a fourth program before metgrid, not available in the Domain Wizard:

- exit Domain Wizard just before executing metgrid;
- copy the just created namelists from the DW folders to your WPS and WRF folders;
- correct the paths within the namelists;
- add "PRES" (including the "") to namelist.wps, section metgrid, row fg\_name;
- create a new file named ecmwf\_coeffs with the content of [http://www.ecmwf.int/products/data/technical/model\\_levels/model\\_def\\_60.html](http://www.ecmwf.int/products/data/technical/model_levels/model_def_60.html) at your WPS directory;
- execute calc\_ecmwf\_p.exe found at /WPSversion/util/

## O The jobscript used on Tornado

Here for the case of executing wrf.exe with OpenMPI 1.4.3. Change OpenMPI version or wrf.exe to real.exe as you need.

```
#-----SGE directives-----
#$ -N yourWRFRun # select a meaningful name
#$ -cwd
#$ -S /bin/csh
#$ -l s_cpu=99:00:00 # adjust this to the foreseen runtime of your model run
#$ -l s_vmem=3500M # adjust this to the amount of RAM each core has but left some space free
#$ -j y
#$ -q cluster # operational mode asking for multi-core runs (replace with serial if you need to run on a single core)

#-----start-----
echo -n " Job started at: "
date
date +%s
echo -n " Execution host: "
hostname

#-----user command section-----
setenv MPIROOT /sw/sles10-x64/ofed/openmpi-1.4.3-pgill # your MPI path
setenv MPIBIN $MPIROOT/bin
$MPIBIN/mpixec --prefix $MPIROOT ./wrf.exe # your binary / program to execute

#-----end-----
echo -n " Job completed at: "
date
date +%s
echo "Dauer"
time
echo "complete"
```

To submit the jobscript for example to distribute the domain to 8 cores we used the command  
qsub -pe orte 8 job.script

## P WRF Post Processing and evaluation through combined DB data

1) Queries to extract data from met stations and bus measurements to combine them in a new DB:

a) Bus measurements:

```
CREATE TABLE combinedb2 AS
SELECT * from (
(SELECT * from messwerte where station_fk > 0 AND messgroesse_fk =1
      AND ((EXTRACT (MONTH FROM zeitstempel) = 05)
      OR (EXTRACT (MONTH FROM zeitstempel) = 06
      AND EXTRACT (DAY FROM zeitstempel) <= 24)))
as a
JOIN (SELECT *, ST_X(the_geom) AS utm_x, ST_Y(the_geom) AS utm_y from stationsnetz)
as b
ON (a.station_fk = b.stations_id))
as c
ORDER BY c.zeitstempel ASC
```

b) Station measurements

```
CREATE TABLE combineds2 AS
SELECT * from (
(SELECT * from tb_messwerte where
```

```

(EXTRACT (YEAR FROM zeitstempel) = 2011
AND EXTRACT (MONTH FROM zeitstempel) = 05)
OR (EXTRACT (YEAR FROM zeitstempel) = 2011
AND EXTRACT (MONTH FROM zeitstempel) = 06
AND EXTRACT (DAY FROM zeitstempel) <= 24))
as a
JOIN (SELECT id_messreihe, station_fk from tb_messreihe)
as c
ON (a.messreihe_fk = c.id_messreihe)
JOIN (SELECT *, ST_AsText(ST_Transform(location_latlon, 32632)) AS utm from
tb_station_meta)
as b
ON (c.station_fk = b.id_station))
as c
ORDER BY c.id_station ASC

```

2) This is a three-piece Bash script. The first and third part ran local, the second part on the HPC Tornado that was decommissioned 19 July 2012.

a) This first part of the script selects data from the combined DB for the 5 min time span around the 30 min WRF output files and writes them into a point shape with their MEZ time transformed into UNIX time (time\_sec). The file names got an index, the same as the WRF output files. First data point is at 1 Mai 01:55 local summer time or in UNIX time 3513376500 s. The last time step is 25 June 01:55 local summer time or 23:55 UTC. This was done with a Bash for loop invoking psql and pgsql2shp:

```

for ((i=0; ${i}<2592; i++))
do echo "drop TABLE ten;
CREATE TABLE ten as
SELECT * from alltemp062011 where time_sec >= 3513376500+(1800*${i})
AND time_sec < 3513377100+(1800*${i});" > ./x.sql &&
psql -h ip-adress -p 5432 -U username -w -d combined_dev2 -f x.sql &&
pgsql2shp -r -h ip-adress -p 5432 -u username -P password -f out${i}.shp combined_dev2
ten
done

```

Project the shapes from UTM to WRFs Lambert Conformal Conic projection with SAGA GIS' command line saga\_cmd within a Bash for loop:

```

for ((i=0; ${i}<2592; i++))
do saga_cmd libpj_proj4 "Set Coordinate Reference System" -CRS_METHOD=0
-CRS_PROJ4="+proj=utm +units=m +datum=WGS84 +zone=32" -SHAPES=./out${i}.shp
done

for ((i=0; ${i}<2592; i++))
do saga_cmd libpj_proj4 "Coordinate Transformation (Shapes)" -CRS_METHOD=0
-CRS_PROJ4="+proj=lcc +units=m +datum=WGS84 +lat_1=53,515 +lat_2=53,515" -SOURCE=./out$
{i}.shp -TARGET=./projected/outp${i}.shp
done

```

To copy the shapes to a server with WRF data use scp (secure copy):

```

scp ./projected/out* username@login.yourserver.de://yourpath/

```

b) Now extract and convert T2 of the WRF netCDF formatted output into a SAGA sgrid. Therefore rename the WRF output, using a running index (to get rid of ':'). The first day of the model was trashed due to the transient time. More exactly the first 22 h and 5 min were trashed to get the UTC time-stamped data in sync with the first data point of the local summer time measurement data, using Bash script and saga\_cmd. To compare the measurement data to the other runs replace WRF330nLUC with your folder name. Replace T2 by another WRF output variable like U10 and V10 to analyze the wind.

```

Index=0
for file in ./username/WRF330nLUC/run/wrfout_d03_2011-0*
do newfilename=wrfout_d03_2011-${Index}
mv "$file" ./username/WRF330nLUC/run/$newfilename
echo mv $file $newfilename
let "Index=Index+1" done

```

```
mkdir ./username/WRF330nLUC/T2grids
mkdir ./username/WRF330nLUC/T2result
```

```
for ((i=0; ${i}<2592; i++))
do saga_cmd libio_gdal 0 -GRIDS="./username/WRF330nLUC/T2grids/wrfnLUC_T2_2011-${i}" \
-FILES=NETCDF:"./username/WRF330nLUC/run/wrfout_d03_2011-${i}":T2;
done
```

The resulting saga grids have to get a coordinate system description .sgrd file:

```
for ((i=0; ${i}<2592; i++))
do echo "
NAME = wrfd3_T2_2011-${i}
DESCRIPTION = NETCDF VARNAME=T2
NETCDF_DIMENSION_Time=1
UNIT = Kelvin
DATAFILE_OFFSET = 0
DATAFORMAT = FLOAT
BYTEORDER_BIG = FALSE
POSITION_XMIN = 612707.7595808203
POSITION_YMIN = 6750584.9665848
CELLCOUNT_X = 120
CELLCOUNT_Y = 120
CELLSIZE = 1000.0000000000
Z_FACTOR = 1.000000
NODATA_VALUE = 9969209968386869046778552952102584320.000000
TOPTOBOTTOM = TRUE
" > ./username/WRF330nLUC/T2grids/wrfnLUC_T2_2011-${i}.sgrd
done
```

```
for ((i=0; ${i}<2592; i++))
do echo
"PROJCS[Lambert_Conformal_Conic,GEOGCS[GCS,DATUM[Datum,SPHEROID[WGS84,6378137.0,298.25722
36],TOWGS84[0,0,0,0,0,0]],PRIMEM[Greenwich,0],UNIT[degree,0.01745329251994328]],PROJECT
ION[Lambert_Conformal_Conic],PARAMETER[central_meridian,9.848],PARAMETER[latitude_of_orig
in,53.515],PARAMETER[standard_parallel_1,53.515],PARAMETER[standard_parallel_2,53.515 ],U
NIT[Meter,1.0]]" \
./username/WRF330nLUC/T2grids/wrfnLUC_T2_2011-${i}.prj
done
```

The data points of the WRF output have to be interpolated onto the points of the measurements' point shapes.

```
for ((i=0; ${i}<2592; i++))
do saga_cmd libshapes_grid 0 -SHAPES=./username/T2shapes/ouptp${i}.shp \
-GRIDS=./username/WRF330nLUC/T2grids/wrfnLUC_T2_2011-${i}.sgrd \
-RESULT=./username/WRF330nLUC/T2result/ouptpWRFnLUC-${i}x \
-INTERPOL=3
done
```

This generates a list of all shapes and merges it with a script that merges all shape files:

```
for (i=1; ${i}<2592; i++)
do echo "T2result/ouptpWRFnLUC-${i}x.shp\;\\" >> shplist.sh
done

echo " saga_cmd libshapes_tools 2 \
-OUT=./username/WRF330nLUC/T2result/allouptpWRF-T2nLUC \
-MAIN=./username/WRF330nLUC/T2result/ouptpWRFnLUC-0x.shp \
-LAYERS=\\ " > script.sh && \
cat shplist.sh >> script.sh && sh script.sh
```

The resulting shape contains the final .dbf that can easily be imported into a spreadsheet program or R for further analysis. To redo the analysis with the ERA-I data, the scripts above have to be adapted to the 6 hourly time step of ERA-I. The easiest way to get 2 m air temperature data from ERA-I was to follow the normal preprocessing of WRF until metgrid. Then real has to run for every 6 h time step of the whole model run period. Every real run creates the initial boundary conditions (as the file wrfinput\_d03) including T2 at the same (interpolated) resolution as the WRF output. From this point on it is easy to use the

above procedure to compare ERA-I with the measurement data. Now the steps necessary to semi-automate the multiple runs of real. This creates all the namelist.input files, needed for the real runs:

```
time1=(01 01 01 01 02 02 02 02 03 03 03 03 04 04 04 04 05 05 05 05 06 06 06 06 07 07 07
07 08 08 08 08 09 09 09 09 10 10 10 10 11 11 11 11 12 12 12 12 13 13 13 13 14 14 14 14 15
15 15 15 16 16 16 16 17 17 17 17 18 18 18 18 19 19 19 19 20 20 20 20 21 21 21 21 22 22 22
22 23 23 23 23 24 24 24 24 25 25 25 25 26 26 26 26 27 27 27 27 28 28 28 28 29 29 29 29 30
30 30 30 31 31 31 31)
time2=(00 06 12 18 00 06 12 18 00 06 12 18 00 06 12 18 00 06 12 18 00 06 12 18 00 06 12
18 00 06 12 18 00 06 12 18 00 06 12 18 00 06 12 18 00 06 12 18 00 06 12 18 00 06 12
06 12 18 00 06 12 18 00 06 12 18 00 06 12 18 00 06 12 18 00 06 12 18 00 06 12 18 00
18 00 06 12 18 00 06 12 18 00 06 12 18 00 06 12 18 00 06 12 18 00 06 12 18 00 06 12
06 12 18 00 06 12 18)
```

```
for ((i=0;i<${#time1[@]};i++));
do echo "&time_control
run_days = 0,
run_hours = 6,
run_minutes = 0,
run_seconds = 0,
start_year = 2011, 2011, 2011,
start_month = 06, 06, 06,
start_day = ${time1[$i]}, ${time1[$i]}, ${time1[$i]},
start_hour = ${time2[$i]}, ${time2[$i]}, ${time2[$i]}, ...
```

Please insert the rest of namelist.input, see Appendix M

```
" > namelist.input-${time1[$i]}-${time2[$i]}
done
```

4 parallel runs of real and moving namelists and results from runs before to the right run directories:

```
mv wrfinput_d03 ../runERA/wrfinput_d03-212 && mv namelist.input-24-00 namelist.input
&& rm rsl.* && rm WRFoLUC.* && qsub -pe orte 8 qreal.job && cd ../run1 &&\
mv wrfinput_d03 ../runERA/wrfinput_d03-213 && mv namelist.input-24-06 namelist.input
&& rm rsl.* && rm WRFoLUC.* && qsub -pe orte 8 qreal.job && cd ../run2 &&\
mv wrfinput_d03 ../runERA/wrfinput_d03-214 && mv namelist.input-24-12 namelist.input
&& rm rsl.* && rm WRFoLUC.* && qsub -pe orte 8 qreal.job && cd ../run3 &&\
mv wrfinput_d03 ../runERA/wrfinput_d03-215 && mv namelist.input-24-18 namelist.input
&& rm rsl.* && rm WRFoLUC.* && qsub -pe orte 8 qreal.job && cd ../run0
```

c) The .dbf files can be exported as .csv to load them into R-Studio (get rid of NA, 99999 etc. before) to calculate the spatial correlation between measurements and WRF:

```
library("plyr")
z = ddply(csvFILE, .(StationID), summarize,
coroLUC = cor(WRFoLUC, Measurements), sigoLUC = if(length(StationID) < 3) {NA} else
{cor.test(WRFoLUC, Measurements)$p.value},
coroLUC = cor(WRFoLUC, Measurements), sigoLUC = if(length(StationID) < 3) {NA} else
{cor.test(WRFoLUC, Measurements)$p.value},
n = length(StationID))
write.csv(z, file="./out.csv")
```

This calculates the hourly means for a diurnal analysis between different WRF runs and measurements:

```
library("plyr")
z = ddply(alloutpWRF.54uPSFC, .(hour), summarize,
meanMeasurements = mean(Measurements),
meanoLUCTemp = mean(XoLUCTemp),
meanoLUCPSFC = mean(XoLUCPSFC),
meanoLUCWIND = mean(XoLUCWIND),
meanoLUC_Temp = mean(XoLUC_Temp),
meanoLUC_PSFC = mean(XoLUC_PSFC),
meanoLUC_WIND = mean(XoLUC_WIND),
n = length(hour))
write.csv(z, file="./hourly-means.csv")
```

# Abbreviations and acronyms

AMD	Advanced Micro Devices, Inc.	IFSAR	Interferometric SAR
ANOVA	Analysis of variance	InSAR	SRTM
ARW	Advanced Research WRF	IUHI	Intra UHI
ATKIS	Amtliches Topographisch Kartographisches Informationssystem = Official Topographic Cartographic Information System	KLIMZUG	NORD Klimawandel in Regionen zukunfts-fähig gestalten, Region Nord = future proof adaption on regional climate change, region north
BEM	Building energy model	l.a.	last accessed
BEP	Building effect parameterization	LAT	Latitude
CBD	Central business district	LCZ	Local climate zone = U.S. optimized LUC by Stewart and Oke (2009, 2012)
CEST	Central European Summer Time	LGV	Landesbetrieb Geoinformation und Vermessung der Stadt Hamburg = State Office of Geoinformation and Measurement of the city of Hamburg
CET	Central European Time		
cf.	confer = compare	LiDAR	Light detection and ranging
CFD	Computational fluid dynamics	LON	Longitude
CliSAP	Integrated Climate System Analysis and Prediction	LSM	Land surface model
CPU	Central processing unit	LUC	Land use classification or land use classes
CWRF	Climate WRF	nLUC	New LUC by Daneke, Bechtel, and Langkamp (2010)
DK	Driesen+Kern GmbH	MI	Meteorological institute of the university of Hamburg
DB	Database	ML	Model levels
DD	Dynamical downscaling	MPI	Message passing interface
DDR	Double data rate	NCAR	National Center for Atmospheric Research
DEM	Digital elevation model	NCEP	National Centers for Environmental Prediction
DKRZ	Deutsches Klima-Rechenzentrum = German climate computing center	netCDF	Network common data format
DSM	Digital surface model	NMM	Nonhydrostatic Mesoscale Model
DTM	Digital terrain model	NOAA	National Oceanic and Atmospheric Administration
DWD	German weather service	Noah LSM	N for NCEP, O for Oregon state university, A for air force, H for hydrologic research lab
ERA-I	ERA Interim Reanalysis		
et al.	et alii = and others		
etc.	et cetera = and the rest		
EULAG	Eulerian / semi-Lagrangian fluid solver		
GCC	GNU compiler collection		
GCM	Global climate model		
GIS	Geographical information system		
GK3	Gauß-Krüger 3 projection		
GmbH	Gesellschaft mit beschränkter Haftung = Ltc.		
GNU	GNU's Not Unix (recursive acronym)	NWS	National weather service
GRIB	Gridded binary	oLUC	Original LUC of WRF
GUI	Graphical user interface	PGI	Compiler of The Portland Group
GWL	Grosswetterlagen = large / major circulation types	pNetCDF	Parallel netCDF
HaLm	Hamburger Luftmessnetz = ambient air pollution network of Hamburg	PSFC	Pressure at the surface
HP	Homepage	$\rho$	Spearman rank correlation coefficient
HPC	High performance cluster	r	Pearson product-moment correlation coefficient
		R <sup>2</sup>	coefficient of determination
		RAM	Random access memory

RCM	Regional climate model	T2	2 m air temperature of WRF
RH	Relative humidity	UHI	Urban heat island
RMSE	Root mean square error	U.S.	United States
$\sigma$	Standard deviation	USGS	U. S. Geological Survey
SAGA	System for Automated Geoscientific Analysis	UTC	Coordinated Universal Time
SAR	Synthetic Aperture Radar	UTM	Universal Transverse Mercator projection
SD	Statistical downscaling	v	version
SFHC	Heat capacity	vs.	versus
SLH	Surface layer heights	VSH	Variance of sectors height
SLUCM	Single layer urban canopy model	WPS	WRF preprocessing system
SRHH	Stadtreinigung Hamburg = Hamburg city cleaning service	WRF	Weather research and forecasting model
SRTM	Shuttle Radar Topography Mission	$z_0$	Aerodynamic roughness length in meter
ST	Surface temperature	ZMAW	Zentrum für Marine und Atmosphärische Wissenschaften = Center of marine and atmospheric sciences
SVF	Sky view factor		
T	(2 m) air temperature of measurements		

## Units

"	arc second
'	arc minute
°	arc hour
°C	degree Celsius
d	day
h	hour
J	joule
K	kelvin
km	kilometer
m	meter
mm	millimeter
min	minute
s	second
W	watt

# Acknowledgments

I thank Prof. Jürgen Böhner for his absolute trust and constant support. He made this possible.

I thank my wife Sandra (and our unborn child) for their patience especially in the last months ;).

I thank my working group, and all the people of the universities Hamburg, RWTH Aachen, and Berlin, that provided thousands of hints, tips, and months of hard work that is now part of this thesis. I especially thank:

D Arnds (bus measurements)

B Bechtel ( $z_0$  and countless stuff that made my research a better one)

M Buttstädt (bus measurements RWTH Aachen)

O Conrad (SAGA GIS, bug fixing, and programming art)

H Dietrich (logger and circulation type knowledge)

C Daneke (nLUC, DB, fun, and friendship)

T Kawohl (bus measurements)

B Leitl (support, bolster, and wind tunnel stuff)

J Oßenbrügge (support and supervision)

E Rauch (american english)

J Schilling (friendship and trust in my work, without even knowing what I am doing)

I thank all the people that provided us with the invaluable measurement data and technical infrastructure:

A Bugl and R Weigle (DB help)

T Blümel (bus measurement logistics)

U Dietze and T Nass (winter clearance service measurement data)

A Hansen (school measurement data)

Intermap Technologies (IFSAR DEM)

P Kirschner (HaLm data)

I Lange and B Brümmer (MI-station data)

D Matzen (HaLm meta data)

T de Paus (KLIMZUG NORD data)

C Peek (processed  $z_0$  data of MI-station)

S Sandoval and F Ament (HUSCO data)

B Schüen (DKRZ and WRF help)

SICCS and CliSAP (money and seminars)

A huge high five goes out to my whole family and my friends from Amsterdam to Bremen over Karlsruhe and Postbauer-Heng to Napoli! It's done! I have time again! The computer<sup>35</sup> did not eat me in the end ;)

---

<sup>35</sup> Last but not least I thank the wrfhelp-line and the whole open source community, as 95% of this research was accomplished with open source software like SAGA GIS, WRF, PostgreSQL, pgAdmin, R-Studio, Mozilla, Quantum-GIS, GNU Debian. This research was written and edited with Focuswriter, then Libreoffice, Gnumeric, and Gimp on OpenSuse Tumbleweed with KDE. Great stuff!

# Bibliography

- Argüeso D, JM Hidalgo-Munoz, SR Gamiz-Fortis, MJ Esteban-Parra, J Dudhia, Y Castro-Diez, 2011: Evaluation of WRF parameterizations for climate studies over Southern Spain using a multistep regionalization, *Journal of Climate* 24, 5633–5651, doi:10.1175/JCLI-D-11-00073.1
- ATKIS HP, 2012: Arbeitsgemeinschaft der Vermessungsverwaltungen der Länder der Bundesrepublik Deutschland (AdV), <http://www.adv-online.de>, l.a. 3 July 2012
- Auer AH, 1978: Correlation of land use and cover with meteorological anomalies, *Journal of Applied Meteorology* 17, 636–643
- Baur F, P Hess, H Nagel, 1944: Kalender der Großwetterlagen Europas 1881-1939, Forschungsinstitut für langfristige Wettervorhersage, Bad Homburg
- Bechtel B, C Daneke 2012: Classification of local Climate Zones based on multiple Earth Observation Data, *IEEE Journal of Selected Topics in Applied Earth Observations and Remote Sensing*, doi: 10.1109/JSTARS.2012.2189873
- Bechtel B, T Langkamp, F Ament, J Böhner, C Daneke, R Günzkofer, B Leitl, J Oßenbrügge, A Ringeler, 2011: Towards an urban roughness parameterisation using interferometric SAR data taking the Metropolitan Region of Hamburg as an example, *Meteorologische Zeitschrift* 20, 1, 29–37, doi: 10.1127/0941-2948/2011/0496
- Bechtel B, T Langkamp, R Günzkofer, C Daneke, B Leitl, J Oßenbrügge, A Ringeler, J Böhner, 2009: Urban roughness parameter estimation using Interferometric SAR data in the Metropolitan Region of Hamburg, METTOOLS 2009 Poster
- Bechtel B, K J Schmidt, 2011: Floristic mapping data as a new proxy for the mean urban heat island, *Climate Research* 49, 45–58, doi: 10.3354/cr01009
- Böhner, J, O Antonic, 2008: Land-Surface Parameters Specific to Topo-Climatology. – In: Hengl, T & Reuter, H.I. [Eds.]: *Geomorphometry: Concepts, Software, Applications. – Developments in Soil Science* 33, Elsevier, 772 pp.
- Bottema M, 1995a: Aerodynamic roughness parameters for homogeneous building groups, Part 2: Results Document SUB-MESO 80, Ecole Centrale de Nantes, France
- , 1995b: Parameterisation of aerodynamic roughness parameters in relation to air pollutant removal efficiency of streets, Brebbia C A, H Power, N Mous-Siopoulos, *Air Pollution III, Volume 2 Air Pollution Engineering and Management, Ecology Environment* 10, 235–242
- Bottema M, 1997: Urban roughness modelling in relation to pollutant dispersion, *Atmospheric Environment* 31, 3059–3075
- Burian S J, SW Stetson, WS Han, J Ching, D Byun, 2004: High-resolution dataset of urban canopy parameters for Houston 5th Conference on Urban Environment 93, extended abstract
- Buttstädt M, T Sachsen, G Ketzler, H Merbitz, C Schneider, 2011: A new approach for highly resolved air temperature measurements in cities, *Atmospheric Measurement Techniques Discussion* 4, 1001–1019
- CCCSN HP, 2012: A general downscaling figure, <http://www.cccsn.ec.gc.ca/?page=downscaling>, l.a. 29 June 2012
- CERA HP, 2011: Climate and Environmental Retrieval and Archive, <http://cera-www.dkrz.de>, l.a. 29 June 2012
- Chang S, G Huynh, 2007: A Comparison of Roughness Parameters for Oklahoma City from Different Evaluation Methods 7th Symposium on the Urban Environment 92

- Chen F, H Kusaka, R Bornstein, J Ching, CSB Grimmond, S Grossman-Clarke, T Loridan, KW Manning, A Martilli, S Miao, D Sailor, F P Salamanca, H Taha, M Tewari, X Wang, AA Wyszogrodzki, C Zhang, 2010: The integrated WRF/urban modelling system: development, evaluation, and applications to urban environmental problems International, Journal of Climatology
- Ching J, M Brown, T McPherson, S Burian, F Chen, R Cionco, A Hanna, T Hultgren, D Sailor, H Taha, D Williams, 2009: National Urban Database and Access Portal Tool, NUDAPT, Bulletin of the American Meteorological Society 90, 8, 1157–1168
- CLWRF HP 2012: CLimate WRF – WRF modifications for regional climate modelization, <http://www.meteo.unican.es/en/software/clwrf>, l.a. 15 August 2012
- Counihan J, 1975: Adiabatic atmospheric boundary layers: A review and analysis of data from the period 1880–1972, Atmospheric Environment 9, Issue 10, October 1975, 871–905, ISSN 0004-6981
- CWRF HP 2012: Climate Weather Research and Forecasting Model, <http://cwrf.umd.edu>, l.a. 22 June 2012
- Daneke C, B Bechtel, J Böhrner, T Langkamp, J Oßenbrügge, 2011: Conceptual approach to measure the potential of Urban Heat Islands from Landuse datasets and Landuse projections, Computational Science and Its Applications - ICCSA 2011 Lecture Notes in Computer Science 6782, 381-393, doi: 10.1007/978-3-642-21928-3\_27
- Daneke C, B Bechtel, T Langkamp, 2010: Classification Scheme of Urban Structures based on climatic Characteristics, designed for Land Use Modeling Applications 17th Conference International Seminar on Urban Form, ISUF, Formation and Persistence of Townscape, Hamburg and Lübeck, 20–23 August 2010
- Davenport AG, 1960: Rationale for determining design wind velocities, Journal of Structural Division, American Society of Civil Engineers 86, 39–68
- Davenport AG, CSB Grimmond, TR Oke, J Wieringa, 2000: Estimating the roughness of cities and sheltered country, preprint for the 12th AMS Conference, Applied Climatology, Asheville, NC, 96–99
- DK, 2010: Driesen+Kern GmbH "rugged" data logger series, <http://www.driesen-kern.de/downloads/dk3xxloggerserierrugged.pdf>, l.a. 25 May 2011
- Dudhia J, D Gill, K Manning, W Wang, C Bruyere, 2005: PSU/NCAR Mesoscale Modeling System Tutorial Class Notes and Users' Guide, MM5 Modeling System Version 3 – Updated for MM5 Modeling System Version 37 – Released January 2005, <http://www.mmm.ucar.edu/mm5/documents/tutorial-v3-notes.html>, l.a. 25 June 2011
- Dudhia J, 2011: WRF Modeling System Overview, [http://www.mmm.ucar.edu/wrf/users/tutorial/201104\\_Korea/01\\_WRF\\_Overview\\_Dudhia.pdf](http://www.mmm.ucar.edu/wrf/users/tutorial/201104_Korea/01_WRF_Overview_Dudhia.pdf), l.a. 3 July 2011
- DW HP, 2011: WRF Domain Wizard, <http://wrfportal.org/DomainWizard.html>, l.a. 30 January 2012
- DWD HP, 2012a: The objective circulation type classes of the DWD, [http://www.dwd.de/bvbw/appmanager/bvbw/dwdwwwDesktop?nfpb=true&pageLabel=dwdwww\\_result\\_page&portletMasterPortlet\\_i1gsbDocumentPath=Navigation%2FOeffentlichkeit%2FKlima\\_Umwelt%2FKlimadaten%2Fkldaten\\_kostenfrei%2Fwfk\\_kennzahlen\\_node.html%3F\\_nnn%3Dtrue](http://www.dwd.de/bvbw/appmanager/bvbw/dwdwwwDesktop?nfpb=true&pageLabel=dwdwww_result_page&portletMasterPortlet_i1gsbDocumentPath=Navigation%2FOeffentlichkeit%2FKlima_Umwelt%2FKlimadaten%2Fkldaten_kostenfrei%2Fwfk_kennzahlen_node.html%3F_nnn%3Dtrue), l.a. 20 August 2012
- DWD HP, 2012b: Data archive of the objective circulation types, [http://www.dwd.de/bvbw/generator/DWD-WWW/Content/Oeffentlichkeit/KU/KU2/KU23/wetterlagenklassifikation/online\\_wlkdaten.templateId=raw.property=publicationFile.txt/online\\_wlkdaten.txt](http://www.dwd.de/bvbw/generator/DWD-WWW/Content/Oeffentlichkeit/KU/KU2/KU23/wetterlagenklassifikation/online_wlkdaten.templateId=raw.property=publicationFile.txt/online_wlkdaten.txt), l.a. 20 August 2012
- DWD HP, 2012c: Data archive of the objective circulation types with additional forecast data, [http://www.dwd.de/bvbw/generator/DWDWWW/Content/Oeffentlichkeit/KU/KU2/KU23/wetterlagenklassifikation/online\\_wlkvorhersage.templateId=raw.property=publicationFile.txt/online\\_wlkvorhersage.txt](http://www.dwd.de/bvbw/generator/DWDWWW/Content/Oeffentlichkeit/KU/KU2/KU23/wetterlagenklassifikation/online_wlkvorhersage.templateId=raw.property=publicationFile.txt/online_wlkvorhersage.txt), l.a. 20 August 2012
- DWD WebWerdis HP, 2012: climatological database of the DWD, [http://werdis.dwd.de/werdis/start.js\\_JSP.do](http://werdis.dwd.de/werdis/start.js_JSP.do), l.a. 25 July 2012
- ECMWF HP, 2011: European Centre for Medium-Range Weather Forecasts, <http://www.ecmwf.int/research/era/do/get/index>, l.a. 23 May 2012

- EEA HP, 2012: Coordination of Information on the Environment (CORINE) data at the European Environment Agency, <http://www.eea.europa.eu/data-and-maps/data/clc-2006-vector-data-version-2>, l.a. 19 June 2012
- Ellefsen R, 1991: Mapping and measuring buildings in the urban canopy boundary layer in ten US cities, *Energy Building* 15–16, 1025–1049
- Feddersen B, 2005: Wind tunnel modelling of turbulence and dispersion above tall and highly dense urban roughness, ETH Zürich, doi: 103929/ethz-a-004941441
- Fischer M, 2010: Analyse des Hamburger Stadtklimas anhand von Schulwetterstationen, unpublished bachelor thesis, meteorological institute of the university of Hamburg
- Flagg DD, R Schoetter, BH Fock, D Grawe, P Kirschner, KH Schlünzen, 2012: From Land-Use to Surface Cover for Mesoscale Atmospheric Models, Submitted to Theoretical and Applied Climatology
- Gál T, J Unger, 2009: Detection of ventilation paths using high-resolution roughness parameter mapping in a large urban area, *Building Environment* 44, 1, 198–206
- Garratt JR, 1992: *The Atmospheric Boundary Layer*, Cambridge University Press, Cambridge, 316
- Golem.de, 2012: Google with 3D- and Offlinemaps vs. Apple, <http://www.golem.de/news/google-mit-3d-und-offline-karten-gegen-apple-1206-92362.html>, l.a. 25 June 2012
- Grimmond CSB, TR Oke, 1999: Aerodynamic properties of urban areas derived from analysis of surface form, *Journal of Applied Meteorology* 38, 9, 1262–1292
- Grimmond CSB, M Best, J Barlow, AJ Arnfield, J-J Baik, A Baklanov, S Belcher, M Bruse, I Calmet, F Chen, P Clark, A Dandou, E Erell, K Fortuniak, R Hamdi, M Kanda, T Kawai, H Kondo, S Krayenhoff, SH Lee, S-B Limor, A Martilli, V Masson, S Miao, G Mills, R Moriwaki, K Oleson, A Porson, U Sievers, M Tombrou, J Voogt, T Williamson, 2009: Urban surface energy balance models: Model characteristics and methodology for a comparison study, *Meteorological and Air Quality Models for Urban Areas*, Editors: A Baklanov, S Grimmond, A Mahura, M Athanassiadou, Dordrecht: Springer
- Grimmond CSB, M Blackett, MJ Best, J-J Baik, SE Belcher, SI Bohnenstengel, I Calmet, F Chen, A Dandou, K Fortuniak, ML Gouvea, R Hamdi, M Hendry, T Kawai, Y Kawamoto, H Kondo, ES Krayenhoff, SH Lee, T Loridan, A Martilli, V Masson, S Miao, K Oleson, G Pigeon, A Porson, YH Ryu, F Salamanca, GJ Steeneveld, M Tombrou, JVoogt, D Young, N Zhang, 2010: The International Urban Energy Balance Models Comparison Project: First results from Phase 1, *Journal of Applied Meteorology and Climatology* 49, 1268–1292, doi: 101175/2010JAMC23541
- Grimmond CSB, M Blackett, MJ Best, J-J Baik, SE Belcher, JBerlinger, SI Bohnenstengel, I Calmet, F Chen, A Coutts, A Dandou, K Fortuniak, ML Gouvea, R Hamdi, M Hendry, M Kanda, T Kawai, Y Kawamoto, H Kondo, ES Krayenhoff, S-H Lee, T Loridan, A Martilli, V Masson S Miao, K Oleson, R Ooka, G Pigeon, A Porson, Y-H Ryu, F Salamanca, G-J Steeneveld, M Tombrou, JA Voogt, D Young, N Zhang, 2011: Initial Results from Phase 2 of the International Urban Energy Balance Comparison Project, International, *Journal of Climatology* 31, 244–272, doi: 101002/joc2227
- HaLm HP, 2012: Ambient air pollution network of Hamburg, <http://www.hamburger-luft.de>, l.a. 2 June 2012
- Hanna SR, JC Chang, 1992: Boundary layer parameterisations for applied dispersion modelling over urban areas, *Boundary-Layer Meteorology* 58, 229–259
- Hess P, H Brezowsky, 1977: Katalog der Großwetterlagen Europas 1881-1976, 3. verbesserte und ergänzte Auflage, *Berichte des Deutschen Wetterdienstes* 15
- HOBO, 2010: Pro v2 User's Guide, [http://www.onsetcomp.com/files/manual\\_pdfs/10694-H-MAN-U23.pdf](http://www.onsetcomp.com/files/manual_pdfs/10694-H-MAN-U23.pdf), l.a. 1 June 2012
- Holt T, J Pullen, 2007: Urban canopy modeling of the New York city metropolitan area: a comparison and validation of single- and multilayer parameterizations, *Monthly Weather Review* 135, 1906–1930
- HPC Advisory Council 2010: Weather Research and Forecasting (WRF) Performance Benchmark and Profiling, Best Practices of the HPC Advisory Council, [http://www.hpcadvisorycouncil.com/pdf/WRF\\_Analysis\\_and\\_Profiling\\_Intel.pdf](http://www.hpcadvisorycouncil.com/pdf/WRF_Analysis_and_Profiling_Intel.pdf), l.a. 25 June 2012

- HUSCO HP, 2012: The Hamburg urban soil climate observatory of the university of Hamburg, <http://www.mi.uni-hamburg.de/index.php?id=6566&L=3>, l.a. 25 May 2012
- HVV HP, 2010: metro bus lanes, <http://www.hvv.de/streckennetz/produktplaene/?netzplan=MetroBusse+%28geografisch%29>, l.a. 8 July 2012
- ICDC, 2012: Integrated climate data center - Land surface parameters, <http://www.icdc.zmaw.de/land.html>, l.a. 11 October 2012
- Joint Urban, 2003: Urban field program, <http://www.noaa.inel.gov/projects/ju03/ju03.htm>, l.a. 11 October 2012
- KLIMZUG NORD HP, 2009: The metropolitan regions of Hamburg, <http://klimzug-nord.de/index.php/page/2009-03-30-REGION>, l.a. 2 August 2012
- KLIMZUG NORD HP, 2012: Future proof adaption on regional climate change, region north, <http://klimzug-nord.de>, l.a. 23 May 2012
- Kondo J, H Yamazawa, 1986: Aerodynamic roughness over an inhomogeneous ground surface, *Boundary-Layer Meteorology* 35, 331–348
- Kusaka H, F Chen, M Tewari, M Duda, J Dudhia, Y Miya, Y Akimoto, 2009: Performance of the WRF model as a high resolution regional climate model: model intercomparison study, *Proceedings of ICUC-7 (in CD-ROM)*
- Kutzbach J, 1961: Investigations of the modifications of wind profiles by artificially controlled surface roughness – MS Thesis, Department of Meteorology, University of Wisconsin, Madison, 58
- Langkamp T, J Böhner, 2011: Influence of the compiler on multi-CPU performance of WRFv3, in *Geoscientific Model Development*, 4, 611–623, 2011, doi:105194/gmd-4-611-2011
- Lemonsu A, A Leroux, S Belair, S Trudel, J Mailhot, 2006: A General Methodology of urban cover classification for atmospheric modeling, 6th Symposium on the Urban Environment, 55, Atlanta
- Leroux A, J-P Gauthier, A Lemonsu, S Belair, J Mailhot, 2009: Automated urban land use and land cover classification for mesoscale atmospheric modelling over Canadian cities, *Geomatica* 63, 1, 393–406
- Liu J, Bray M, Han D, 2012: Sensitivity of the Weather Research and Forecasting (WRF) model to downscaling ratios and storm types in rainfall simulation, *Hydrological Processes*, doi: 10.1002/hyp.8247
- LGV HP, 2012: Landesbetrieb Geoinformation <http://www.hamburg.de/startseite-landesbetrieb-geoinformation-und-vermessung>, l.a. 22 June 2012
- Lo JCF, AKH Lau, F Chen, JCH Fung, KKM Leung, 2007: Urban modification in a mesoscale model and the effects on the local circulation in the Pearl River Delta Region, *Journal of Applied Meteorology and Climatology*, 46, 457–476
- Loridan T, CSB Grimmond, S Grossman-Clarke, F Chen, M Tewari, K Manning, A Martilli, H Kusaka, M Best, 2010: Trade-offs and responsiveness of the single-layer urban parameterization in WRF: an offline evaluation using the MOSCEM optimization algorithm and field observations, *Quarterly Journal of the Royal Meteorological Society* 136, 997–1019
- Martilli A, 2007: Current research and future challenges in urban mesoscale modelling in *International Journal of Climatology* 27: 1909–1918, doi: 101002/joc1620
- Martilli A, A Clappier, MW Rotach, 2002: An Urban Surface Exchange Parameterisation for Mesoscale Models, *Boundary-Layer Meteorology*, 104, 261–304
- Matheron G, 1963: Principles of Geostatistics, *Economic Geology* 85, 1246–1246
- , 1973: The Intrinsic Random Functions and their Applications – *Advances in Applied Probability* 5, 1097–1105
- Meijering E, 2002: A Chronology of Interpolation: From Ancient Astronomy to Modern Signal and Image Processing, *Proceedings of the IEEE* 90, 319–342, <http://bigwww.epfl.ch/publications/meijering0201.pdf>

- Memon RA, DYC Leung, C-H Liu, 2010: Effects of building aspect ratio and wind speed on air temperatures in urban-like street canyons, *Building and Environment* 45, 1, 176–188, doi: 10.1016/j.buildenv.2009.05.015
- , 2008: A review on the generation, determination and mitigation of urban heat Island, *Journal of Environmental Sciences*, 20, 120–8
- MI HP, 2012: Wettermast Hamburg, <http://wettermast-hamburg.zmaw.de/AktDatIndex.htm>, l.a. 25 May 2012
- Miao S, F Chen, MA LeMone, M Tewari, Q Li, Y Wang, 2009: An observational and modeling study of characteristics of urban heat island and boundary layer structures in Beijing, *Journal of Applied Meteorology and Climatology* 48, 3, 484–501
- Mitas L, H Mitasova, 1999: Spatial Interpolation, P Longley, MF Goodchild, DJ Maguire, DW Rhind (Editors), *Geographical Information Systems: Principles, Techniques, Management and Applications*, Wiley
- Morton D, O Nudson, C Stephenson, 2009: Benchmarking and Evaluation of the Weather Research and Forecasting (WRF) Model on the Cray XT5, *Cray User Group Proceedings*, Atlanta, GA, 04–07
- Niu G-Y, 2011: The community Noah land-surface model (LSM) with multi-physics options, updated from the User's Guide Public Release Version 2.7.1 [Mitchell et al. 2005]
- NUDAPT, 2012: National Urban Database and Access Portal Tool, <http://nudapt.org>, l.a. 11 October 2012
- Oke TR, 1987: *Boundary Layer Climates*, Methuen, UK, Wiley, Sons, New York, 372
- Oke TR, 2004: Initial Guidance to Obtain Representative Meteorological Observations at Urban Sites, IOM Report 81, WMO, Geneva
- Oleson KW, GB Bonan, J Feddema, M Vertenstein, CSB Grimmond, 2008: An urban parameterization for a global climate model: 1, Formulation & evaluation for two cities, *Journal of Applied Meteorology and Climatology* 47, 1038–1060, doi:10.1175/2007JAMC1597.1
- Orlanski I, 1975: A rational subdivision of scales for atmospheric processes, *Bulletin American Meteorology Society* 56, 527–530
- Oßenbrügge J, B Bechtel 2010: Klimawandel und Stadt - Der Faktor Klima als neue Determinante der Stadtentwicklung, *Hamburger Symposium Geographie 2*
- Oßenbrügge J, B Bechtel, J Böhner, C Daneke, T Langkamp, T Pohl, S Schempp, 2012: Climate change as a topic for urban research and urban governance - The example of Hamburg/Germany (submitted)
- Otte TL, A Lacser, S Dupont, JKS Ching, 2004: Implementation of an urban canopy parameterization in a mesoscale meteorological model, *Journal of Applied Meteorology* 43, 1648–1665
- OtterBox HP, 2012: OtterBox 3000 Clear, <http://www.otterbox.com/OtterBox-3000-Clear/OTR3-3000S-01.default.pd.html>, l.a. 25 June 2012
- Owen PR, 1971: Buildings in the wind, *Quarterly Journal of Royal Meteorology Society* 97, 396–413
- Pedro M, M Soares, RM Cardoso, PMA Miranda, J de Medeiros, M Belo-Pereira 2012: WRF high resolution dynamical downscaling of ERA-Interim for Portugal, *Climate Dynamics*, doi: 10.1007/s00382-012-1315-2
- Peeck C, 2011: Untersuchung des Einflusses urbaner Rauigkeitsstrukturen auf die Entwicklung des mittleren und turbulenten Windfeldes am Beispiel der Stadt Hamburg, University of Hamburg, Department Geosciences, diploma thesis (falsely labeled as dissertation thesis at <https://kataloge.uni-hamburg.de/DB=1/PPNSET?PPN=665963475>, l.a. 27 June 2012)
- pNetCDF HP, 2012: <http://trac.mcs.anl.gov/projects/parallel-netcdf>, l.a. 27 April 2012
- Ratti C, S Di Sabatino, R Britter, 2006: Urban texture analysis with image processing techniques: winds and dispersion, *Theoretical and Applied Climatology* 84, 77–90
- Raupach MR, 1992: Drag and drag partition on rough surfaces, *Boundary-Layer Meteorology* 60, 375–395
- , 1994: Simplified expressions for vegetation roughness length and zero-plane displacement as functions of canopy height and area index, *Boundary-Layer Meteorology* 71, 211–216
- , 1995: Corrigenda, *Boundary-Layer Meteorology* 76, 303–304

- Raupach MR, RA Antonia, S Rajagopalan, 1991: Rough wall turbulent boundary layers, *Applied Mechanics Rev* 44, 1–25
- Roman D, 2009: Performance hints for WRF on Intel® architecture, <http://software.intel.com/en-us/articles/performance-hints-for-wrf-on-intel-architecture>, l.a. 9 February 2011
- Rotach MW, R Vogt, C Bernhofer, E Batchvarova, A Christen, A Clappier, B Feddersen, SE Gryning, G Martucci, H Mayer, V Mitev, TR Oke, E Parlow, H Richner, M Roth, YA Roulet, D Ruffieux, JA Salmond, M Schatzmann, JA Voogt, 2005: BUBBLE – an urban boundary layer meteorology project, *Theoretical and Applied Climatology* 81, 231–61
- Ruth M, 2006: Smart growth and climate change, Regional development, infrastructure and adaptation, Cheltenham, UK, Northampton
- Sailor DJ, M Hart, 2006: An anthropogenic heating database for major U.S. cities, Sixth Symposium on the Urban Environment, Atlanta, GA, 28 January – 2 February, American Meteorological Society, Boston, MA, Paper 5.6
- Sändig B, E Renner, 2011: The urban impact on the regional climate of Dresden, D G Steyn, S Trini Castelli (Editors), *Air pollution modeling and its application XXI*, Proceedings of the 31 NATO/SPS International Technical Meeting on Air Pollution Modelling and Its Application, Torino, Italy, 27 September - 1 October 2010, Springer, Dordrecht, 181–185, NATO Science for Peace and Security Series - C: Environmental Security
- Schlünzen KH, D Hinneburg, O Knoth, M Lambrecht, B Leidl, S Lopez, C Lüpkes, H Pankus, E Renner, M Schatzmann, T Schoenemeyer, S Trepte, R Wolke, 2003: Flow and transport in the obstacle layer – First results of the microscale model MITRAS, *Journal of Atmospheric Chemistry* 44, 113–130
- Schmid HP, 1994: Source areas for scalars and scalar fluxes, *Boundary-Layer Meteorology* 67, 293–318
- Smolarkiewicz PK, R Sharman, J Weil, SG Perry, D Heist, G Bowker, 2007: Building resolving large-eddy simulations and comparison with wind tunnel experiments, *Journal of Computational Physics* 227, 633–653
- SRHH HP, 2012: The winter road clearance service of the Hamburg city cleaning service, <http://www.srh-h.de/srhh/opencms/privatkunden/winterdienst/index.html>, l.a. 25 May 2012
- Stewart ID, TR Oke, 2009: Newly developed "thermal climate zones" for defining and measuring urban heat island magnitude in the canopy layer, Preprints, 8th Symposium on Urban Environment, January 11–15, Phoenix, Arizona, extended abstract
- Stewart ID, TR Oke, 2012: 'Local Climate Zones' for urban temperature studies, *Bulletin of the American Meteorological Society*, doi: 10.1175/BAMS-D-11-00019.1
- Taha H, JKS Ching, 2007: UCP/MM5 Modeling in conjunction with NUDAPT: model requirements, updates, and applications, Seventh Symposium on the Urban Environment, San Diego, CA, 10–13 September, American Meteorological Society, Boston, MA, Paper 6.4
- Tewari M, H Kusaka, F Chen, WJ Coirier, S Kim, A Wyszogrodzki, TT Warner, 2010: Impact of coupling a microscale computational fluid dynamics model with a mesoscale model on urban scale contaminant transport and dispersion, *Atmospheric Research* 96, 656–664
- Tornado HP, 2012: Tornado documentation, <http://www.dkrz.de/Nutzerportal-en/doku/tornado>, l.a. (restricted) 29 August 2012
- UCAR, 2002: Data Format Handbook for Agricultural Meteorology modeling system (AGRMET), [http://www.mmm.ucar.edu/mm5/documents/DATA\\_FORMAT\\_HANDBOOK.doc](http://www.mmm.ucar.edu/mm5/documents/DATA_FORMAT_HANDBOOK.doc), l.a. 1 August 2012
- Variotek HP, 2012a: BT-Q1000XT Bluetooth GPS Travel Recorder, <http://variotek.de/?p=285>, l.a. 25 June 2012
- , 2012b: Mobile Power Pack VT-PP-320, <http://variotek.de/?p=215>, l.a. 25 June 2012
- VDI, 1997: Umweltmeteorologie Klima- und Lufthygienekarten für Städte und Regionen, VDI-Richtlinie 3787, Blatt 1

- Voogt, JA, TR OKE, 2003: Thermal remote sensing of urban climates. *Remote Sensing of Environment*, 86, 370–384
- Wang W, C Bruyere, M Duda, J Dudhia, D Gill, H-C Lin, J Michalakes, S Rizvi, X Zhang, JD Beezley, JL Coen, J Mandel, 2012: ARW Version 3 Modeling System User's Guide, [http://www.mmm.ucar.edu/wrf/users/docs/user\\_guide\\_V3/contents.html](http://www.mmm.ucar.edu/wrf/users/docs/user_guide_V3/contents.html), l.a. 2 September 2012
- Wentz M, 2000: Die kompakte Stadt, Frankfurt am Main, New York, Campus Verlag, Die Zukunft des Städtischen, 11
- Werner PC, FW Gerstengarbe, 2010: Katalog der Großwetterlagen Europas (1881-2009) nach Paul Hess und Helmut Brezowsky, 7. verbesserte und ergänzte Auflage, PIK Report 119, <http://www.pik-potsdam.de/research/publications/pikreports/.files/pr119.pdf>, l.a. 5 July 2012
- Westfalia Ltc. HP, 2011: Magnets of a tools company, [http://www2.westfalia.de/shops/agrishop/landmaschinen\\_zubehoer/fuer\\_schlepper\\_traktoren\\_anhaenger/arbeits\\_frontscheinwerfer/924-universal\\_magnethalterung\\_einfach.htm](http://www2.westfalia.de/shops/agrishop/landmaschinen_zubehoer/fuer_schlepper_traktoren_anhaenger/arbeits_frontscheinwerfer/924-universal_magnethalterung_einfach.htm), l.a. 15 June 2012
- Wetterzentrale.de HP, 2012: Archive of the AVN-Nordhemisphärenanalysen since 27.01.1998, <http://www.wetterzentrale.de/topkarten/tkhavnar.htm>, l.a. 29 July 2012
- Wieringa J, AG Davenport, CSB Grimmond, TR Oke, 2001: New revision of Davenport roughness classification, 3rd European, African Conference on Wind Engineering, Eindhoven, Netherlands, July 2001
- Wilby RL, SP Charles, E Zorita, B Timbal, P Whetton, LO Mearns, 2004: The guidelines for use of climate scenarios developed from statistical downscaling methods. Supporting material of the Intergovernmental Panel on Climate Change (IPCC), prepared on behalf of Task Group on Data and Scenario Support for Impacts and Climate Analysis
- Wilby RL, 2008: Constructing climate change scenarios of urban heat island intensity and air quality, *Environment and Planning B: Planning and Design* 35, 902–919, doi:10.1068/b33066t
- WRF basics, 2012: Online tutorial basics, [http://www.mmm.ucar.edu/wrf/OnLineTutorial/Basics/WRF/run\\_directory.html](http://www.mmm.ucar.edu/wrf/OnLineTutorial/Basics/WRF/run_directory.html), l.a. 29 June 2012
- WRF HP, 2012: <http://www.wrf-model.org>, l.a. 18 June 2012
- WRF oLUC, 2009: original land use data of WRF, [http://www.mmm.ucar.edu/wrf/src/wps\\_files/geog\\_v3.1.tar.gz](http://www.mmm.ucar.edu/wrf/src/wps_files/geog_v3.1.tar.gz), l.a. 25 June 2012
- WRF online tutorial, 2012: <http://www.mmm.ucar.edu/wrf/OnLineTutorial/index.htm>, l.a. 19 June 2012

## Erklärung

Hiermit versichere ich, die vorliegende Arbeit selbstständig angefertigt und nur die angegebenen Hilfsmittel verwendet zu haben. Diese Arbeit hat in gleicher oder ähnlicher Form noch keiner Prüfungsbehörde vorgelegen. Der Veröffentlichung in der Bibliothek stimme ich zu.

Hamburg, den 15. March 2013